Project Number: ME-RLN-01

Reduction of Audible Noise Due to Hard Stops in an Assembly Machine

A Major Qualifying Project Report:

submitted to the Faculty

of the

WORCESTER POLYTECHNIC INSTITUTE

in partial fulfillment of the requirements for the

Degree of Bachelor of Science

by

Tyler Angers **Muhammad Azeem** **Sean Mokler** **Timothy Souza**

Date: December 13, 2007

Approved:

Professor Robert L. Norton, Major Advisor

1. cam
2. noise
3. impact

This report represents the work of one or more WPI undergraduate students
submitted to the faculty as evidence of completion of a degree requirement.
WPI routinely publishes these reports on its web site without editorial or peer review.

ACKNOWLEDGEMENTS:

We would like to thank the following people from the sponsoring company and WPI for their guidance and help throughout the course of the project.

- Professor Robert Norton
- Charlie Gillis
- Marty D'Agostino
- Ernie Chandler
- Greg Aviza
- Daniel LaBelle
- Adriana Hera
- Steve KilKelly
- Jamie Ulery
- Corey Maynard
- Dave Morris

ABSTRACT:

This project focuses on the reduction of audible noise emitted from an assembly machine at the sponsoring company. We modeled the system initially using assumed and calculated values, and the simulated data reflects the displacement, velocity, and acceleration in the system. A comparison of the tested and simulated data verified that the model does accurately portray the system's dynamic behavior, minus the impact events. Given the relationship between emitted noise and kinetic energy, the source of the audible noise problem was the high velocity impacts on the hard stops. We achieved the desired positions and velocities through redesign of the cams that generate system motion. Following the production of new cams and the gathering of data after installation, a comparison to the original experimental data showed a large decrease in peak accelerations. The comparison indicates that the new cams provide a significant improvement over the old cams. Peak accelerations at the hard stops were decreased which corresponds to a drop in velocity at impact. This resulted in lower emitted noise as measured on a sound level meter. According to the originally outlined goals, this project provides a successful solution to the problem encountered by the sponsor.

EXECUTIVE SUMMARY:

The goal of this project was to identify and redesign components of an assembly machine that contributed to excessive machine noise and increased part wear. The mechanisms targeted for improvement were the horizontal and vertical mechanisms on one station of the assembly machine.

The first task was to create dynamic models of the current system, and verify those models by comparison to test data. Part geometry was modeled using Pro/Engineer and Unigraphics. Application of material properties allowed the masses of each part to be determined using the computer models. To view the properly phased motion of the two mechanisms, a kinematic model was created in Pro/Engineer. This required properly defining an assembly as well as joint definitions between parts to create a single degree of freedom model for reference purposes. We found the stiffnesses in the system using hand calculations and finite element analysis with SolidWorks. By applying the proper boundary conditions for each of the pins and subjecting the part to an arbitrary force that causes distortion, the spring rate can be determined as a ratio of the force required per displacement.

The mass and stiffness data for each of the components were converted into a lumped model. The lumped model considers component location and provides the effective mass and stiffness of each link as if they were located at the cam follower. The air spring preload experienced by the follower arm was calculated using the pressure in the air spring and the surface area that it acts upon.

All of this calculated data was substituted into program *Dynacam* along with the provided cam profile. After making assumptions, the dynamic simulation provides the displacement,

velocity, and acceleration functions for the system. These functions are used to verify experimental data gathered.

Test data was collected using multiple methods for comparison to the dynamic simulation as well as determination of data that cannot be predicted in the models. The air preload was verified using a pressure transducer to measure cylinder pressure throughout the cycle. Hammer tests provided natural frequencies of various links while a linear variable differential transformer (LVDT) measured the extension or compression of the pneumatic link. These tests verified calculations and assumptions made for the dynamic model. The acceleration correlation is established by placing accelerometers in the system at certain locations. The intent of this is to provide acceleration data on the hard stop impacts as well as the cam profile.

The transfer of kinetic energy due to high velocities upon hitting the hard stops was determined to be the biggest contributor to the noise emitted by the machine. The focus on the cam redesign is primarily based on the reduction of velocity at impact, but must also take over travel into consideration. Reducing velocity at the hard stop and decreasing the over travel improved noise as well as machine operation.

Once the cam profile had been established and approved, we had them fabricated and installed them in the machines. We took accelerometer data in the same fashion as it was for the original cams. Acceleration profile was compared to the original cams as well as the dynamic simulation to determine correlation and improvement. A sound level meter gave readings of the magnitude of the collision in decibels, with the difference being taken as the overall improvement of the system.

Results indicated that the accelerations for the vertical cam dropped from 24 g's to 3.5 g's upon impact and from 16 g's to 3.5 g's for departure. The velocity range decreased from

26.76 – 30.73 deg/sec to 3 – 5.92 deg/sec. The sound reduction was 4 dB. Acceleration for the vertical motion mechanism dropped from 36 g's to 2 g's upon hitting and 45 g's to 11 g's upon departure. The velocity range decreased from 19.9 – 28.0 deg/sec to 3 – 7.5 deg/sec. The sound reduction was 4.39 dB.

The result of this project was successful and after analyzing the data, it is recommended that the changes made to the single station be implemented throughout all relevant stations on all machines. In addition to the changes already made, several additional recommendations have been explored that offer potential improvement. Implementing these suggestions has been shown by our testing to improve dynamics, cause quieter operation, both of which provide longer component life, and overall improved performance.

TABLE OF CONTENTS:

List of Figures

List of Tables:

1. Introduction

Assembly machines are a crucial type of equipment for the sponsoring company. These machines have evolved over several product lines and been subject to redesigns that promote higher running speeds to satisfy increased product demand. One problem resulting from increased running speeds is that there has been an increase in sound output from the machine. The particular problem that this project addresses is the sound output by one of the systems on a particular assembly machine. The goal of this project was to analyze this system, find the source(s) of sound output, and test means to reduce the noise emitted by this system.

The first step was to model and understand the original system. We then generated dynamic models of the system that provided theoretical data, which we used to verify the experimental data taken from the machine. This process was performed for both mechanisms in the system. Through the creation of a lumped mass model, we created a single degree of freedom model using the program *Dynacam*. We then verified the output of the *Dynacam* model using accelerometers, pressure transducers, and hammer tests on the actual machine to ensure that our simulated data closely correlated to the experimental data. Once completed, the components that contributed the most towards noise generation were redesigned.

After completing the redesign phase, prototype parts were manufactured. We then had the prototype parts installed in the machine and repeated the tests initially performed on the machine. These verified that the redesigned theoretical models were accurate and provided test data to quantify the improvements over the previous components. With this knowledge in mind, we made further recommendations as to potential changes to be made to the system to improve noise generation and overall operation.

The following design report discusses the functionality of each mechanism within the system and the components of interest. The report provides the results of all tests done, analysis of these results, and recommendations. This feedback was then presented to the sponsoring company.

2. Background

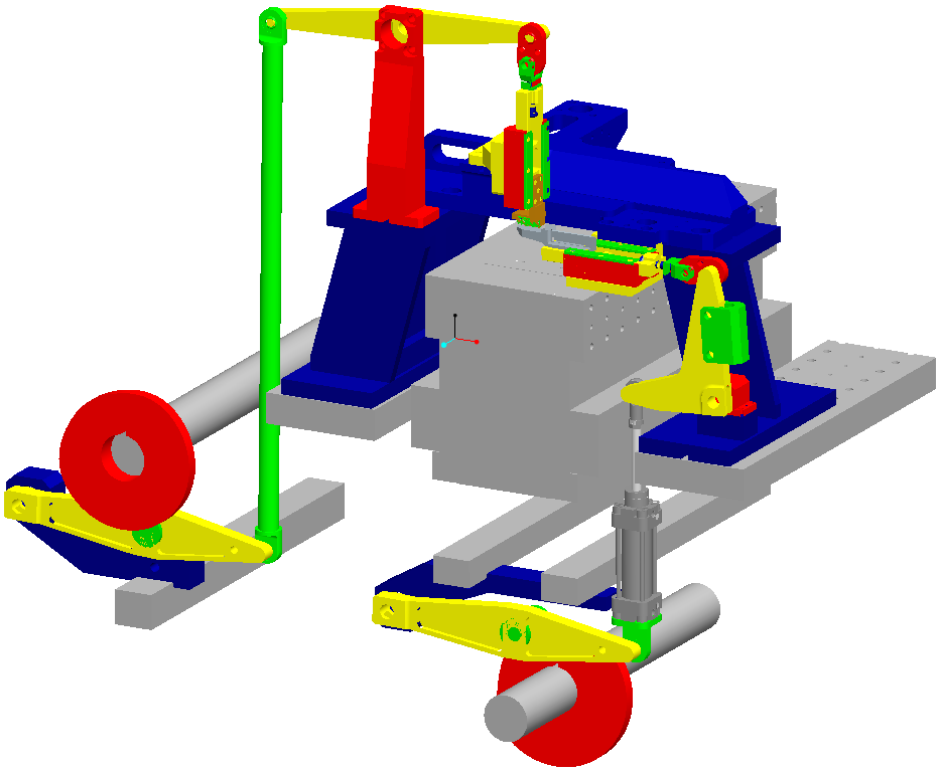

Figure 1 – Model of one station of the assembly machine

The subject station of the assembly machine, shown in **Figure 1**, assembles individual components to form a final product. Classified as an indexing machine, the component is delivered to the system on a conveyor belt that runs beneath the tooling. When it reaches its desired position, the conveyor stops while the two mechanisms in the station perform their respective functions. Since the product part is small, the position of the tooling end effectors at the extremes of their motion is critical. Ideally, the profile of the cam solely dictates the final position achieved by the tooling. Realistically, this is not possible due to the translation of motion throughout the linkage train on route to the end effector. Part tolerances, vibrations, masses and link stiffness must be taken into account during the translation of this motion, each manipulating the input and transforming the output. The positional precision required by the

tooling is subject to this transformed output resulting in a motion path that is unique to each mechanism.

The current configuration, as explained by the engineers, generates excessive audible noise. The noise is the result of the impact between the tooling and the hard stop, which is used to gain the precision of the necessary location. **Figure 2** shows the concept of a hard stop with the inclusion of an over-travel spring.

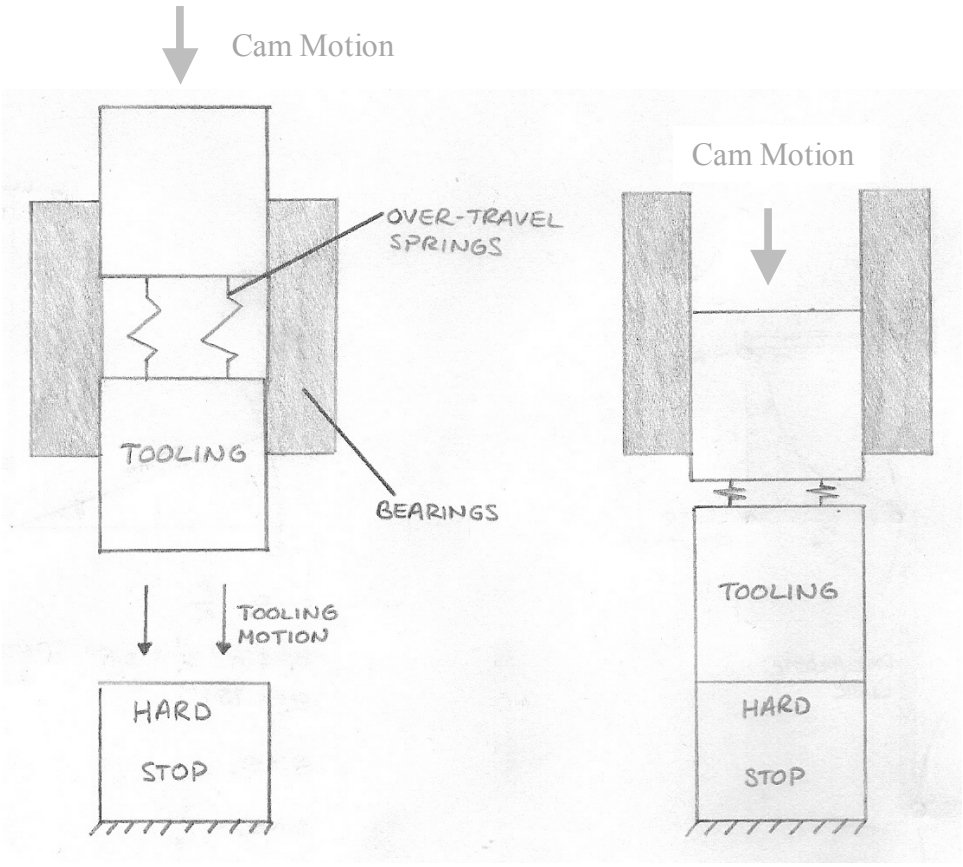

Figure 2 - Hard stop and over-travel condition

A system similar to the one pictured is featured in the horizontal and vertical motion mechanisms to achieve the required positions. Over-travel is motion that drives the tooling beyond the final position allowed by the hard stop, which is necessary to ensure that the tooling stays on the hard stop through the dwell. Given that each machine is different, the over-travel also exists to guarantee that the tooling will contact the hard stop. By specifying a range that

encompasses variance due to tolerances and setup procedures, any variations are essentially negated.

The kinetic energy, $E_{kinetic}$, is a function of the mass, m, times the velocity, v, squared as seen in *Equation 1*.

$$E_{kinetic} = \frac{1}{2}mv^2 \quad \textbf{(1)}$$

Given this relationship, the kinetic energy can be reduced by decreasing either the mass or the velocity at impact.

Most of the parts within the machine are fabricated from hardened steel. While providing excellent strength and hardness, which is necessary for certain components, it is a very dense material. There is the potential for some components to be fabricated in a fashion that will increase critical dimensions, but being less dense than steel will achieve a similar stiffness with a decrease in mass.

Another method of reducing the mass present at the cam is by reducing the link ratio applied to masses to account for their displacement from the cam follower. The effective masses calculated from this property relate to the link factor, defined as the ratio between the lengths of the input and output of the lever arms. Decreasing the ratio will lessen the effective mass at the cam follower. This lowers vibrations, which in turn lowers noise.

Reduction of velocity upon hitting the hard stop is the other way to lessen the kinetic energy of the impact. Since velocity is simply the integral of the acceleration, reduction of acceleration at this point would provide the same results. This is significant because accelerations are analyzed in this project rather than velocities due to equipment available.

The force, *F*, experienced by the hard stop due to the impact of the tooling is given in *Equation 2*.

$$F = m \times a \tag{2}$$

Force is equal to the mass, *m*, times the acceleration, *a*. Decreasing the collision force ensures that the hard stop does not prematurely wear, a condition that would result in imprecise positions, the exact reason the hard stop is present. Eliminating this premature wear will result in better precision as well as less maintenance.

The ideal goal would reduce the kinetic energy to zero which would result in no impact noise. In order to achieve this goal, the velocity must equal zero at the hard stop since mass is never zero. While ideal, this solution is unrealistic. Due to imperfections in the system, it is impossible to reduce the velocity to zero at impact on every station unless an individual cam was developed for each and every station.

As with any engineering problem associated with a multi-component system, it is difficult to trace the problem back to a single source. The system must be analyzed as a whole and the determination made as to which components are the greatest offenders and whose redesign stands to provide the most benefit. The goal of this project is to determine areas of improvement for this system in order to reduce the audible noise, redesign them, and test the result.

2.1 Horizontal Motion Mechanism

The purpose of the horizontal motion mechanism is to remove a component from a stack and deliver it to the vertical motion mechanism. After reaching the vertical mechanism, the

tooling dwells while the vacuum system within the vertical mechanism picks up the component. The tooling then retracts while the vertical motion mechanism performs its function.

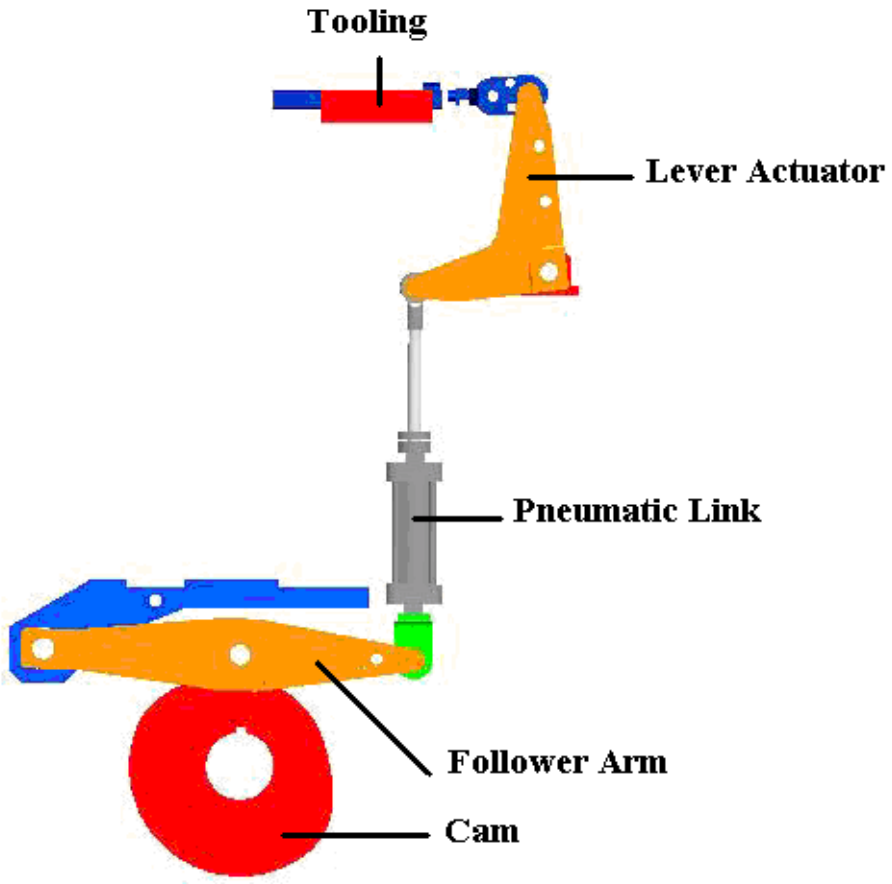

Figure 3 – Horizontal motion mechanism

The horizontal motion mechanism, shown in **Figure 3**, is composed of a cam follower system connected through a series of levers to a tooling assembly. The cam generates the motion with the output translated through the follower attached to the follower arm. For the tooling in-stroke, the follower arm descends and pulls the pneumatic link down. The lever actuator rotates and drives the tooling in. Once the tooling contacts the hard stop on the in-stroke, cam motion drives the linkage into over-travel where there is a dwell. Upon exiting from the dwell, the

follower arm rises, pulling the pneumatic link down, rotating the lever actuator and retracting the tooling from the nest.

The problem with the horizontal motion mechanism is the high velocity of the tooling as it hits the hard stop. Contact with the hard stop produces impact noise also resulting in higher forces due to rapid deceleration.

2.2 Vertical Motion Mechanism

The purpose of the vertical motion mechanism is to receive the component from the horizontal motion mechanism, and pushes it down into the product in a nest. **Figure 4** shows the mechanism.

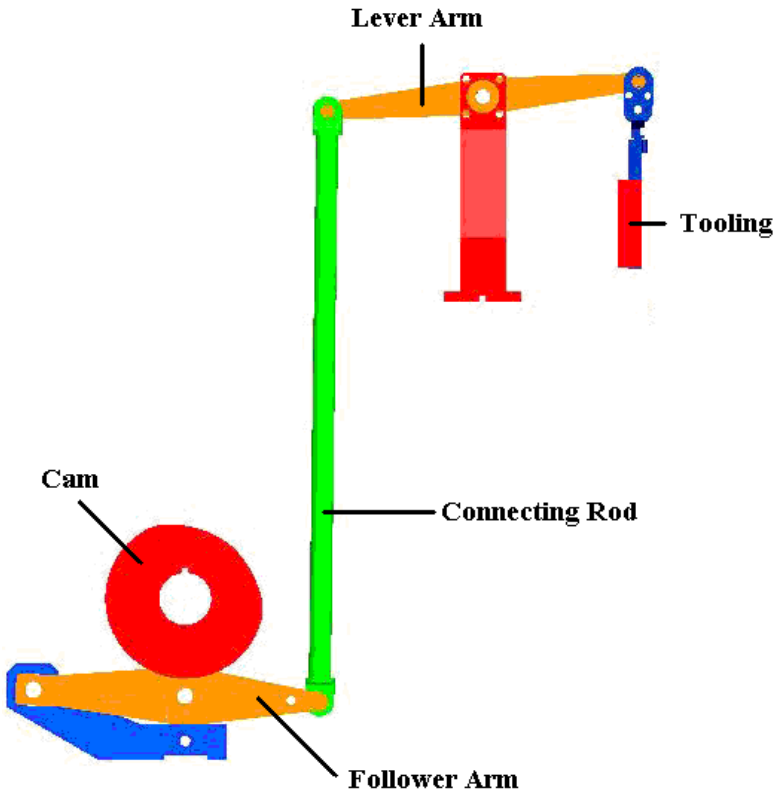

Figure 4 – Vertical motion mechanism

The vertical motion mechanism is composed of a cam follower system connected through a series of levers to a tooling assembly. The cam generates the motion with the output translated through the follower attached to the follower arm. For the tooling in-stroke, the follower arm ascends and pushes the connecting rod up. The lever arm will rotate and drive the tooling in, performing the lowering action. For the tooling out stroke, the follower arm descends and pulls the connecting rod down. The lever arm rotates and retracts the tooling from the nest. The tooling makes contact with the hard stop on the outstroke and cam drives the mechanism into over travel.

The issue with the vertical motion mechanism is the high velocity of the tooling as it hits the hard stop. Contact with the hard stop produces impact noise also resulting in higher forces due to rapid deceleration.

3. Modeling and Analysis

The first step towards a solution is the modeling and analysis of the systems, in this case, horizontal and vertical motion mechanisms. In order to predict their dynamic response, a basic model was developed that provided simulated data for the given system parameters. This simulated data was then compared to test data taken from accelerometers mounted strategically throughout the machine.

The simulated data of interest is the displacement, velocity, and acceleration. Specifically, the effect of linkage train's stiffness and effective mass at the follower must be known. This effective mass and system stiffness is a combination of the individual stiffnesses and masses of the included components and is necessary for the creation of a lumped mass model. This lumped mass model is required for a single degree of freedom system. The analysis is performed on a single degree of freedom model due to its simplicity and acceptable accuracy. Using *Dynacam*, vertical and horizontal mechanisms can be analyzed using their respective cams to determine the variation in output due to mass and stiffness for the given linkage train. Unfortunately, *Dynacam* does not take into account the hard stops present and therefore excludes any impact forces and vibrations due to the collision. Its value however lies in the prediction of simulated data immediately before impact, providing a predictable model for the system at the critical point, impact.

3.1 Creation of Simulated Models

To create the simulated dynamic model in *Dynacam* the system stiffness and spring preload were calculated. This way we could make the most accurate models of the system possible.

3.1.1 Finite Element Analysis

To properly estimate the stiffness of all major parts in the system, finite element analysis (FEA) must be used. FEA must be performed on the lever followers, the lever actuator, the lever arm, and the connecting rods. The forces on the connecting rods are only tensile and compressive, so their stiffness can be calculated using simple formulae rather than FEA. Parts such as the bearings and small brackets will have stiffness that is insignificant compared to that of the larger parts, so they can be excluded from the analysis. All finite analysis shown in this report was done in SolidWorks Cosmos.

The first part that finite element analysis was done on was the lever follower, as can be seen in **Figure 5**. This part is on both mechanism, and is affixed the same way, so only one finite element analysis needs to be done for this.

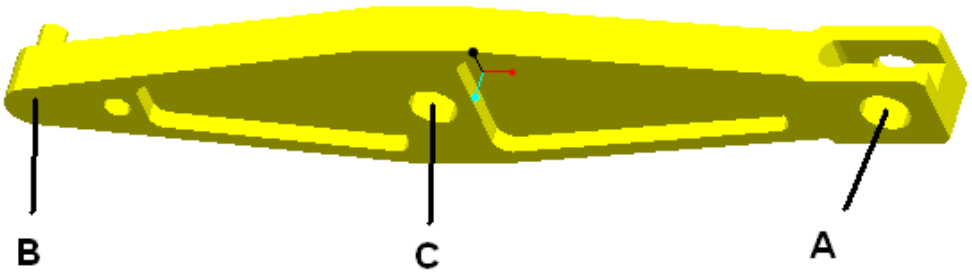

Figure 5 - Follower arm constraints

In the mechanism, this part rotates around point A, with the cam roller pushing in one direction on point C, and the connecting rod pushing in the opposite direction on point B. Both the cam roller and connecting rod bearings are connected on the same side of the follower arm.

The restraints added to the part were on points A and C, with a bearing load placed on point B. The restraint on point A was a hinge joint, which restricts translational motion in all directions, but allows rotational motion around the axis of the hole. This means that the pinhole will not move, but it will allow rotation in the direction it realistically can rotate. Point C needed to mimic the force of the cam roller pushing up on a pin going through that hole. To do this we created a pin coming out to the center point of the cam roller. A restraint was then placed on the face of the pin that restricted the motion in the vertical direction, without restricting rotation or motion in any of the other directions.

With the proper restraints in place, a force was placed on point B. To do this we added a pin to the part that extended the width of the bearing that attaches the follower arm to the connecting rod. This made it so the addition of a 500 Newton bearing load onto the pin was accurate to the actual mechanism. The FEA was then run, as can be seen in **Figure 6**. The stiffness was then from this by dividing the displacement of the endpin by the applied force.

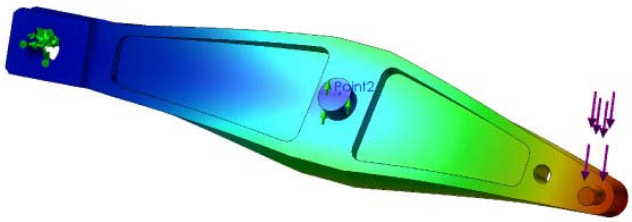

Figure 6 - FEA follower arm

Finite element analysis was next performed on the lever arm and lever actuator. The process for these parts was very similar to that of the follower arm. The primary difference is that the lever actuator and lever arm rotate around their center holes, which we reflected in the restraints. This meant that the hinge joint placed at the end of the follower arm is now placed in

the center hole (point A). Pins were then made, similarly to how the pin where the connecting rod attached to the follower arm, in the two remaining axis where the other restraint (point C) and the load (point B) are. The same bearing load of 500 Newtons was applied to pin C, and a restraint was made that allows rotation in all directions and translation in all but the direction the force is primarily acting in. With these restraints in place, we then ran the FEA on the lever actuator (**Figure 7**) and the lever arm, and in turn, the stiffness of the parts found.

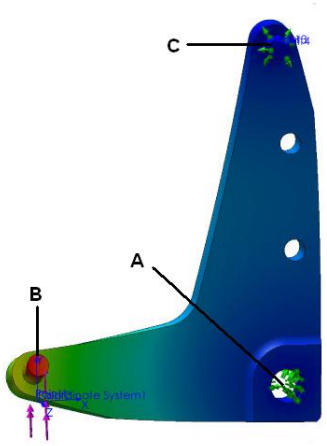

Figure 7 - FEA lever actuator

3.1.2 Effective System Mass

The idea behind making lumped model is to convert the distributed mass of each rotating link in the mechanism to a single point mass or 'lumped' mass at the point where it is connected to the adjacent link. The mass moment of inertia of the link at that point should be equal to that of the point mass. The total effective mass on the cam is then calculated by adding up effective

masses of each part according to their attachment with the adjacent link. This way it becomes easier to evaluate the mass effect of each part in the system.

This project focuses on two separate mechanisms of the machine, one with horizontal motion and the other with vertical. Each mechanism is operated by a separate cam, therefore each mechanism need to have its own lumped model. Below are the figures for lumped models for the two mechanisms. Distributed mass of each linkage is converted to one 'lumped' point mass or 'lollipop' at a position where it is easy for further evaluation, as seen in **Figure 8**.

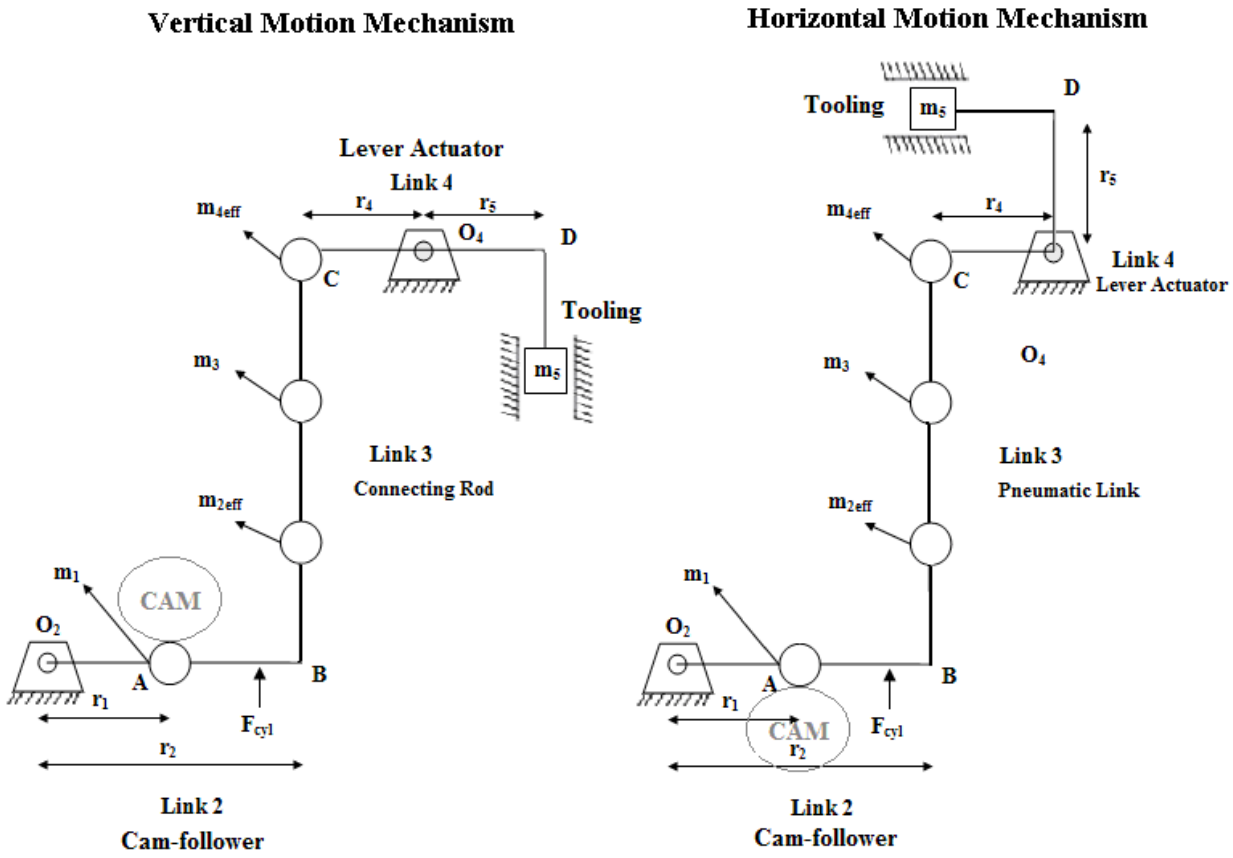

Figure 8 - Lumped model of vertical and horizontal mechanisms

The two mechanisms are similar, with different lever actuators. The connecting rod for the vertical tooling is a simple metal tube while in the horizontal tooling it is a pressurized pneumatic link. The geometry of a link does not affect the lumped mass model as long as its

mass moment of inertia at the pivot point is known. This can be easily found out with the Pro/Engineer CAD model after applying appropriate material properties.

Starting from the tooling mass, its effective mass at point C can be calculated by multiplying it by the ratio squared of the distances about the pivot point of the lever actuator. This can be represented by *Equation* 3.

$$EF_C = (\frac{r_5}{r_4})^2 \times m_t \quad \textbf{(3)}$$

The effective mass of the lever actuator at point C is then calculated by dividing the moment of inertia (about pivot point O_4) by square of the distance between pivot and point C (r_4). All the masses are then converted down to point B, which is the end of the cam-follower. Since the pushrods are in line with point B, their effective masses at that point will be their actual masses. Mass for the pneumatic link was determined by simply weighing it on a precise lab scale. Effective masses of tooling and lever actuator are also in line with connecting rod above point B, therefore they will have same effect as at point C. The total effective mass of the overall system at point B will be the sum of the following:

1. Effective mass of Tooling at point C (m_{5C})
2. Effective mass of Lever Actuator at point C (m_{4eff})
3. Actual mass of the connecting rod (m_3)
4. Effective mass of Cam-follower converted to point mass at B (m_{2eff})

The sum of the above masses is then converted back to the roller follower by dividing it by the ratio squared of the distances between pivot O_2 to point C (r_2) and pivot O_2 to roller-follower (r_1). The final step was to add the mass of the roller-follower to get the overall effective

mass of the whole mechanism on the cam. All of these calculations were carried out in a MathCAD model that can be found in **Appendix C** and **Appendix D**. The effective mass on cam for vertical tooling turned out to be 8.35 kg and for horizontal tooling 13.89 kg.

3.1.3 Effective System Stiffness

In addition to the effective mass, vibrations in a mechanism are also dependent on another parameter of the lumped model, the effective system stiffness. All links undergo deflection as force is applied, and they tend to vibrate as the magnitude of the applied force changes rapidly. In this case, low stiffness of the system might be the cause of vibrations. Therefore, the effective stiffness of the system needs to be calculated for further analysis in *Dynacam* model.

The system stiffness is calculated in a similar way as the effective mass. First, the stiffness of each part in the system is determined and then the values are summed according to the position and link ratios. However, finding out the spring rate of a part is not as simple as finding its mass. For complex geometry and shape like that of lever actuators and cam-follower, it is quite impractical to determine stiffness with simple calculations by hand and would be inaccurate. The most reliable and precise method of finding stiffness is through Finite Element Analysis (FEA) model of the part. We used the FEA package of SolidWorks to find out stiffnesses for Bell-Crank, Lever Actuator and Cam-follower. While doing the FEA forces were carefully placed in the right position and direction to get correct stiffness.

For the pushrods, it was easier to determine the stiffness of the connecting rod, in vertical tooling mechanism, as it is mainly a long hollow metal tube than of that of air-cylinder of horizontal tooling. For the connecting rod, its cross-sectional area was multiplied by elastic modulus of the material, dividing the result by length of connecting rod to get stiffness. The

pneumatic link in reality has two spring rates, one in extension and one in compression. The compression spring rate is determined by the calculation of stiffness using the piston rod. The extension spring rate was measured using a linear variable differential transformer, and will be discussed in a later section. The calculations for stiffnesses of the connecting rod and the pneumatic link in compression can be found in **Appendix F.** **Figure 9** shows the diagram of the lumped mass model with stiffness *k* of each part.

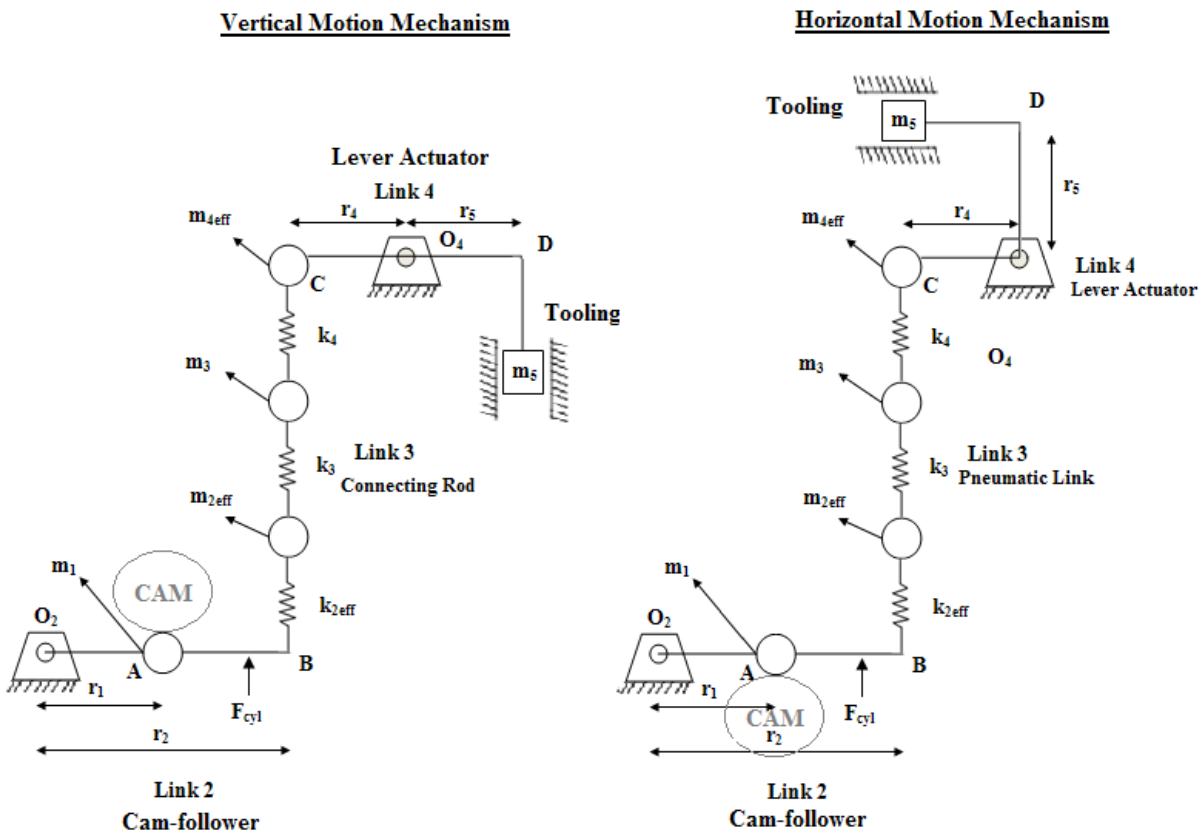

Figure 9 - Lumped mass model with effective stiffnesses

We apply the same technique as for the effective mass to find the effective spring rate on the cam i.e. by calculating the effective spring rate at point B and then transferring it back to the roller-follower. The FEA for the lever actuators was done with the whole link as one part (and not dividing it about the pivot). Therefore, their spring rate could be added on only one side of

the link (k_4), which is over link 3 in our cases for both mechanisms (see Figure 9). The same method applies on the cam-follower and its stiffness (k_{2eff}) is assumed to be at point B.

All the stiffnesses are in line over point B for both mechanisms. They were added by evaluating the reciprocal of the sum of reciprocals of the stiffnesses. This can be represented by *Equation 4*.

$$k_B := \frac{1}{\frac{1}{k_2} + \frac{1}{k_3} + \frac{1}{k_4}} \tag{4}$$

Equation 4 gives the effective system stiffness at point B. This was transferred back to roller-follower to find out the total effective stiffness of the mechanism on the cam, done by multiplying it by the ratio squared of the distances between pivot O_2 and point B (r2) and pivot O_2 and roller-follower (r1). Effective stiffness for vertical mechanism is 5.80e06 N/m and horizontal mechanism is 9.52e06 N/m.

Values for the effective mass and effective spring rate for both mechanisms are inserted in the *Dynacam* model for further vibrational analysis. Effective masses and spring rates for individual parts can be summarized in **Table 1**.

Table 1 - Spring rates and effective masses of individual links

Vertical Tooling Mechanism

		A		B		C	
						Stiffness	
		Weight/ lb	Mass/ kg	W_eff/ lb	m_eff/ kg	lb/in	N/m
M1	Roller Follower	0.33	0.15	0.33	0.15		
Link 2	Lever, CAM Follower	1.07	0.48	3.79	1.72	32,354	5.67E+06
Link 3	Conrod	1.45	0.66	5.16	2.34	14,867	2.60E+06
Link 4	Lever, Actuator	0.95	0.43	3.37	1.53	13,934	2.44E+06
M5	Tooling	1.62	0.74	5.77	2.62		
	Effective values on CAM			**18.41**	**8.35**	**33,125**	**5.80E+06**

Horizontal Tooling Mechanism

		A		B		C	
						Stiffness	
		Weight/ lb	Mass/ kg	W_eff/ lb	m_eff/ kg	lb/in	N/m
M1	Roller Follower	0.33	0.15	0.33	0.15		
Link 2	Lever, CAM Follower	**1.07**	**0.48**	**3.79**	**1.72**	32,354	5.67E+06
Link 3	Pneumatic Link (Air Cylinder)	2.45	1.11	8.71	3.95	278,781	4.88E+07
Link 4	Lever, Actuator (Bell-Crank)	**1.64**	**0.74**	**5.82**	**2.64**	152,841	2.68E+07
M5	Tooling	1.89	0.86	11.97	5.43		
	Effective values on CAM			**30.62**	**13.89**	**54,369**	**9.52E+06**

Column A in the above tables indicates actual mass of each link with column B indicating its contribution in the effective mass of the system. It is quite clear that the tooling is the highest contributor to effective mass of the system, although its actual mass is very low in both mechanisms. This is due to the link ratio that amplifies mass affect on the cams. It can be observed that amplification due to link ratios is quite significant in increasing the effective mass on the cam.

Column C indicates spring rates of individual parts determined through FEA or simple calculation. We can see that lever actuators are the weakest links in mechanism and cam-followers are the stiffest.

3.1.4 Air Spring Preload

For an accurate dynamic analysis of the system, the spring preload on the cam follower arm was determined. Even though both systems use the same air spring, the systems are not identical so the calculations were performed twice. This was due to the vertical motion cam using the air spring to push up on the cam follower (**Figure 10**) and the horizontal motion cam

uses the air spring to pull the cam follower down on the cam (**Figure 11**). This means that the air springs act in different directions depending on which part they are on. The calculations for these preloads are in **Appendix E**.

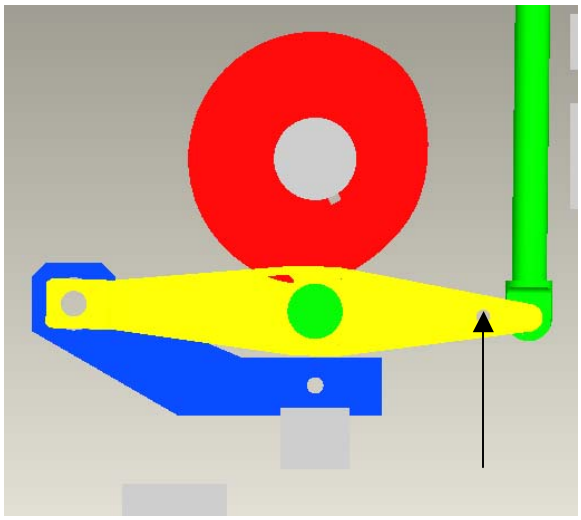

Figure 10 - Vertical air spring location

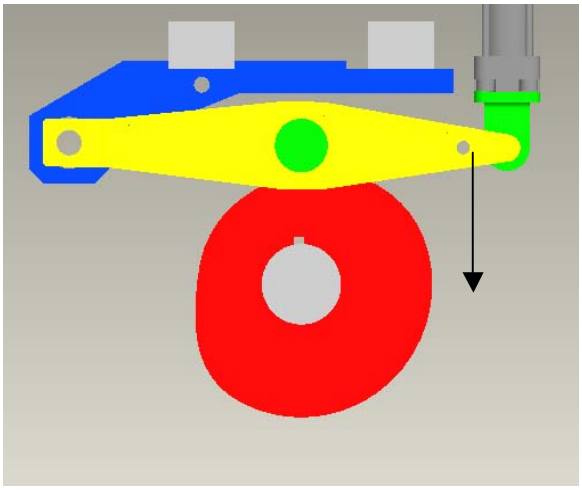

Figure 11 - Horizontal air spring location

3.1.5 *Dynacam* Model

Before we can have a full understanding of the motion of the current mechanisms, a computer model of the system must be analyzed. The CAD drawings of the cam were able to show us where features such as the rise, fall, and dwells were located, but they could not show us the actual function used to create the rise and falls. The original cams were created in the

program *Dynacam*, so rather than trying to recreate the cams using the program; the original files of the cams were used for the analysis.

Using *Dynacam,* many aspects of the original horizontal motion mechanism could be ascertained. The rise and fall were split with a dwell in the middle of them, so two separate functions were used to create these motions. The original cam design used a 3-4-5 polynomial function, which immediately told us there was room for improvement in the cam. Simply changing it to a higher order polynomial or a B-spline function would likely decrease peak accelerations and vibrations. The model also showed us that there were significant vibrations in the system.

We performed analysis of the original vertical motion mechanism in a similar fashion to the horizontal mechanism. Due to the cam not needing a dwell at both ends of its motion, the cam's design had the rise and fall in a single motion. This original motion was done using a B-spline function with even knots, which is a more advanced motion than the 3-4-5 polynomial used in the horizontal motion mechanism, and is made to minimize accelerations and jerk. This indicates to us that any improvements made in decreasing the velocity upon impact would also likely increase the peak acceleration and jerk in the system.

The data acquired from *Dynacam* on the old cams was used to make comparisons between the original cams and the new cam design. From this data the peak velocity, acceleration, and jerk were ascertained. We also used this data to calculate the velocity at impact, as described in the cam redesign section (Sections 4.1 and 4.2).

3.2 Horizontal Motion Mechanism

The base component of the horizontal motion mechanism is the cam. Its rotation generates linkage motion, and its profile determines the displacement, velocity, and acceleration

of the tooling throughout the entire stroke. For this reason, it makes sense to model the original cam in *Dynacam* to determine the theoretical characteristics of the cam. This data can later be verified using accelerometers to verify the theoretical model.

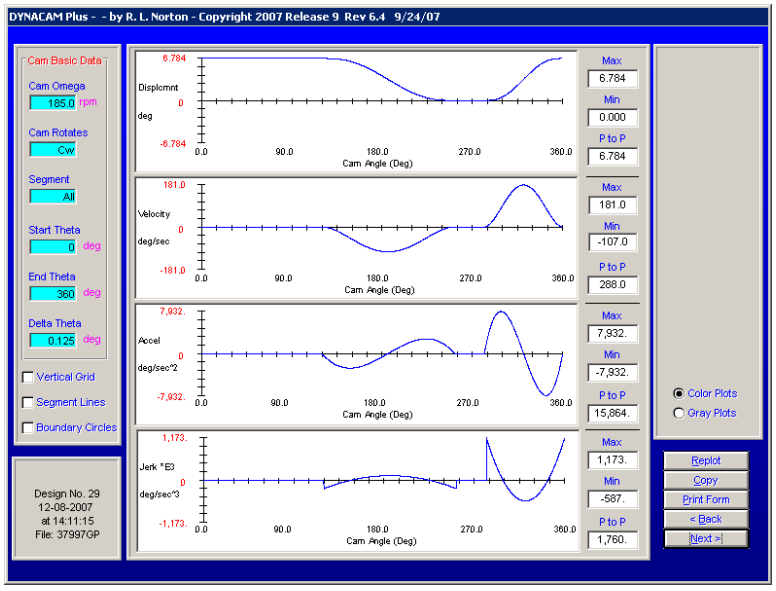

Figure 12 – Original horizontal motion cam SVAJ

Figure 12 shows the displacement, velocity, acceleration, and jerk curves for the original cam that is present on the machine. These curves and values are important because they are necessary to generate the dynamic model of the system.

The dynamic model is the combination of the cam profile, the effective system stiffness, and the effective system mass, all modeled as a single degree of freedom system. **Figure 13** shows the horizontal motion mechanism as a system, with the effective masses modeled as point masses and the stiffnesses of each link present.

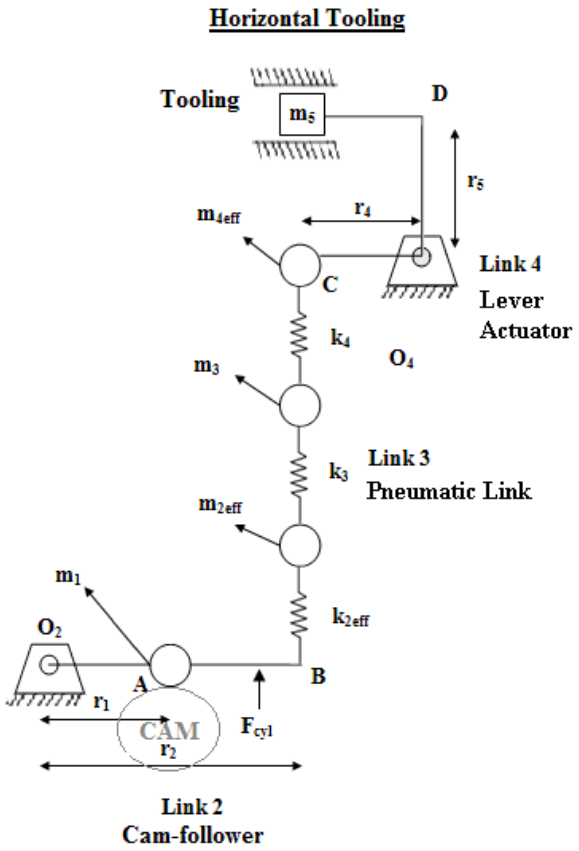

Figure 13 – Horizontal motion mechanism lumped mass model

The circular symbols or 'lollipops' in the figure represent the point masses of respective links with equivalent mass moment of inertia as of their original distributed mass at that point. The zigzag symbols represent effective spring rates of each part. Effective mass and effective spring rate of the overall system are calculated separately.

First, effective masses of tooling and lever actuator are transferred onto pin-connection between lever actuator and air-cylinder, labeled as m_{4eff} in the figure. Effective mass of the cam-follower arm is then calculated at the pin-connection between pneumatic link and the cam-follower arm, labeled as m_{2eff}. All masses now are in line with the pneumatic link, or link three. They can be added together to find the effective mass of the whole system at point B. The aggregate is then transferred back onto the roller-follower to find the effective mass of the whole

mechanism on the cam, by multiplying it by the square of the ratio (r_2/r_1). Table 2 shows the values for individual effective masses.

Table 2 – Horizontal mechanism effective mass

Link Mass	Effective Mass (kg)
m_{4eff}	2.64
m_3	3.95
m_{2eff}	1.72
Overall	13.89

We calculated the spring rate of the overall system in the same way. k_4 represents the effective spring rate of lever actuator on the pneumatic link. Notice that the tooling spring rate is not taken into account as it is a free moving slider attached to one arm of the lever actuator and its effective spring rate on the entire system is negligible. k_3 is the pneumatic link's spring rate and k_{2eff} is the effective spring rate of the cam-follower on the pneumatic link, or link3. Upon completing all the calculations of the individual effective spring rates, the reciprocals were added to create a single effective spring rate for the system. We then transferred the result back onto the cam by multiplying it by square of the ratio r2/r1. **Table 3** shows the values of the respective spring rates.

Table 3 - Horizontal mechanism effective stiffness

Link Mass	Spring Rate (N/m)
k_4	2.68e07
k_3	4.88e07
k_{2eff}	5.67e06
Overall	9.52e06

Please refer to **Appendix D** for detailed calculations regarding the lumped mass model for the horizontal motion mechanism.

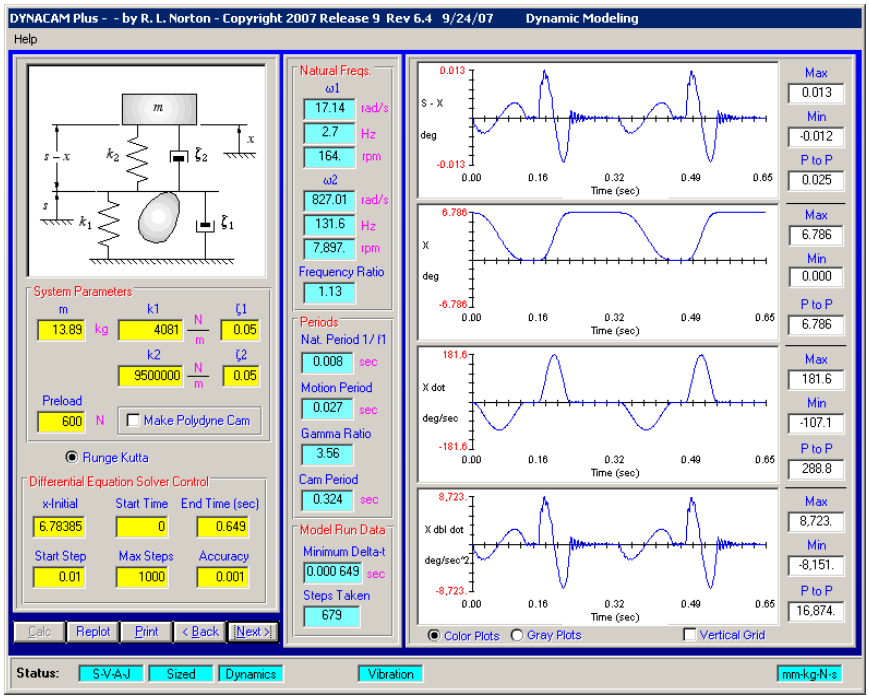

Figure 14 - Horizontal motion mechanism dynamic vibrations

Figure 14 shows the dynamic vibrations for the horizontal motion mechanism once the proper system parameters were plugged into *Dynacam*.

3.3 Vertical Motion Mechanism

The vertical motion mechanism runs the same way as the horizontal motion mechanism. By using *Dynacam*, we generated **Figure 15**, which shows the SVAJ for the vertical motion mechanism. **Figure 16** shows the vertical motion mechanism as a system, with the effective masses modeled as point masses and the stiffnesses of each link present.

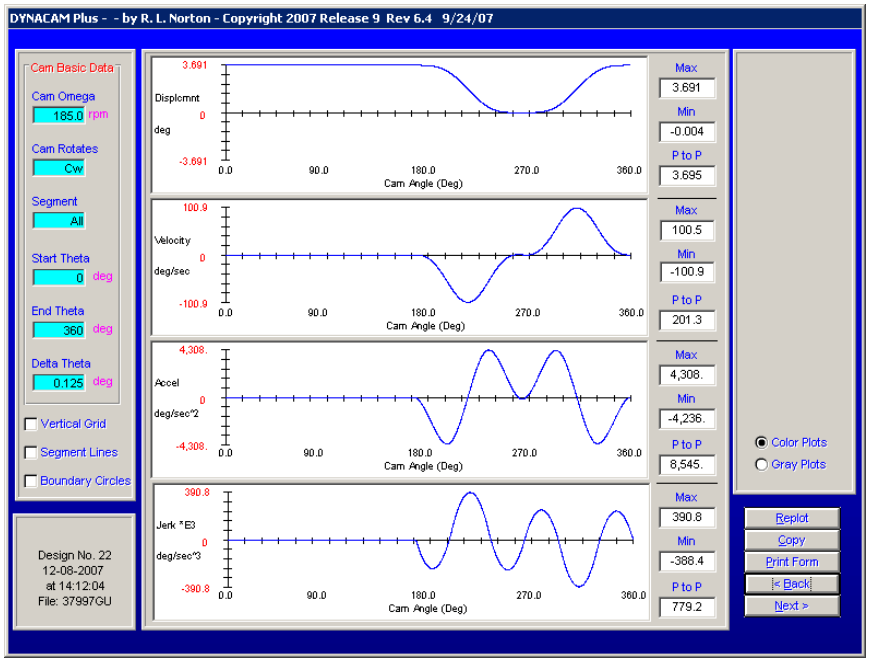

Figure 15 - Vertical motion mechanism SVAJ

Vertical Tooling

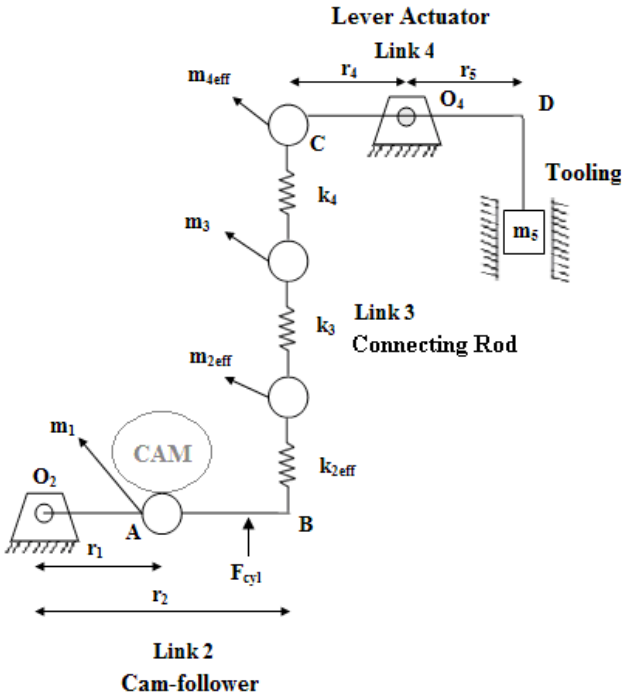

Figure 16 - Vertical motion mechanism system

Notice that lumped model for the vertical mechanism is very similar to the lumped model of the horizontal mechanism. There is difference in geometry of the lever actuators but their functions are the same, both of them are rockers. For the horizontal mechanism, the lever actuator is L-shaped and for the vertical mechanism, it is a straight horizontal beam. There is similar method to transfer effective mass for the tooling and lever actuators in line with pushrods (link 3) and same procedure is carried out in estimating the effective mass and the spring rate of the whole system for both mechanisms. Effective masses of the individual parts for vertical mechanism are listed in **Table 4**.

Table 4 - Vertical motion mechanism effective mass

Link Mass	Eff_Mass/ (kg)
m_{4eff}	1.53
m_3	2.34
m_{2eff}	1.72
Overall	8.35

The effective spring rates for individual parts are as follows in **Table 5**.

Table 5 - Vertical motion mechanism effective stiffness

Link Mass	Spring Rate (N/m)
k_4	2.44e06
k_3	2.60e06
k_{2eff}	5.67e06
Overall	5.80e06

Please refer to **Appendix C** for detailed calculations regarding the lumped mass model for the horizontal motion mechanism.

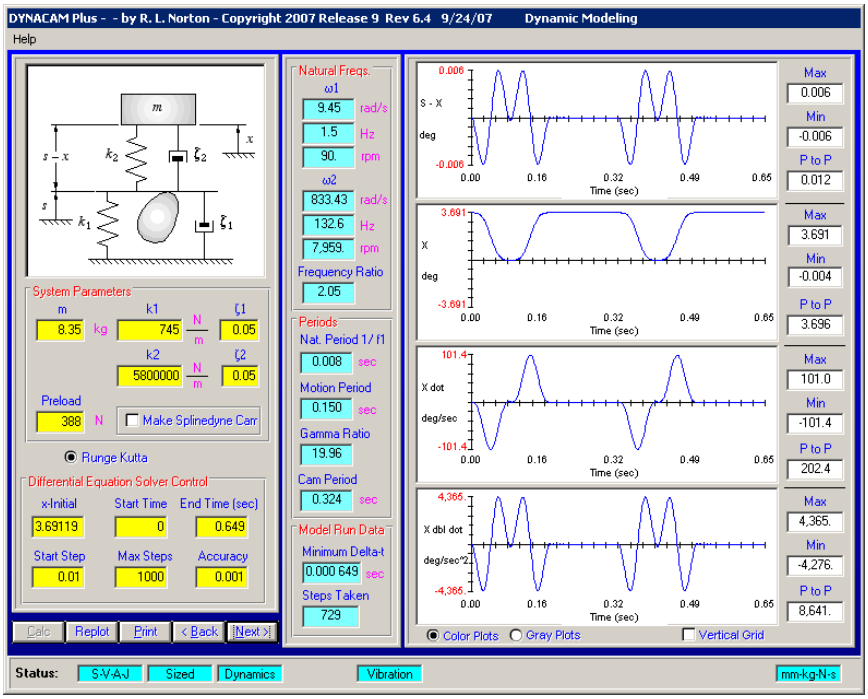

Figure 17 - Vertical motion mechanism dynamic vibrations

Figure 17 shows the dynamic vibrations for the horizontal motion mechanism once the proper system parameters were plugged into *Dynacam*.

3.4 Verification of Theoretical Models

Having generated theoretical data through various procedures, we performed tests to verify that the theoretical data could be used as a basis of comparison. To do so, accelerometers, pressure transducers, a linear variable differential transformer (LVDT), a signal hammer and high-speed video was used to perform the necessary tests. We then compared the collected data to the theoretical to check for correlation.

3.4.1 Accelerometers

Accelerometers were introduced to specific points on the linkage trains to measure the acceleration experienced throughout the cycle. Using a dynamic signal analyzer, the input of the accelerometer, given in volts, was multiplied by the given calibration factor of the accelerometer which would return acceleration readings in g. An external trigger was used to synchronize the beginning of the acceleration cycle with the transfer of parts on the conveyor belt. Once this phased acceleration data was collected for the horizontal and vertical motion mechanisms, it was compared to the dynamic accelerations generated in *Dynacam*.

For the vertical motion mechanism, the accelerometers were placed on the end effector, shown as point A, the follower arm, shown as point B, and the lever arm, shown at point C. **Figure 18** shows the mechanism with the corresponding accelerometer placements.

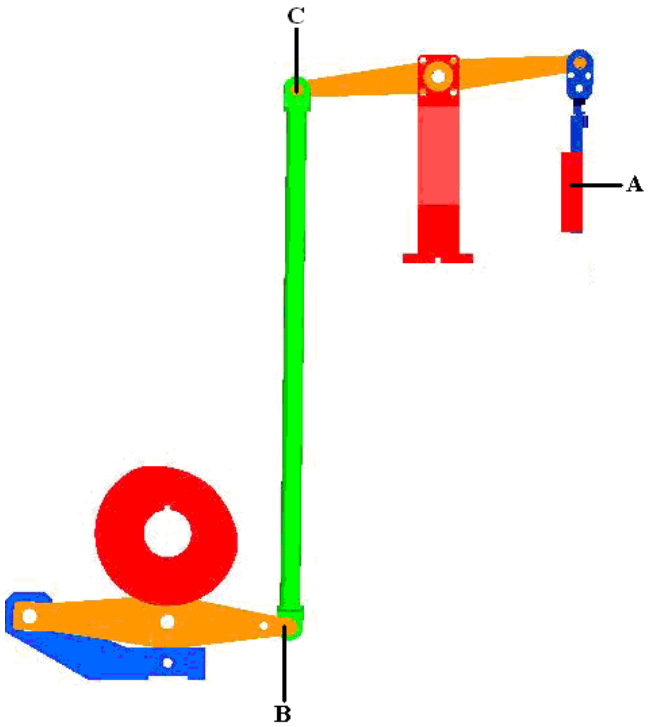

Figure 18 – Vertical motion mechanism accelerometer placement

These positions provide specific data. The accelerometer placement at A shows the magnitude of the impact with the hard stop. The hard stop collision data at the end effector should provide accurate results, although it is subject to the influence the over-travel spring and its affects.

The accelerometers located at B and C in theory provides similar data. The intent behind their placement in the system is to record the acceleration due to the profile of the cam with no input due to the hard stop. Comparison of the two provides insight into how the acceleration function transmits across the linkage train.

All measured accelerations in the system are subject to both orientational and magnitudinal scaling. The accelerometer has a predetermined coordinate system that defines the direction of positive acceleration. Depending on the orientation of the accelerometer within the system, the data might require multiplication by negative one to account for this. The acceleration data taken from the horizontal motion mechanism is subject to the link ratio's that govern motion through the lever actuator. Since the ratio of the input to the output is not equal to one to one, the multiplication of the acceleration by the ratio to account for translation away from the cam follower is necessary. In addition to this, a common unit must be chosen for the two as the output of *Dynacam* is in deg/sec^2 while the measured data is in g force. Please reference **Appendix A** and **Appendix B** for calculations regarding the link ratios and conversions.

Figure 19, **Figure 20**, and **Figure 21** show the acceleration data gathered from the original cam at the specified points. All graphs show a single revolution of the cam versus the acceleration measured. A moving average has been applied to the curve to cancel out the noise and give a true indication of the data path over the cycle.

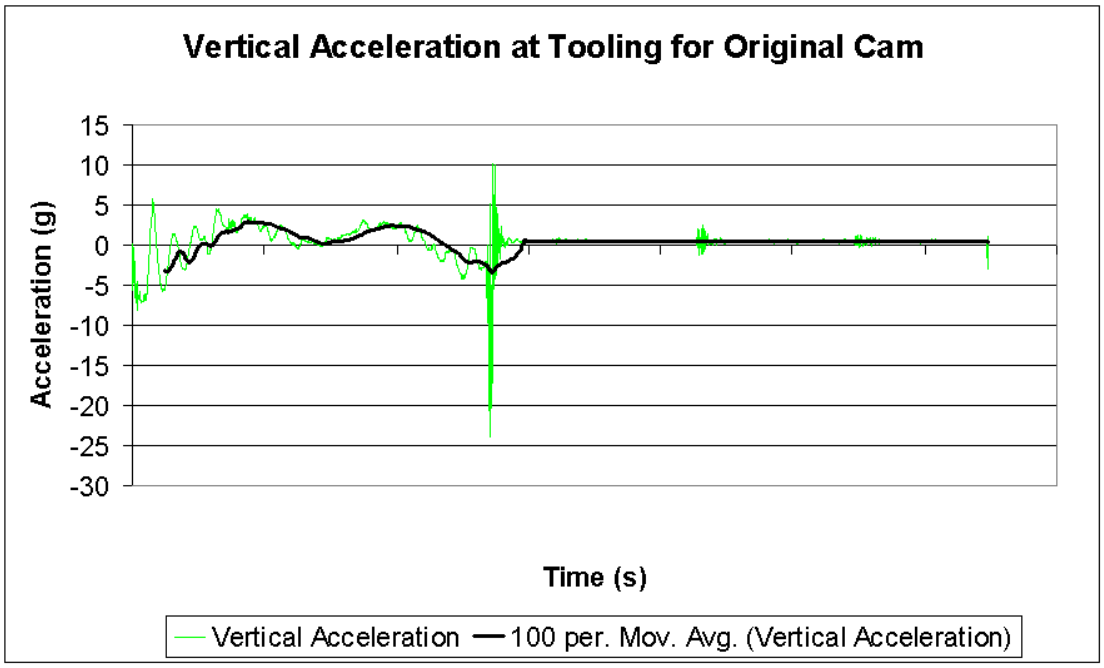

Figure 19 - Vertical mechanism acceleration for the original cam at point A

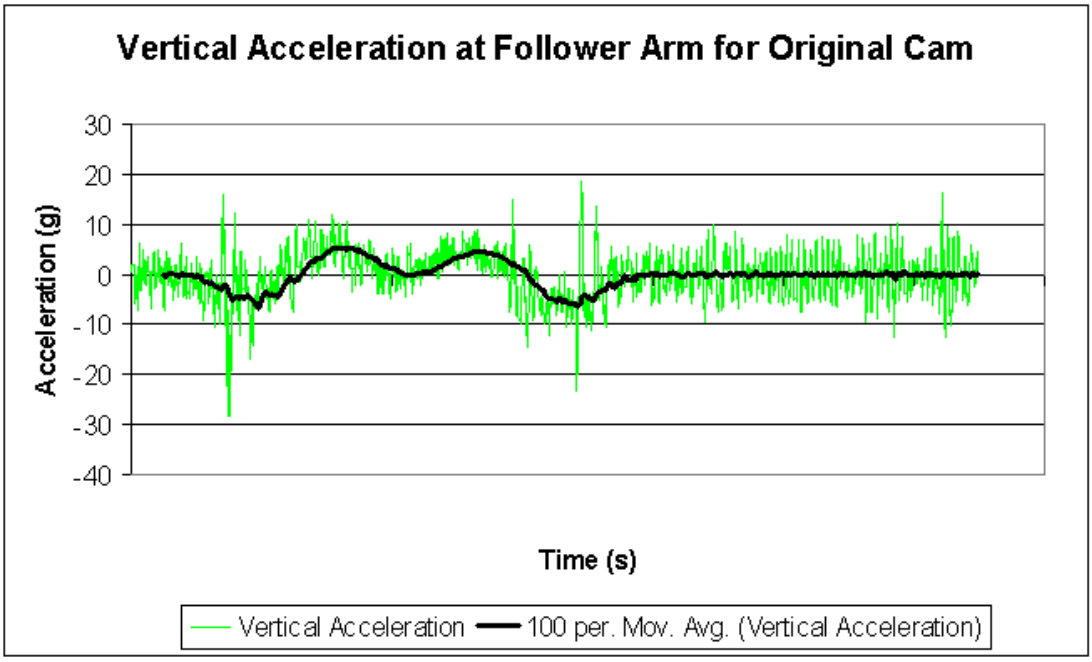

Figure 20 – Vertical mechanism acceleration for original cam at point B

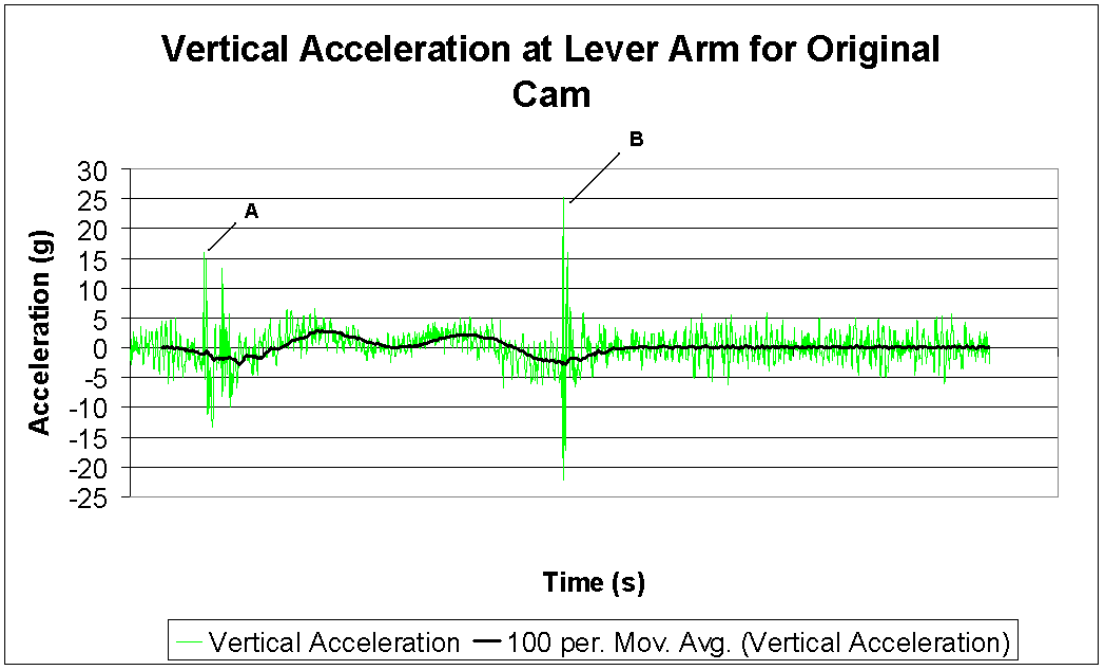

Figure 21 – Vertical mechanism acceleration for original cam at point C

The first comparison that we did was of the theoretical acceleration data for the original cam to the measured data from the machine. As previously mentioned, the data from the follower arm was chosen due to its location and ability to provide the most accurate acceleration data. **Figure 22** shows a graph of this comparison.

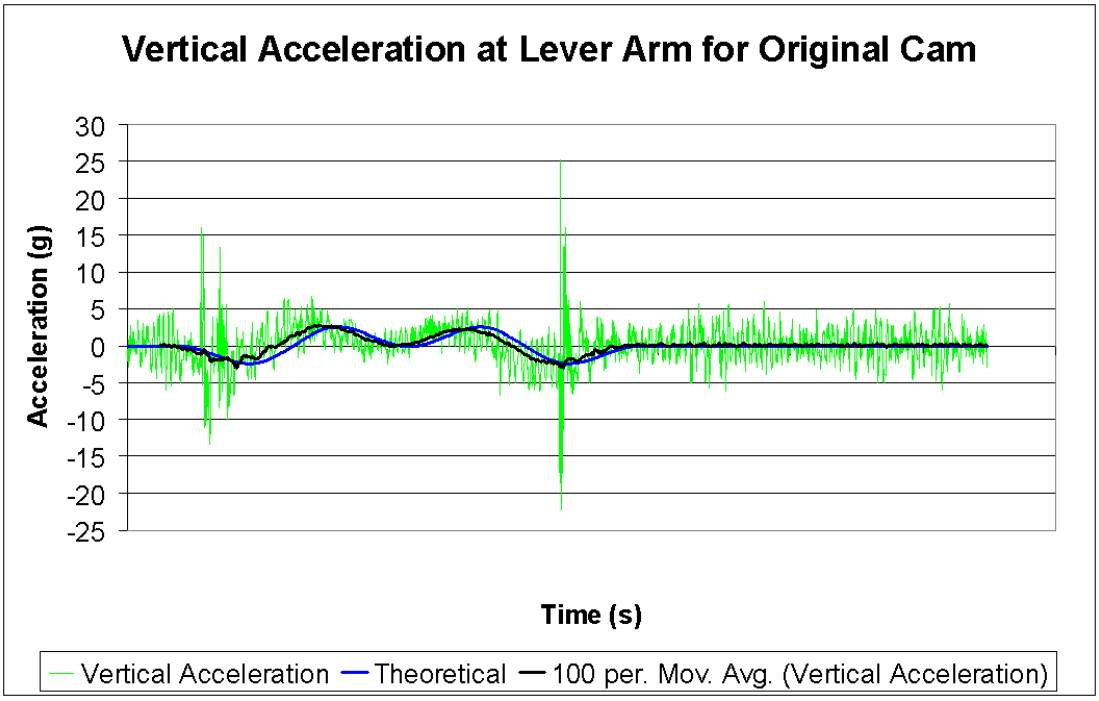

Figure 22 - Theoretical vs. measured data correlation for original vertical cam

Note that the comparison performed is between the theoretical data and the moving average. The curves are similar with the only slight discrepancy being their phasing. This is the result of manual data comparison, but it is clear that the two feature similar timing as their peaks occur at the same interval. A moving average requires a certain amount of data points before it can begin averaging, which reflected the shift in the moving average. The magnitude of the data is close and affects the moving average and the influence of the peaks. It is clear from the graph that the experimental data closely models the theoretical data, allowing the use of the original cam data for the vertical motion mechanism used for improvement analysis.

The impact at A, shown in **Figure 21**, corresponds to the tooling leaving the hard stop while the impact at B corresponds to the tooling hitting the hard stop. Each accelerometer position indicates the collision with the hard stop, shown as spikes in the acceleration. The data taken at A however replaces the spike at A with wild oscillations and does not show the

prominent peak that the other data sets show. The maximum accelerations are present at point C, and were chosen as the curve to analyze for this reason. The spike at A is approximately equal to 16 g's while the spike at B is approximately equal to 24 g's of acceleration. This data provides us with a basis of comparison for future data as well as a starting point for improvements.

For the horizontal motion mechanism, accelerometer placement was located at the end effector, shown as point A, the follower arm, shown as point B, and the lever actuator, shown at point C. **Figure 23** shows the horizontal motion mechanism with the corresponding accelerometer placements.

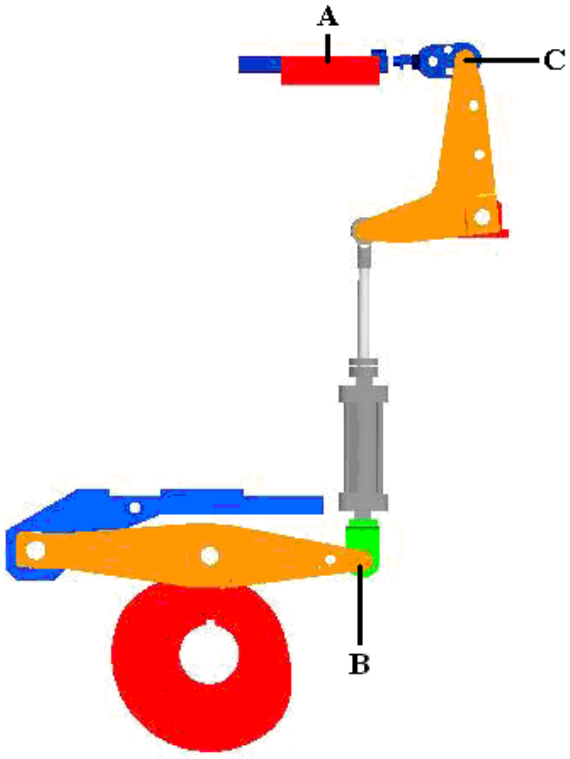

Figure 23 - Horizontal mechanism accelerometer placement

These positions provide specific data. The accelerometer placement at A determined the magnitude of the impact with the hard stop. The hard stop collision data at the end effector

ensures accuracy, unlike the other two locations subject to the dissipation of energy through the over travel spring and links.

The accelerometers located at B and C in theory provides similar data. The intent behind their placement in the system is to record the acceleration due to the profile of the cam with no input due to the hard stop. Comparison of the two provides insight into how the acceleration function transmits across the linkage train.

Figure 24, Figure 25, and **Figure 26** show the acceleration data gathered from the original cam at the specified points. All graphs show a single revolution of the cam versus the g force measured. A moving average was applied to the curve to cancel out the noise and give a true indication of the data path over the cycle.

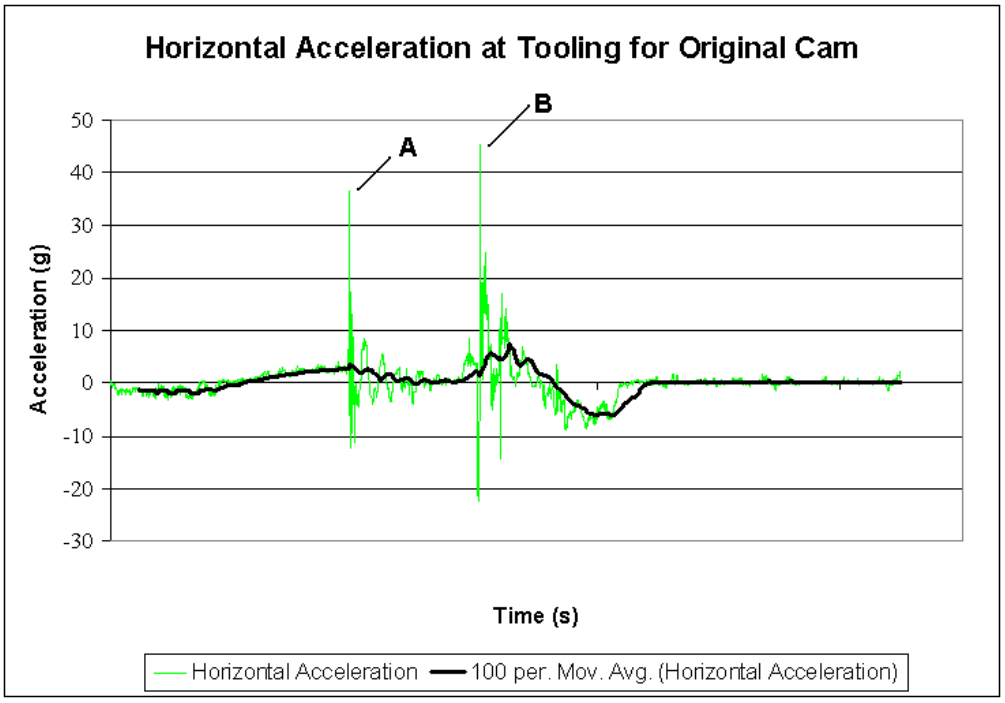

Figure 24 – Horizontal motion acceleration for original cam at point A

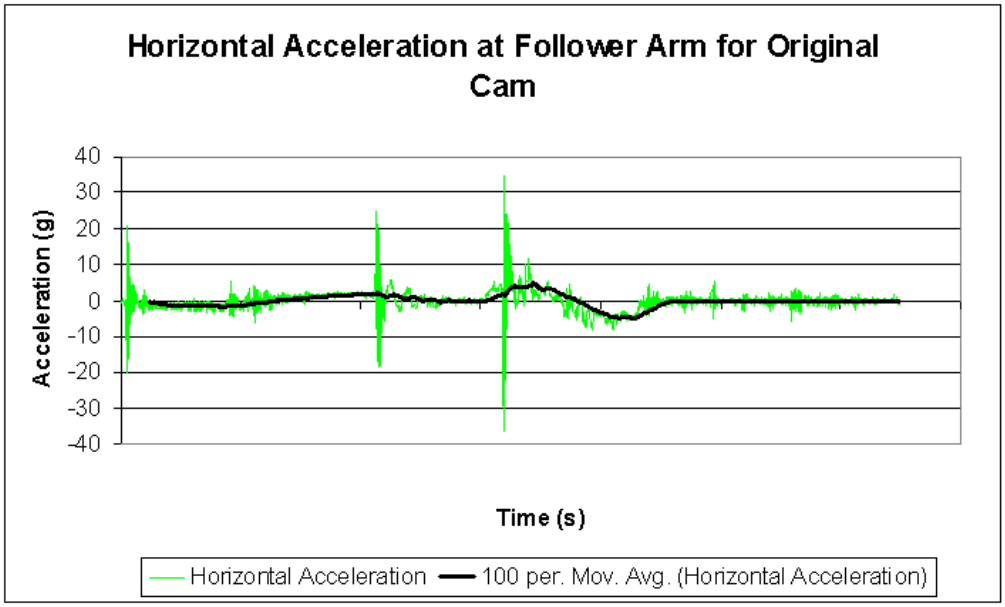

Figure 25 – Horizontal motion acceleration for original cam at point B

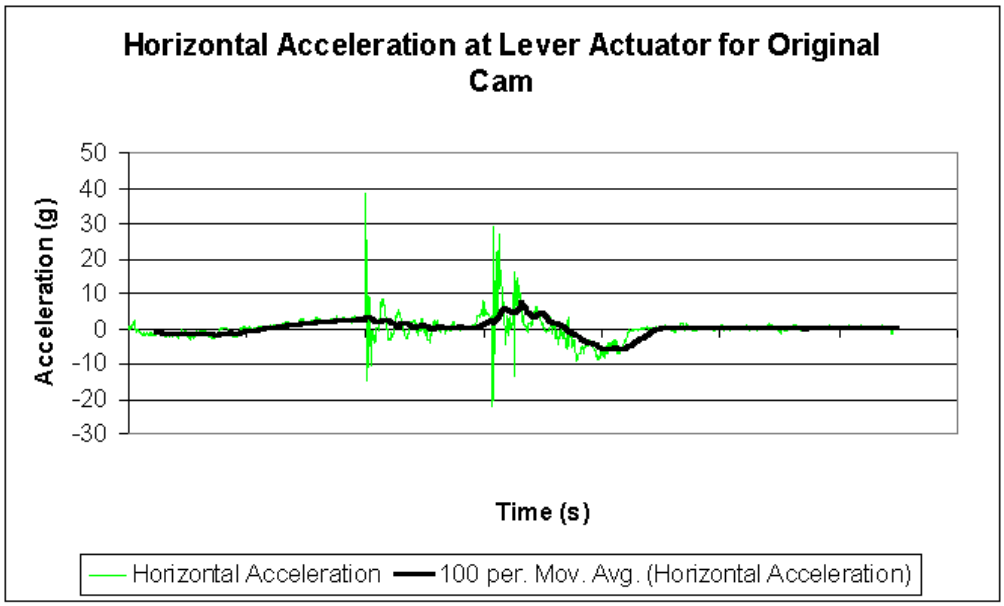

Figure 26 – Horizontal motion acceleration for original cam at point C

The first comparison that done was with the theoretical acceleration data for the original cam compared to the measured data from the machine. **Figure 27** shows a graph of this comparison. Data comparisons made were performed in the same way as with the vertical

motion cam. Since the mechanisms are virtually the same, we made no major changes to analysis procedures.

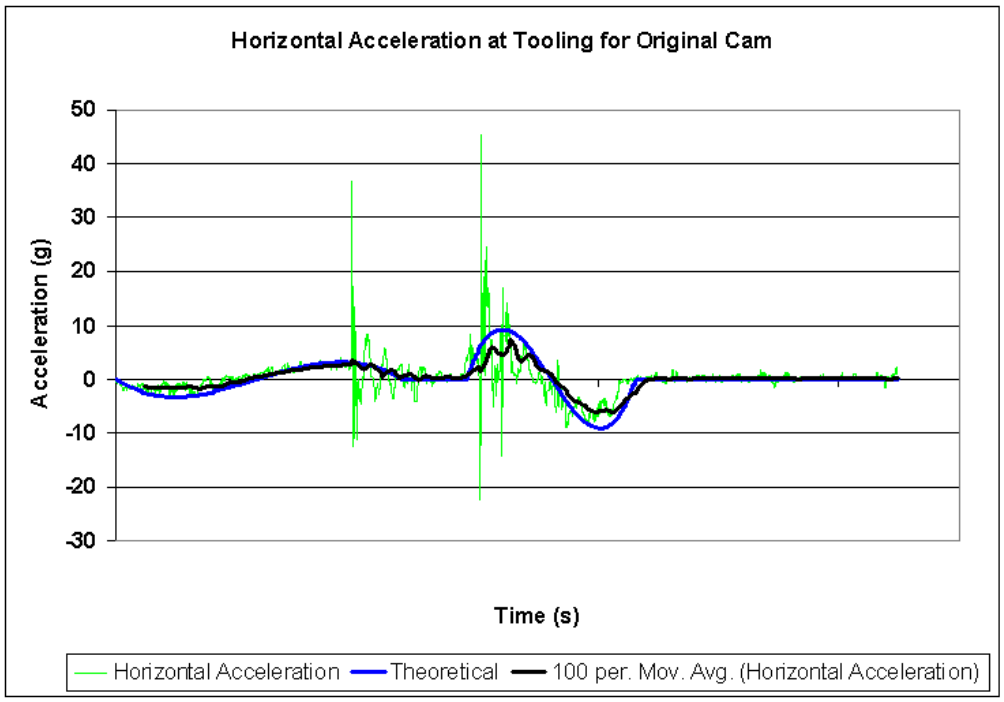

Figure 27 - Theoretical vs. measured data correlation for original horizontal motion cam

The impact at A, shown in **Figure 24**, corresponds to the tooling hitting the hard stop while the impact at B corresponds to the tooling leaving the hard stop. Each accelerometer position indicates the collision with the hard stop, shown as spikes in the acceleration. The spike at A is approximately equal to 36 g's while the spike at B is approximately equal to 45 g's of acceleration. This data provides us with a basis of comparison for future data as well as a starting point for improvements.

Note that we took the acceleration data from the respective machines on multiple occasions. The data shown in this section is purely for the verification of the theoretical models. Other acceleration data may be used in the following sections.

3.4.2 LVDT and Pressure Transducer

One potential problem in the horizontal mechanism was the use of a pneumatic link as a connecting rod. Using a linear variable differential transformer (LVDT) to measure the displacement of the pneumatic link, and a pressure sensor to measure the high side pressure, and comparing the displacement with the change in pressure, it was found that the link is rigid during operations. With a displacement of 0.8 thousandth of an inch and a pressure variation of 119 mpsi, the effective stiffness of the link is limited instead by the cylinder of the connecting rod. The setup for this experiment as well as the calculations can be found in **Appendix E** and **Appendix F**.

3.4.3 Hammer Tests

A metal object when struck by another object tends to vibrate at its natural frequency, as do the linkages in the mechanisms. Vibrations measured through accelerometers on various parts of the machine also include natural frequencies of the parts as well as noise from the surroundings whereas vibrations extrapolated from the *Dynacam* models only account for the driving frequency of the machine. To correlate the simulated and measured vibrations, it is important to make sure that noise and natural frequencies of the parts do not interfere with dynamic frequencies of the machine. Hammer tests are an experimental method to find natural frequencies.

Hammer tests are a simple method by which metal parts are lightly struck by means of an impulse hammer so that they vibrate at their natural frequencies and data is measured through accelerometer mounted on the parts. The hammer has a force transducer and a small tip fixed on the end. The small area of the tip makes sure there are little or no vibrations being transferred from the hammer into the part being tested. With the force transducer, it is assured that natural

frequencies are struck only once by the hammer, which means a there should be a single spike on the transducer data.

The setup is done so that the accelerometer is mounted on one end on the part being tested and the hammer hit is on the opposite end. It is important that hammer hit is done in the same axis as the accelerometer is fixed to get most of the natural frequencies.

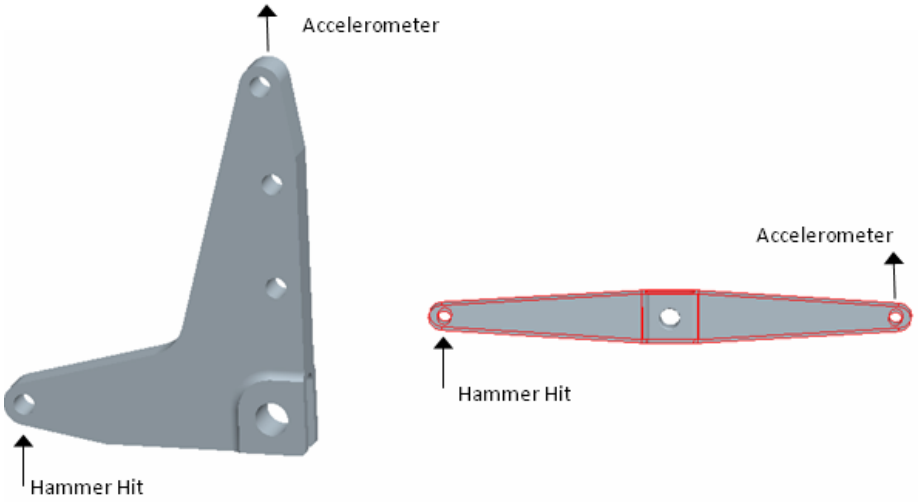

Figure 28 - Hammer hit and accelerometer positions on Lever Actuators

Vibrations are recorded with a dynamic signal analyzer that can capture up to 3.2 KHz of frequencies. Any frequencies higher than that are omitted and not required as they are above the driving frequency of the machine.

The analyzer also calculated Fast Fourier Transform (FFT) of the vibrations where it showed all mode shapes of natural frequency in the given range. The coherence, or legitimacy of our results, was generally greater than 95% meaning the data recorded is clean. Such high coherence was only possible with all machines shutdown in the plant so that there is no outside noise registered through the linkages.

Below is an example of Frequency Response Functions (FRFs) recorded for vertical tooling of the machine at 3.2 KHz bandwidth. The hammer hit was done with the aluminum tip

to pluck higher mode shapes of the part. Notice that the coherence is higher than 99%, indicating clean data. First mode shape is located around 200 Hz range whereas the second is located in 1600 Hz range. This can be seen in **Figure 29.**

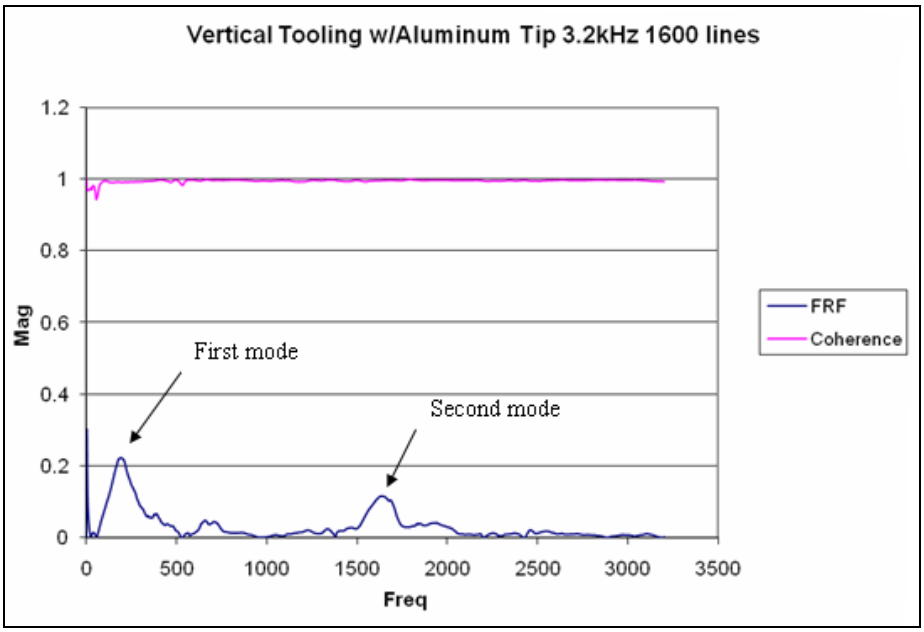

Figure 29 - FRF and coherence response with accelerometer mounted on vertical slider

Frequency range and resolution of the data capture device were carefully adjusted to get the most precise reading possible. The tip of the hammer was changed from plastic to aluminum wherever a higher mode shape was suspected. Generally, an average of five hammer hits was taken to assure the consistency of results.

The FRF's of all parts were carefully analyzed and it was found that all mode shapes were outside the range of driving frequency of our machine. This means natural frequencies do not interfere with correlation between simulated data of *Dynacam* and experimental data measured through accelerometers. All the FRF plots can be found in **Appendix H** of the report.

3.4.4 High Speed Video

It can often be difficult to be certain of what the tooling in a mechanism is actually doing, verses what it is designed and expected to do. One of the tools used to ascertain this information were three high-speed video captures of the tooling, taken before and after changes to the system were made. The video taken at a frame rate of 1000 frames per second slows the motion down by a factor of 40.

The first high speed video taken was of the tooling end-effectors. This gave a good view of how the parts of the mechanisms that handles the product moves in relation to each other. One thing that was immediately evident was that the horizontal motion mechanism started its motion before the vertical motion mechanism had finished its motion, with an overlap of 12 degrees of cam angle. The horizontal tooling did not cross the interference point of the vertical motion until approximately 36 degrees of cam angle into its motion, indicating significant clearance between the two toolings despite their motion phases overlapping a bit. This view also gave us an idea of how much visible vibration there was in the tooling, particularly at the end where there is no hard stop and low frequency vibrations can be expected. The video indicated that any vibrations were minimal and did not appear to affect the machine adversely.

Two more videos were taken, one for each of the mechanisms at the hard stop over-travel spring. The purpose of these videos was to see the amount of compression in the spring and the over-travel.

4. Selection and Redesign

After analysis of the motion of the current system was complete, we decided that a redesign of the cams driving the linkages could greatly reduce the sound output from impact. The strategy was to reduce the velocity of the tooling at the time when it strikes the hard stop, and then to accelerate the tooling again after it hits the hard stop to create the over-travel.

In order to reduce the velocity at the hard stop, we first had to determine the amount of over travel in the system. Due to tolerance stack-ups and slight variances in setup, each mechanism will have a different distance of over travel, so a range of over travel amounts taken into account in the design. Without this information, we would not know at what cam displacement to create the reduced velocity on the cam, and without a range of the point of impact, it is possible that the redesign could create worse velocities at the point of impact in some cases.

The range of values was calculated by taking manual measurements of the over travel on each system. This was done by manually setting the cam shaft to the positions indicated in the setup manual in which the tooling would be fully extended past the hard stop, and then taking manual measurements of each one using feeler gauges. After this was completed, these five measurements were used to create a range of the amount of over travel and a median over travel, which we used as our "target contact point." Due to it only being five measurements we also extended the outer limits of the over travel range by a small amount to error on the side of caution. Since the impact range is not critical to the proper operation of the machine, we did not need to introduce a safety factor.

With the range and target contact point calculated, we were able to begin creating the cams using *Dynacam*. Base data about the cams were taken from the *Dynacam* files of the original cams. This data is in **Table 6.**

Table 6 - Original cam specifications

Known Data to be Used in Design	**Horizontal Motion Cam**	**Vertical Motion Cam**
Revolutions per Minute	Proprietary	Proprietary
Starting Angle	271°	122°
Cam Rotation	Counter-clock-wise	Counter-clock-wise
Follower Arm Rotation	Clock-wise	Clock-wise
Follower Arm Pin Coordinates	x =175mm y =105mm	x =175mm y =-105 mm
Roller Radius	20 mm	20 mm
Follower Arm Radius	175 mm	175 mm
Prime Radius	97.97 mm	100.87mm

Where appropriate, we verified these dimensions using the design drawings of the system. The cams were then created using B-spline functions and dwells, the specifics of which will be explained in the subsequent sections for each cam due to their motions having different characteristics.

The goal in creating each cam was to reduce the velocity along the range of impact as much as possible, while minimizing other ill effects that may come along with the change in design. To accomplish this, boundary conditions were created at the cam angles in which the target contact point should occur when striking the hard stop, where it should reach the furthest point of its displacement, where it should leave the hard stop, and any other points critical to the machine's function. The cam angles used for the boundary conditions ensure that the cam will serve its function and not change the position of the tooling at the times critical to the machine's operation. Next, proper boundary conditions for position, velocity, acceleration, and jerk were

decided upon for each of these cam angles, where appropriate. The values of the cam angles and the boundary conditions varied depending on the cam function.

After these boundary conditions were introduced in *Dynacam*, iterations for the design of the b-spline function were created for each cam. We did this by a combination of changing the spline order, changing the position of the knots in the spline, and adjusting the boundary conditions to optimize the system. These iterations varied based on the individual designs, as explained in the following sections.

Once the iterations were completed, the best designs were compared against each other to assess the gains against the losses, and to decide which design best suits our needs, while at the same time optimizing the other characteristics of the system. Final adjustments were then made to the chosen design to optimize the final cams.

4.1 Horizontal Motion Cam Redesign

The horizontal motion mechanism moves the tooling in the horizontal direction, which is perpendicular to the displacement of the follower at the cam. This horizontal end effector has 4 phases of motion, which are controlled by the cam. First, the cam must dwell at its outermost displacement, for 120 degrees of its motion. This causes the end effector to be motionless in the retracted position while the vertical tooling goes through its motion. The original cam then goes into a fall for 132 degrees of motion in which the tooling moves from the retracted position, hits the hard stop, and goes through over-travel to its innermost position. It then dwells against the hard stop for 30 degrees while the vertical motion linkage picks up the product from the horizontal motion cam. The final phase of motion is a rise that covers the last 72 degrees of the cam motion, which returns the tooling to the outermost position. A graph of the cam motion, with cam zero starting at the fall, are shown in **Figure 30**.

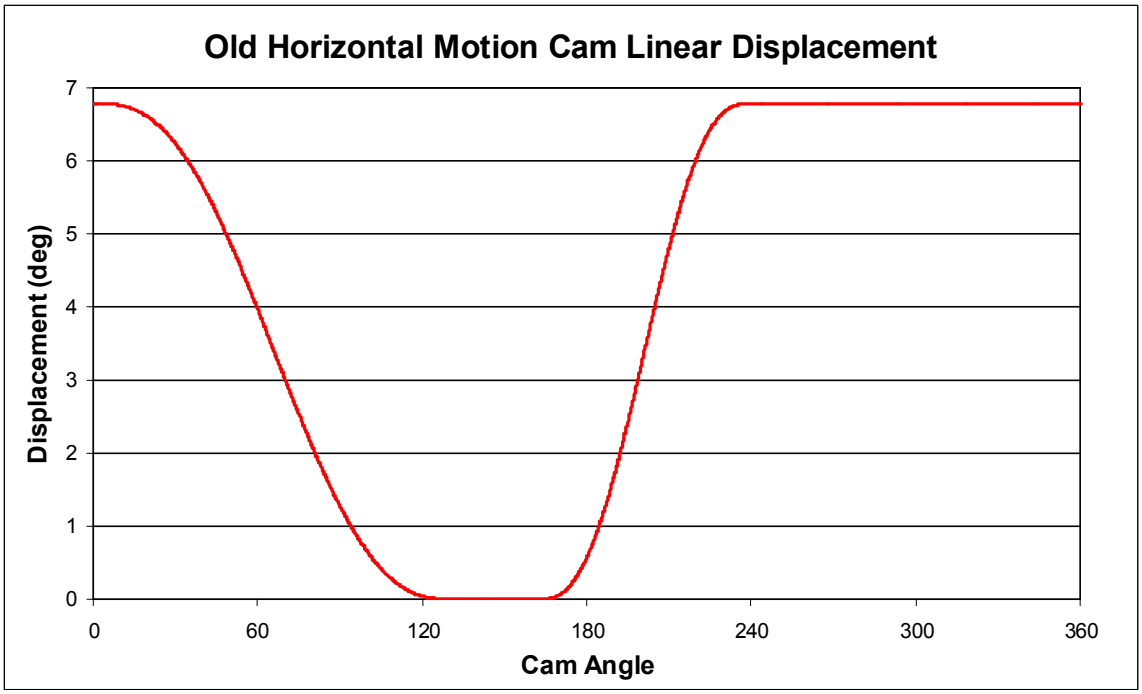

Figure 30 - Old horizontal motion cam displacement

The current cam places the tooling where it needs to be at the correct times, but there are still some deficiencies to the design. The fall and rise motions to the current cam are 3-4-5 polynomials. These are not ideal for reducing peak accelerations, velocities, or vibrations. Due to the fall motion being symmetrical, the velocity at the point of impact is rather large. The goal of redesigning this cam is to reduce the velocity at time of impact while at the same time reducing the peak acceleration and vibrations. One method to reduce the velocity at impact would be to increase the velocity earlier in the fall, creating an asymmetrical fall.

Before creating the new cam design, a calculation of the over-travels must be done. The five measurements of the over-travel obtained were used to calculate the range of points of impact of the cam's angular displacement. To do this we converted the values of the over travel at the tooling to the displacement at the follower using the known link ratios in the mechanism. This value converted to the cam's angular displacement at that point, which is what *Dynacam* uses, as seen in **Table 7**.

Table 7 – Horizontal motion cam over travel for each station.

	Tooling Over-ravel (mm)	Follower Displacement (mm)	Cam Angular Displacement (deg)
1	0.95	0.378	0.124
2	1.2	0.477	0.156
3	0.45	0.179	0.059
4	0.9	0.358	0.117
5	1.35	0.537	0.176

By looking at the over-travel values given, it was evident that the over-travel for linkage number 3 was an outlier to the other values. It was determined an outlier will not cause the machine to function improperly, so we could safely remove it from the range calculation. The range of the other four values was then further extended due to the relatively low number of samples that were taken. We decided on a final cam angular displacement range of 0.104 to 0.182 degrees for the design, with a target contact point at an angular displacement of 0.143 degrees.

With these values calculated, the new cam design began. A major decision made with the new cam was to remove the small dwell that happens after the tooling hits the hard stop. This allowed us to create the entire motion with one b-spline curve. The 30-degree cam angle dwell was replaced with a section of the b-spline function that was in over-travel, therefore not affecting the motion of the tooling.

In the first iteration, we placed constraints at the beginning and the end of the b-spline with a displacement of 6.784 deg (displacement of the cam at the beginning and end of the 120° dwell) and the velocity, acceleration, and jerk set to zero. All iterations included these same end constraints. For the first iteration, the focus was to reduce the velocity to zero at the point of expected impact, which would in turn ideally reduce the sound due to impact to zero. To accomplish this objective both velocity and acceleration were set to zero and the displacement

was set to 0.143 at a cam angle of 112° (20° before the removed dwell began), a final condition of a displacement of 0.143 was then set at a cam angle of 162° (where the removed dwell ended). The knots were then moved around to make it so all the necessary conditions to the motion were met, and the acceleration, jerk, and velocity maximums were minimized. The reduction of the velocity to zero at the target impact point caused the range of impact points to have a greatly varying velocity, meaning the improvement to the velocity was not ideal for all cases.

To improve upon the first design, a few slightly varying iterations were tried. They involved changing the boundary condition of velocity at the point of desired contact to a small value rather than zero. Different values between 2.5 and 5 deg/sec were tried, with the knots being moved to create the desired motion. In each of these attempts, there were positives and negatives. Some had lowered velocity at the target contact point with more variance at the outer limits of the range, while other designs were almost constant throughout the range. In this series of iterations, the cam angle for the impact point boundary condition was moved between 112° and 122°. This ensured that the 30° that is replacing the small dwell was entirely covered by the over-travel section of the motion. A few of these iterations were very promising, and overall had little drawback to them, but it was still felt the design could be made even better.

The next iteration involved three major changes in the boundary conditions. First, a condition was placed at 132°, the latest possible cam angle the tooling can contact the hard stop, which covers the 0.45mm over-travel that was measured in mechanism 3 (0.06 deg). This will cover a “worst case scenario”, and ensures that the tooling will be against the hard stop at the critical 132° cam angle needed for proper machine operation. The value of the displacement at 162° (the end of the removed small dwell) was also changed from the target contact point value of 0.143 deg to the minimum contact point value of 0.104 deg. This change makes it so the

tooling should not leave the hard stop before the point in which it was originally designed for. This value was not changed to the 0.06 deg value because the machine setup instructions indicated that this position is less critical than the point the dwell began. Finally, the minimum value of displacement of the cam was changed from zero to 0.04. This reduces the over-travel, which allows the surrounding values of velocity and acceleration to be lowered which in turn decreases the forces experienced by the system during the over-travel.

The first three iterations have greatly reduced the velocity at the time of impact while at the same time reducing the peak velocity, acceleration, and jerk, however they failed to take into account the velocity of the mechanism as it leaves the hard stop. The sound output by the impact created when the tool leaves the hard stop is known to be significantly less than that at impact, but if the velocity at that point could be reduced, that would be ideal. In order to achieve this, different boundary conditions of velocity were tried at varying cam angles between 162° and 172°. At each value, the knots were changed to optimize the characteristics of motion until a final boundary condition of 10 deg/sec at a 162° cam angle. This change reduced the velocity at the time of impact, but it also increased the peak acceleration and the vibrations significantly.

After all these iterations were completed, a comparison was made to decide between the best design from the iterations where there was no velocity control when the tooling leaves the hard stop, and the iterations where there was reduced velocity at that point. These will be called "single pseudo-dwell" and "double pseudo-dwell" respectively. There were two graphs created and a table made of the other pertinent peak values, to help facilitate the comparison. First, a graph showing the displacement graphs at the points of impact was created, as can be seen in **Figure 31**. This allowed a visual inspection of the motion at the critical times to ensure the motions were acting as intended. It also created a means to calculating the cam angles in which

the contact range occurs. These cam angles can then be matched up with the corresponding velocity plots to evaluate the range of velocity upon impact, as seen in **Figure 32**. It is immediately evident from the two plots that the Single Pseudo-Dwell cam has lower velocity throughout most of the range of initial impact, and the Double Pseudo-Dwell cam has a lower velocity at the release from the hard stop.

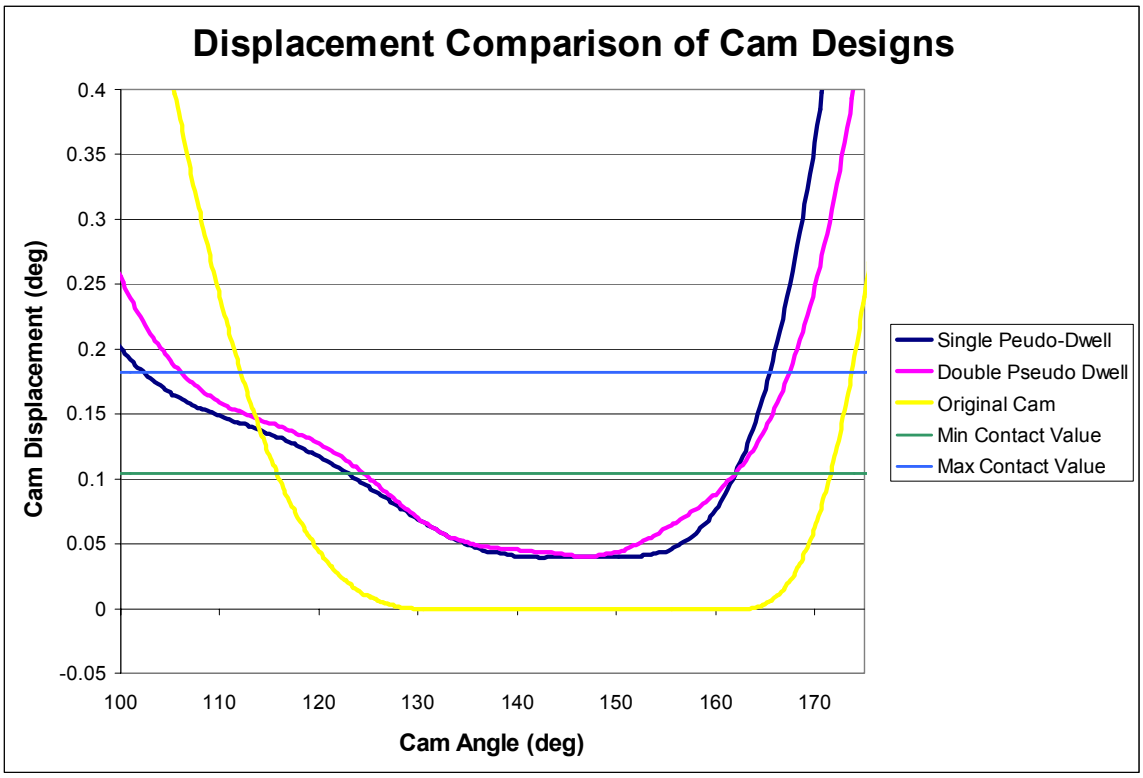

Figure 31 – New horizontal cam displacement comparison

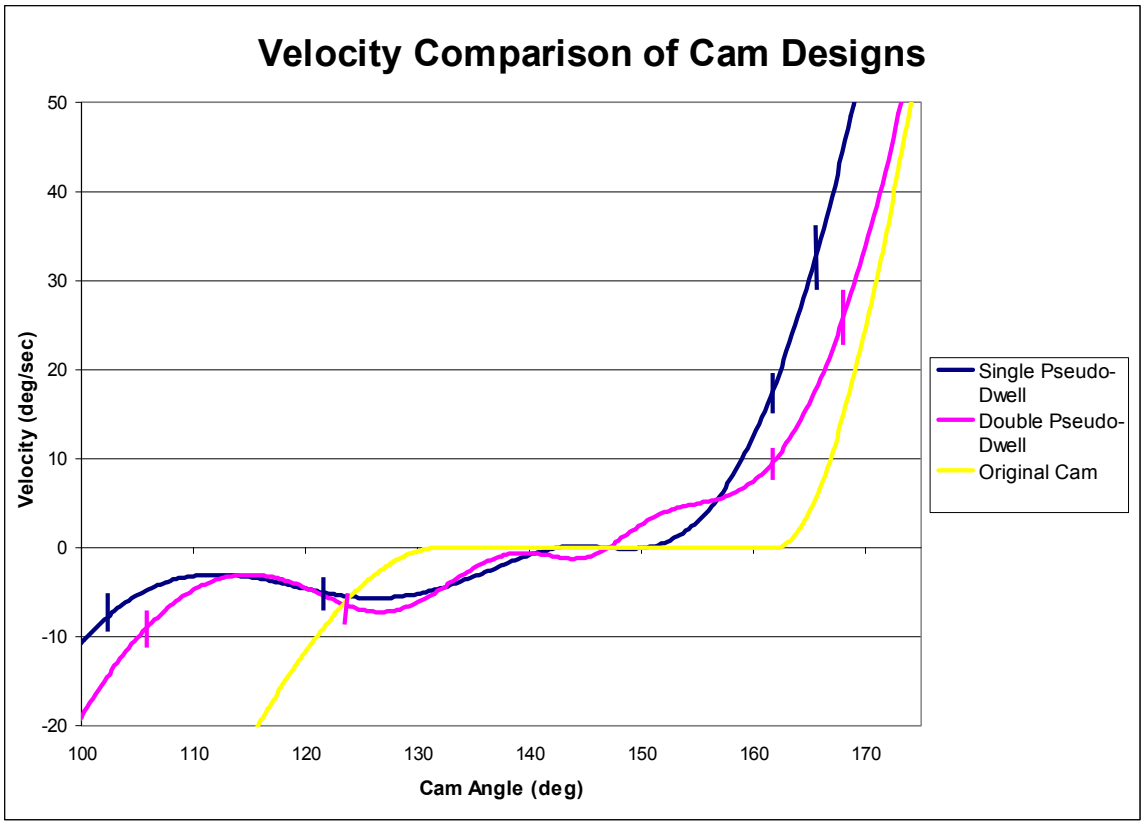

Figure 32 – New horizontal cam velocity comparison

To further weigh the pros and cons of each design, a chart was made of many of the other important characteristics of cam design, which can be seen in **Table 8**. This table shows that even though the double pseudo-dwell option decreases the velocity on impact, the adverse effects to the motion properties outweigh that advantage. This is particularly noticeable in the difference in peak acceleration (directly related to force) and the peak jerk (directly related to vibration). Therefore, the single pseudo-dwell design was chosen as the final design for the horizontal motion cam.

Table 8 - Velocity design comparison for horizontal motion cam

	Single P-D	**Double P-D**	**Advantage?**
Velocity Range at Impact	3 - 7.6 deg	3 – 8.6 deg	Single

Velocity Range at Leaving	18.5 – 32.3 deg	10 – 23.7 deg	Double
Peak Acceleration	7841 deg/sec^2	12,574 deg/sec^2	Single
Peak Jerk	647 deg/sec^3	1351 deg/sec^3	Single
Force Coverage from Jumping	348 N	152 N	Single

The final step in the cam design was to create this new design to the old one to ensure its properties are acceptable and to quantitatively assess its advantages and disadvantages. In this case, the newly designed cam was an improvement over the old cam design in every aspect. These values can be seen in **Table 9**. The new cam design not only should improve the sound output by the hard stops, but will also allow the machine to run more efficiently than in its current state.

Table 9 - Quantitative cam comparison for horizontal motion cam

	Old Cam	New Cam	% reduction
Over-travel past target impact point	~1.1 mm	~0.8 mm	27%
Velocity range at impact	**19.9 – 28.0**	**3 – 7.5**	**73% - 88%**
Velocity at target impact point	24.3	3	88%
Velocity range when leaving	33.8 – 47.4	18.5 – 32.3	32% - 45%
Velocity when leaving at target impact point	40.9	25.8	37%
Peak Acceleration	7,931	7,841	1.2%
Vibrations at dwell: RMS values	0.1612 gs	0.0273 gs	73%

4.2 Vertical Motion Cam Redesign

The purpose of the vertical motion cam is to take part A off the horizontal mechanism and place part A into part B. It does this using four motions. The first, starting at machine zero,

is a dwell that is continued from 45 degrees before cam zero. Then the cam begins a fall until it reaches a pseudo dwell where part A interacts with part B and is detached from the tooling. The final motion is the cam rise, which returns it to the dwell position so that it can receive another part A from the horizontal mechanism. We can see this motion in the displacement diagram in **Figure 33**.

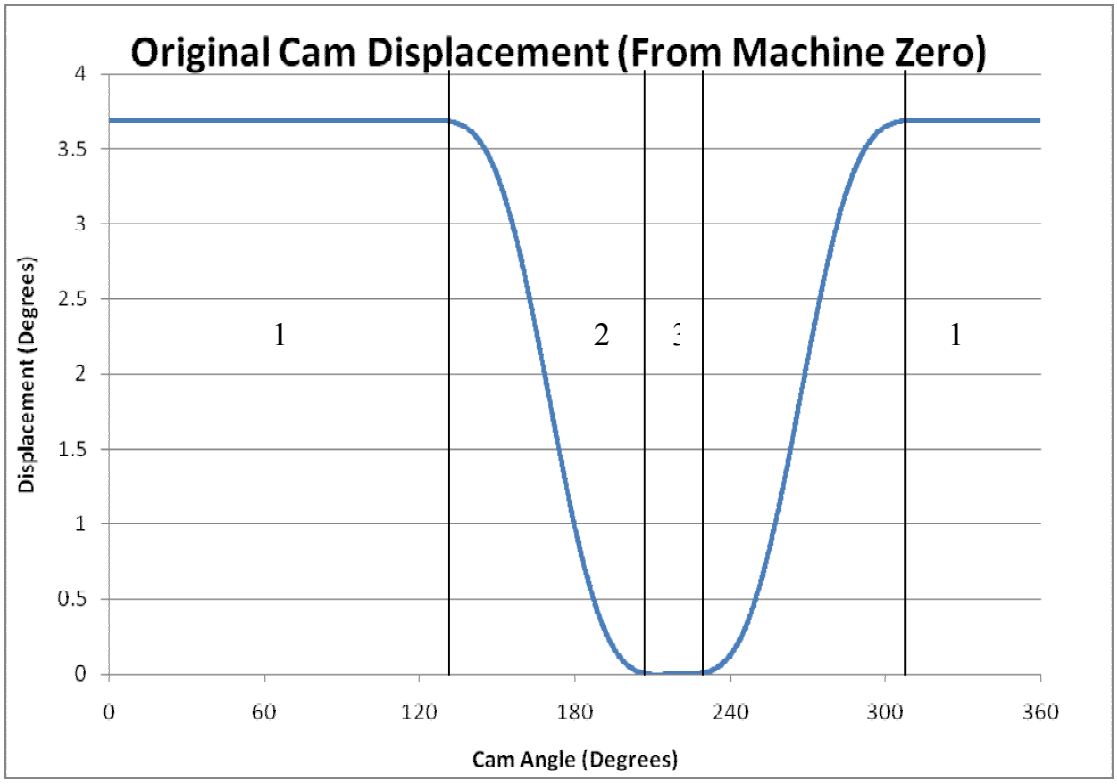

Figure 33 - Original vertical cam displacement motions

At both the dwell and the pseudo dwell, the position of the tooling is very important. We controlled this in two ways. During the setup of the machine, the cam was rotated to where the pseudo dwell was against the cam follower roller, and spacers are ground to ensure proper placement of part A with respect to part B. The dwell incorporates a hard stop design with a spring and over-travel to account for precision placement under all circumstances. This is where the transfer of part A occurs between the horizontal tooling and the vertical tooling.

As with the horizontal mechanism, we can calculate the location of the hard stops by measuring the gap created by the compression of the spring during the over-travel and correlating this distance to a cam angle. Since the hard stop and the resulting gap are during the dwell, we need to subtract this degree correlation from the maximum displacement of the cam. We do this for our five samples in **Table 10** below. The first and second columns refer to the physical distance of the mechanism's over-travel and the final column shows at which degree of displacement the hard stop hits.

Station	Over travel (m)	(degrees)	Hard stop hits at (deg)
1	0.00090	0.156	3.535
2	0.00100	0.174	3.517
3	0.00080	0.139	3.552
4	0.00012	0.021	3.670
5	0.00085	0.148	3.543

Table 10 - Over travel range

It was observed that during the taking of data point number 4, the cam was in the wrong position. For this reason, the data point was removed from the analysis. Since this is only a small sampling of impact ranges possible, the range was extended by twenty percent on both sides in case mechanisms on other machines have slightly varying over-travel ranges.

As stated before, lowering the velocities will lower the kinetic energy at impact and will therefore lower the audible noise created by this impact. To do this, we added more or modified some boundary conditions in the creation of the new cam. The primary additions occurred either at the average of the hard stop locations or at the extremes. The goal was to create a small pseudo dwell during the range of the hard stop. In order to do this it would be necessary to drastically increase the acceleration and velocity before the hard stop hit and after to make sure that the tooling arrived at the pseudo dwell where part A interacts with part B at the correct time.

This increased acceleration was not only excessive, but it also caused large spikes in the jerk and large vibrational issues that affected both dwells. These vibrations occurred even after the cam was put through *Dynacam*'s spline-dyne function to help remove vibrations. While this may have been the best design for reducing the audible noise of the machine, the negative aspects were not worth the gains.

We found that if the target velocity at impact was increased, the peak accelerations were lowered, as were the dynamic vibrations in the system. The goal then became to balance the advantages and disadvantages. The target velocity was then put to 10 deg/s and brought to 0 deg/s in increments of 1 deg/s. It was found that when using two points to attempt to create a pseudo dwell did not work. This was because this created a plateau only at this average impact displacement. Instead, we needed to have a low velocity over a range of impacts. By holding the velocity to a small amount and acceleration to zero at the average hard stop impact displacement, the velocities across the entire impact range would be low.

If the target velocity were put to zero, at either end of the hard stop range, the velocities would have already increased to 13 deg/s. As we increased the target velocity to 3 deg/s, we see that the velocities at the outer edges of the hard stop go down to 5 deg/s. If we raise the velocity above 3 deg/s we see that the outer edge velocities also increase above 5 deg/s (**Figure 34** and **Table 11**). It is shown in **Figure 34** and **Table 10** that on the old cam, the rang of impacts occurred between 21-23 degrees of machine time, while on the new cam this same range of motion is between 17-24 degrees. This is due to reducing the velocity over this time and therefore increasing the time necessary to travel the same distance.

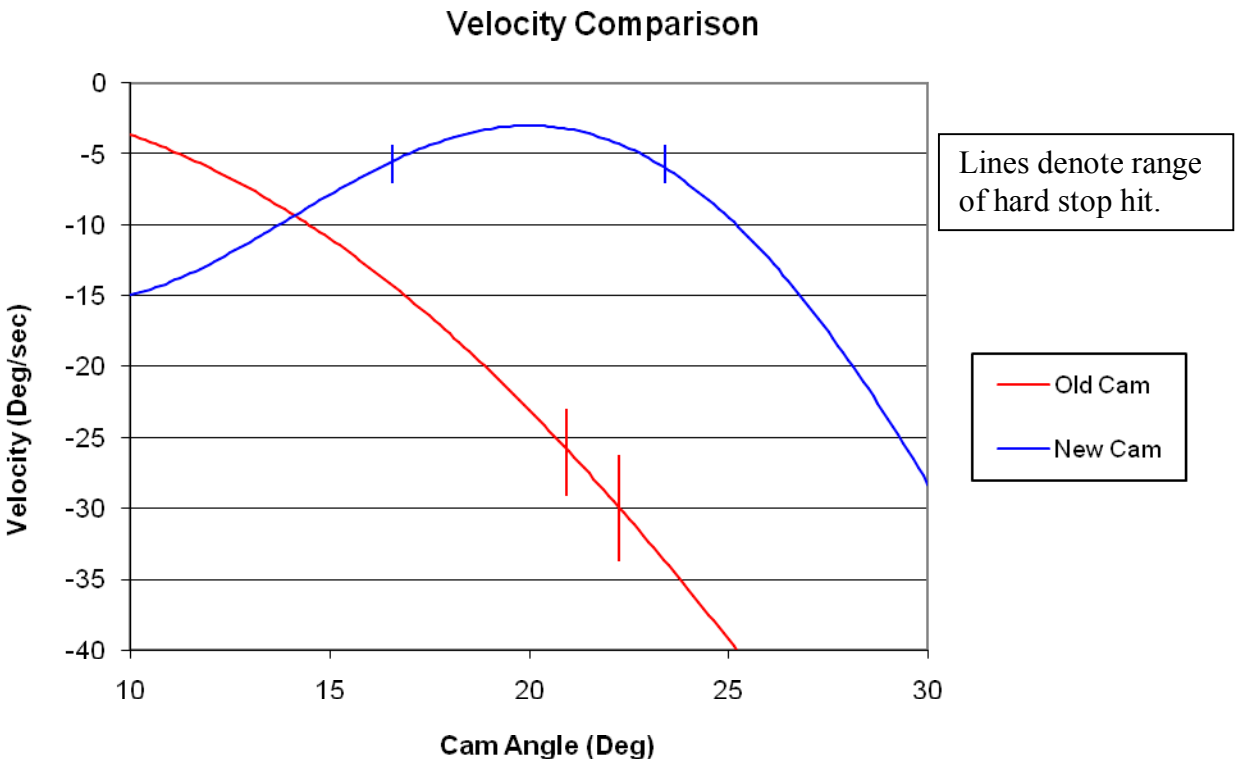

Figure 34 - Hard stop velocity hits

Cam	units	Max Velocity	Percent Decrease	Min Velocity	Percent Decrease
Old	deg/sec	-26.76		-30.73	
New	deg/sec	-3	89%	-5.92	81%

Table 11 - Hard stop velocities

The peak acceleration and jerk can be lowered by moving the target impact point so that the acceleration spikes are minimized and the jerk spikes at either end are also minimized. The knots are then placed to also minimize acceleration and jerk. The resulting displacement, velocities, and accelerations as compared to the old version of the cam can be seen in **Figure 35**, **Figure 36**, and **Figure 37**.

Figure 35 shows the plateau on the new cams where the velocity was reduced and the resulting steeper grades that account for higher peak accelerations and velocities. **Figure 36** shows both ends of the cycle where the velocity goes towards zero. **Figure 37** shows that there

are larger spikes for acceleration, but these were determined to be worth the decrease in velocity at the hard stop impacts.

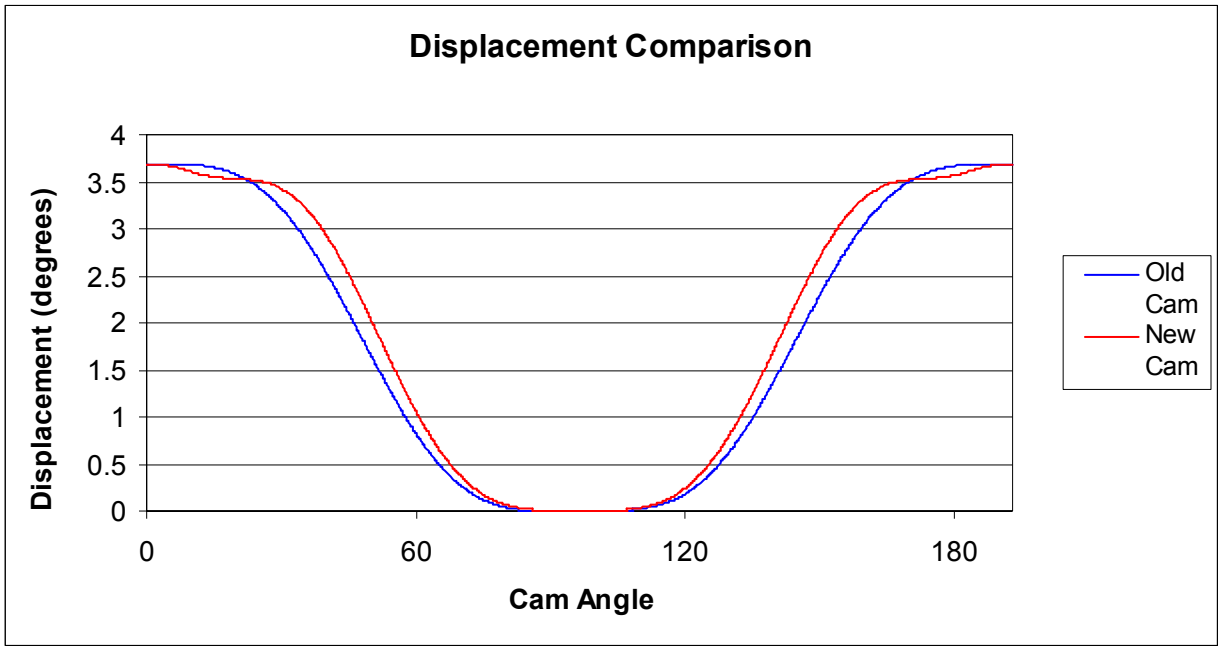

Figure 35 - Displacement comparison

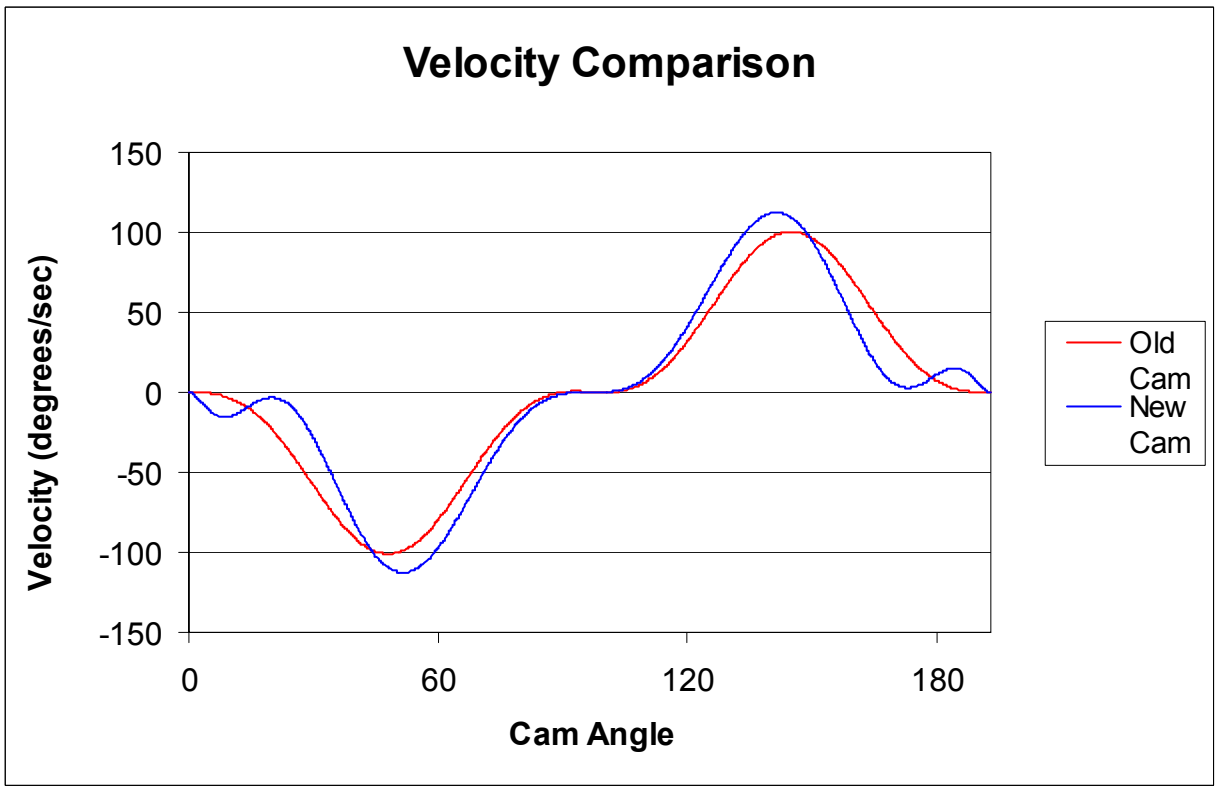

Figure 36 - Velocity comparison

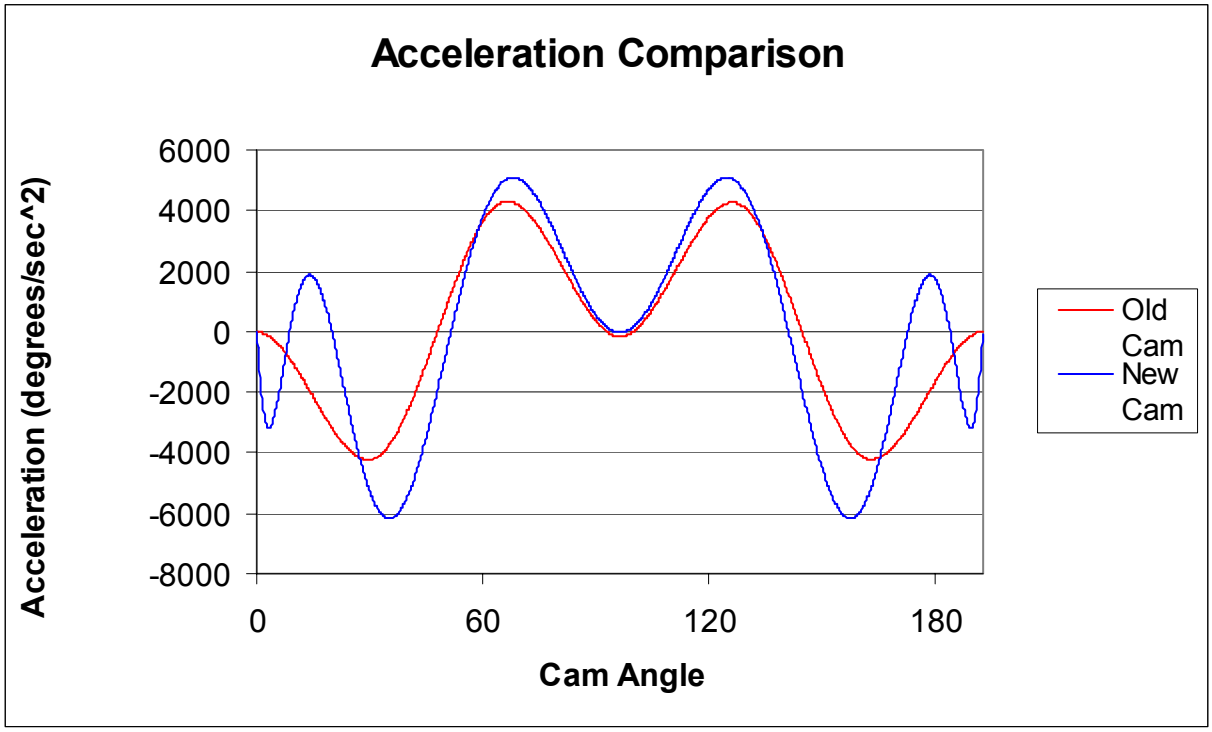

Figure 37 - Acceleration comparison

5. Implementation and Testing

During the period of this project, we had one set of new cams made with the aforementioned cam designs, then had them installed on the mechanism where the previous testing was performed. This allowed the comparison of data before and after the cams were changed, without possibly contaminating the data due to differences in other aspects of the mechanism due to tolerances, differences in over-travel, or variance between tooling that could also have an effect on the data.

5.1 Test Methods

With the redesigned cams on the machine, tests were performed to quantify the improvement of the new design versus the old. This was done using accelerometers and a sound meter. The accelerometer tests were performed much in the same way as they were for the original cams, with three being dispersed throughout the system and readings taken to find correlation to the theoretical data exported from *Dynacam* as well as the data collected from the initial cam design. This will provide a numerical comparison of how much the new cams improved over the old ones in terms of velocity and acceleration of the tooling as it contacts the hard stop. This data is necessary to provide a clear indication of how the new cams helped to achieve the goal of this project.

The second test performed required the use of a sound meter, which measures localized noise within the mechanism. Aimed at the hard stop during operation, it should give a reading in decibels of the noise emitted by the impact of the tooling and the hard stop. Having performed this test on a machine with the old cams, then performing them on the machine with new cams, it

will provide a single, numerical value for the amount of reduction in noise due solely to the new cam profiles.

5.2 Horizontal Motion Cam Results

Accelerometers were attached to three locations labeled A, B, and C in **Figure 38** on the horizontal mechanism, as they were with the original test data. First, an accelerometer was attached to the end effector tooling (Location C) of each of the mechanisms. This gives us the accelerations felt from the impact, and the motion of the device mechanism while it is not against the hard stop. Simultaneously, data was taken from an accelerometer was attached to the top of the lever actuator (Location A), facing in the same direction. This allowed us to see the change in motion across the spring, because the lever actuator has the hard stop damped out of its motion.

The third location that we took acceleration data from was the underside of the cam follower (Location B). The motion of the cam has the only significant effect on this location, due to it being so far from the hard stop. This gave us the cleanest data possible for verifying the proper cam motion.

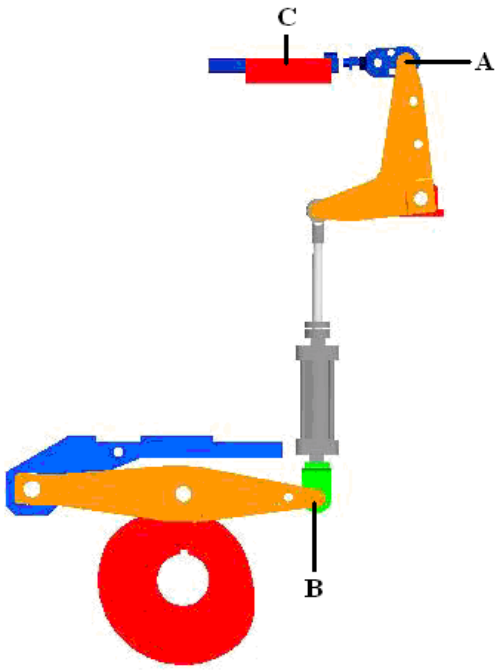

Figure 38 - Horizontal motion mechanism accelerometer placement

From the data gathered in testing, we made graphs in excel using the same techniques outlined in the original cam analysis. First, the cam follower acceleration data was compared to the theoretical cam acceleration data to verify the motion of the mechanism. We did this by converting the theoretical data to Gs at the accelerometer, and then overlaying the graphs. As can be seen in **Figure 39**, the accelerometer data correlates with the theoretical data, showing us that the design is creating the motion intended.

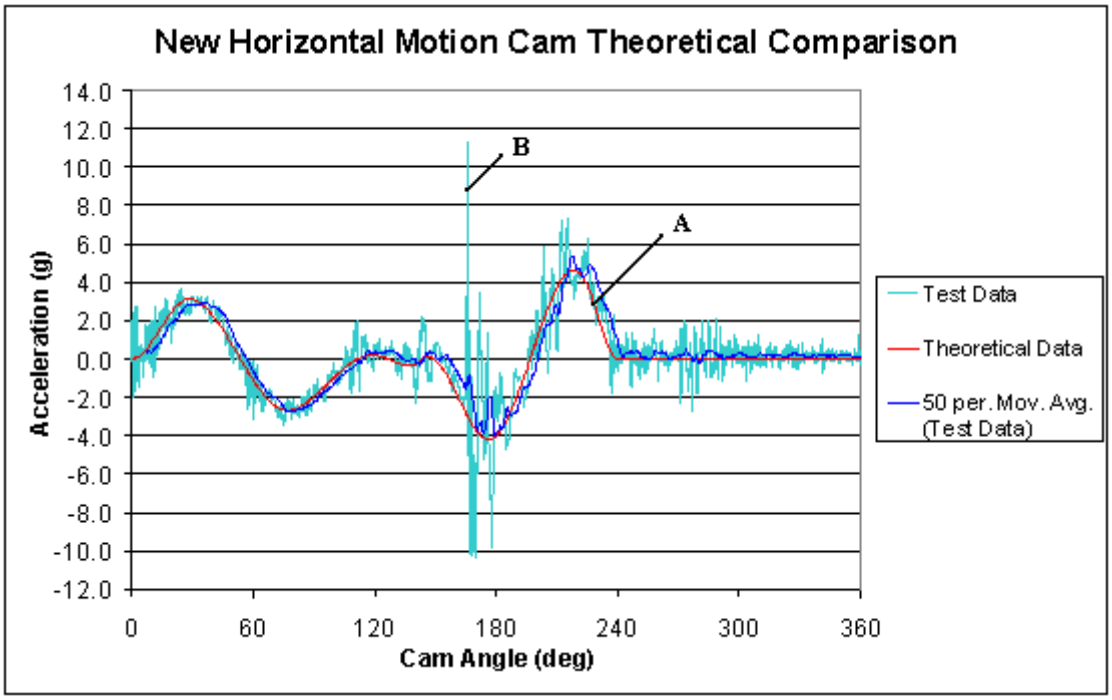

Figure 39 - Horizontal cam motion theoretical comparison

The next comparison made used the data from the accelerometer attached to the end effector is in **Figure 40**. The theoretical data from the old cam, labeled as line A, and the data measured from the new cam, labeled as line B, give a visual representation of this comparison.

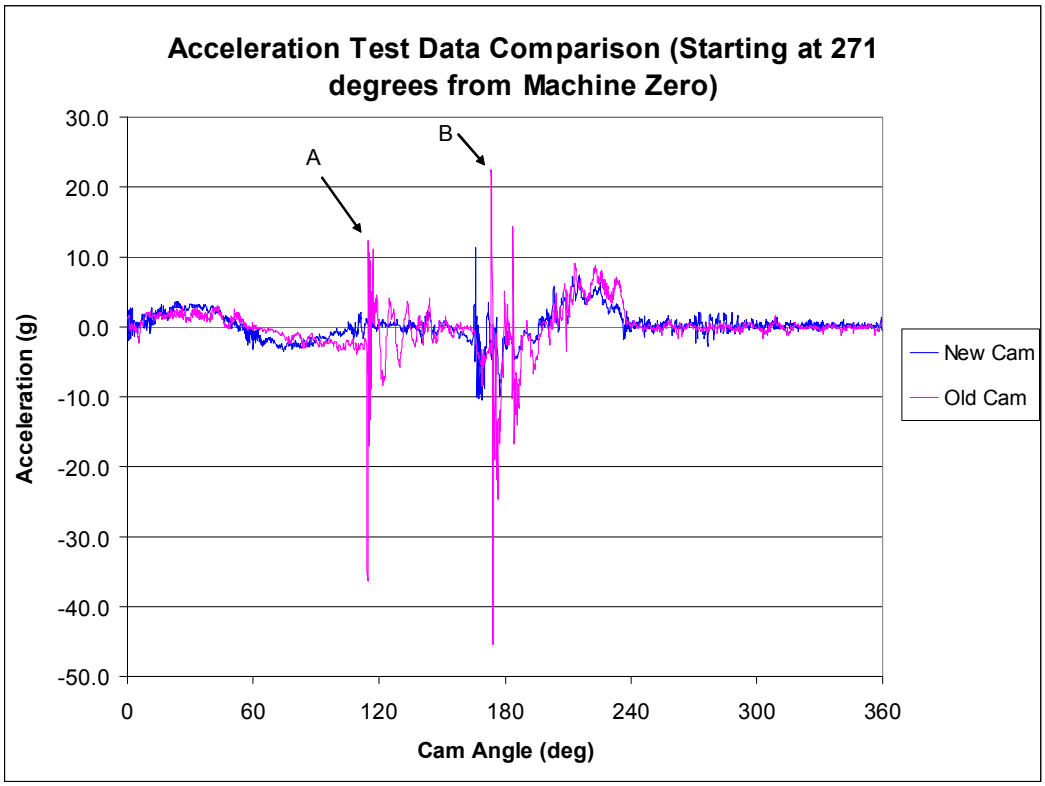

Figure 40 – Old and new cam acceleration comparison for horizontal motion mechanism

It is immediately evident that the new cams have had a significant effect on reducing the impact at the hard stop. The spike that corresponds to the tooling hitting the hard stop, point A in **Figure 40**, was reduced from a peak acceleration of approximately 36gs to less than 2gs (some of which can be attributed to noise), a 94.4% reduction in peak acceleration.

The second spike, at point B, represents the tooling leaving the hard stop. It is evident that this was also significantly reduced, even though not as much so as the spike upon impacting the hard stop was. The peak acceleration with the old cam was approximately 45gs, and the peak acceleration with the new cam was around 11gs; a 75.5% reduction. These results were expected because the cam was primarily designed to reduce the velocity of the tooling upon impact with the hard stop, and less upon leaving the hard stop, as described in the cam design section.

This significant decrease in accelerations means that the velocity upon impact was greatly reduced. Given that it is practically impossible to take a reading of the velocity upon impact, this

data is our best gauge. It is also an accurate gauge because we know that the hard stop is made of hardened steel, which has very high stiffness. This means that the accelerations are not damped out more when the velocity upon impact is increased.

5.3 Vertical Motion Cam Results

We tested the vertical motion mechanism in the same fashion as the horizontal motion mechanism. We placed the accelerometers on the same position on the end effector tooling and the cam follower. The only difference was the location of the accelerometer on the lever arm (because this part is significantly different on the two mechanisms). This data was then used to calculate and verify our findings.

Verification of the cam motion was done by comparing the theoretical data output by *Dynacam* with the data taken from the accelerometer on the cam follower. **Figure 41** shows that the cam is creating the motion expected.

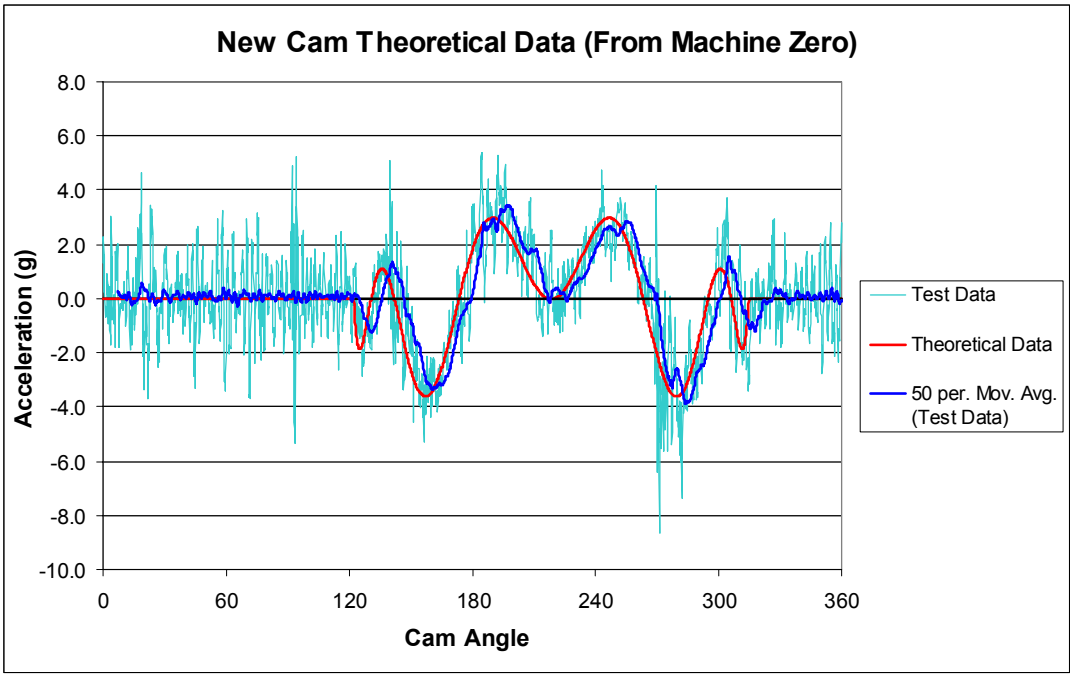

Figure 41 - Vertical motion cam theoretical data

We then compared the data gathered from the accelerometer testing to the old acceleration data to see the effect the new cam had on the hard stops. The two data sets were overlaid on each other for direct comparison, as seen in **Figure 42**. The pink line represents the data from the old cam, and the blue line represents the data from the new cam.

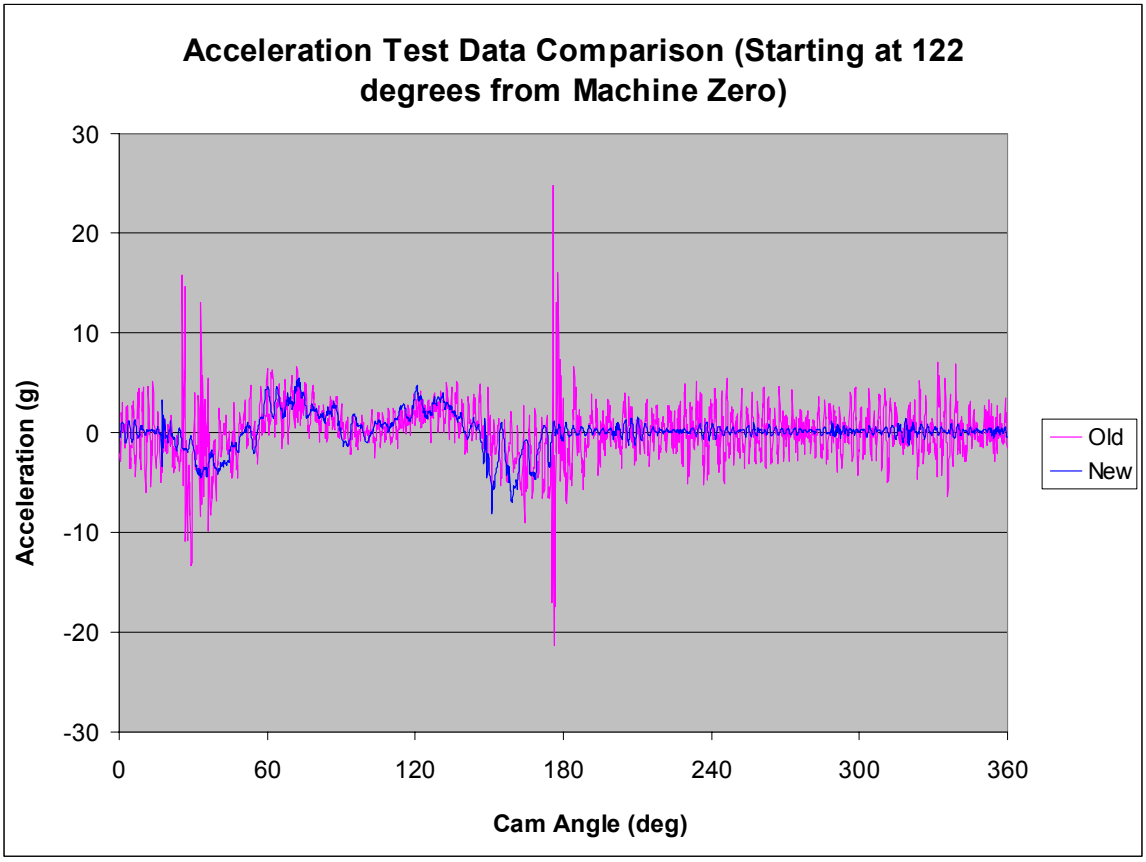

Figure 42 - Acceleration comparison

The impact that happens upon the tooling contacting the hard stop, which happens around 175°, was greatly reduced. The peak acceleration was decreased from around 24g to around 3.5g, which is an 85% reduction. Similarly, the acceleration spike that occurs from the tooling leaving the hard stop is very hard to detect on the graph, and was a reduction from 16g to less than 3.5g, an 81% reduction.

The reduction is significant, and shows a drastically decreased acceleration, and therefore velocity upon impact. This in turn means the sound decibel output from the mechanism should be greatly reduced.

5.4 Sound Testing

After acquiring a sound meter, we took decibel readings on all of the mechanisms on this and on identical machines. Since no readings were taken before the cam was changed, a direct comparison was not possible, but comparisons between the mechanisms with their current cams were made to get the most accurate results possible.

The process used to take the readings was to point the directional microphone towards the point of impact on the vertical mechanism (meter position 1), from about 3 inches away. Since the data is only being used for comparative analysis the absolute distance was not as important as having a consistent distance from the tooling for all tests, so a natural line on the safety guard was used as a point of reference. Three readings were taken on each mechanism to get an average. Next, we performed the same process with the directional microphone facing the point of impact on the horizontal mechanism (meter position 2). There was a different point of reference used, and consistency in the distance the readings were taken from was again maintained. The meter positions can be seen in **Figure 43**.

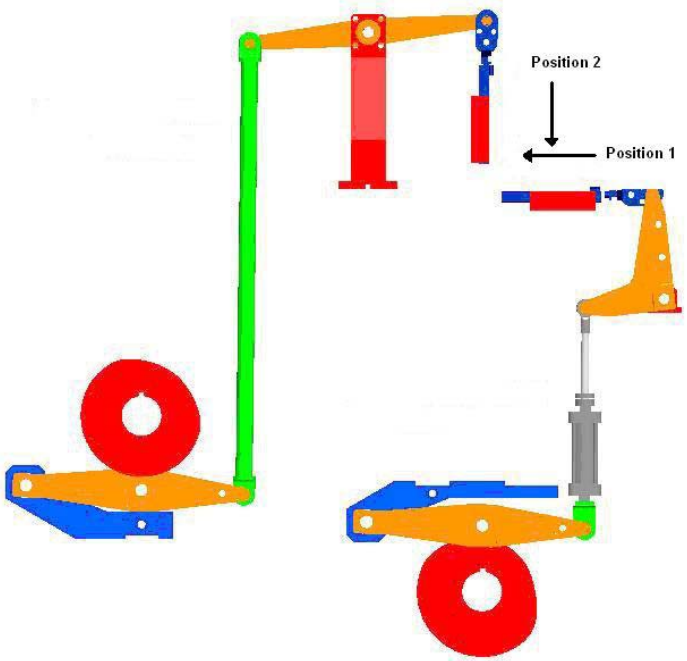

Figure 43 - Sound meter positions

Properly comparing the data of the mechanism with the new cam to the mechanism with the old cam was not quite so simple. Since there were multiple mechanisms on each machine, and the ambient noise around each mechanism was different, the location of the mechanism on the machine needed to be taken into account. To remove this variable, we compared the linkage with the new cams, on the machine that we will call "Machine 1", to the linkage in the same position on the other machine, "Machine 2". Next, our analysis needed to remove the variable of it being in a different location on the factory floor, which may have different ambient noise levels. To do this the reduction in the decibel reading between the mechanisms with the new cams was compared with the other mechanism on the same machine (Machine 1). We then followed the same procedure for the mechanism in the same location on the other machine (Machine 2). Then the change in decibel readings between the two machines could be compared. **Table 12** and **Table 13** show the average readings of each cam, and the comparison of the decibel readings as described above.

Table 12 - Decibels output at the vertical motion mechanism

Meter Pos. 1	dB reading avg for cam 1	dB reading avg for all other cams	Difference
Machine 1	93.53	100.48	6.94
Machine 2	102.33	104.88	2.55
Change in difference between machine 1 and machine 2			4.39

Table 13 - Decibels output at the horizontal motion mechanism.

Meter Pos. 2	dB reading avg for cam 1	dB reading avg for all other cams	Difference
Machine 1	92.37	97.88	5.51
Machine 2	100.90	102.41	1.51
Change in difference between machine 1 and machine 2			4.00

These results show that the linkage in the position where the cams were changed does experience less noise due to outside factors than the other linkages in the system. Machine 2 also showed higher decibel readings, probably because of its proximity to other manufacturing machines. This means that the double comparison, first between the mechanisms in each machine, and then the difference between each machine, was necessary for unbiased analysis.

This analysis shows us that there was an approximate decrease of 4 decibels due to the change of the cams in one mechanism. If each mechanism on the machine were to have the new cams, this result would likely be reduced further because of a reduction of ambient noise. Without testing, it is impossible to conclude this. Nevertheless, a 4dB reduction in sound output from changing the cams on one linkage is significant.

6. Summary

The sponsor company has been experiencing a noise problem with some of their assembly machines. The impact of the hard stops in some of the mechanisms, which must be used to ensure the precision needed to maintain their quality standard, have been causing an increase in decibel levels which are beyond what is considered safe for workers. This means that all workers must wear earplugs, and even then, the sound levels are higher than desirable. The sponsor wanted a way of remedying this problem, and thus our goal for this project was to propose solutions to the sponsoring company on ways to reduce the decibel levels output by the hard stops in the system.

A few potential solutions to the problem were presented to the sponsor. Each of the proposed solutions focused on reducing the kinetic energy (KE = mass * velocity^2) change in the system, which is known to be the primary contributor to noise. This is accomplished by reducing the kinetic energy upon impact or creating means for the kinetic energy to dissipate over a longer time. The change that we expected to have the greatest effect on the system was a reworking of the cams that run the two mechanisms. These were created with a focus on reducing the velocity upon impact, known to be the greatest factor in impact noise.

Another possible change includes removing a non-essential crowbar bracket, and creating a tool that can easily be taken on and off as needed. Other means of reducing the noise emitted was to decrease the vibrations through the hard stop by adding damping materials, or fabricating the tooling out of a different material.

During the time frame of this project only the new cam idea was able to be implemented and tested, with comprehensive comparative data taken. The acceleration spike of the horizontal

and vertical motion end-effector toolings, upon hitting the hard stop, were reduced by 94% and 85% respectively. The corresponding spike when the tooling leaves the hard stop, which should have less of an effect on the sound, was reduced by 75% and 81% respectively. Additionally, decibel readings were taken which showed a drop of 4 decibels when the meter was held a few inches from the guards, upon changing only one set of cams. These acceleration and decibel change results show significant positive change in remedying the problem. The decibel reduction should be even greater if the cams are changed on each mechanism in the machine.

7. Conclusions and Recommendations

Based on the results of test data taken with the old and new cams, it is our conclusion and recommendation that the following changes be implemented with the goal of reducing audible noise and improving operation.

1. Replace existing cams with cams featuring the redesigned profile on all stations This change has been tested and proven Doing this on just one station reduced peak accelerations by 75% to 94% and reduced audible noise by 4 to 7 dB. Replacing these two cams on all stations on all machines will significantly reduce audible noise from the machine.

2 Remove the crowbar bracket from all stations. Alternate means of accomplishing its function are discussed in the Further Work Section.

8. Further Work

While perhaps the single biggest contributor to noise in the machine was reduced by the modification of two cam profiles, a few additional changes to the system could be made to further reduce emitted noise and improve performance. We will discuss several of them in the following section.

8.1 Alternatives to Crowbar Bracket

We previously mentioned that the removal of weight throughout the linkage train is a good way to improve system performance. It will lead to lower forces, less impact noise, improved vibrations, and longer life. For this reason, it is crucial to remove all unnecessary weight from the linkage train.

The lever actuator arm has a bracket bolted onto it, called a crowbar bracket. Its only purpose is to provide a place where the machine operator can get leverage in the event of a jam. While having this capability is important, this bolted on bracket serves as little more than mass during normal operation. For this reason, we suggest removing it during normal operation, only being introduced back into the system when needed.

Several ways to accomplish this vary from no modification required to the fabrication of equipment that can take the place of this bracket. The first and simplest solution requires unbolting the bracket and removing it from the system. This will result in a weight savings of 0.191 kg**.** Question – is this local weight or effective mass at the follower – need to make clear. In the event of a machine jam, the bracket can be bolted back on quickly. In fact, the bracket does not even have to be bolted on, as long as pins are slid through the holes to ensure that it will not fall off, the force of the crowbar should ensure that the pins stay in place. In the event that

the unbolted pins are deemed unsafe, a new set of pins could be fabricated featuring slots that a retaining ring could fit into. This would ensure that the pins would not move during use and provide faster attachment than would a bolt and nut.

The second solution requires the integration of a bracket into the bar that is used for leverage in the event of a jam. There are many ways to do this using the existing bracket as well as by designing a new bracket. The simplest solution would be to weld the current bracket to a lever arm. If a jam occurs, the tool can be inserted into the bolt holes on the lever actuator and the pins can be slid through. The second and more elaborate solution requires fabricating a bar with built-in bracket. Only one is needed per machine and no additional hardware is required. The tool simply slips on the bell crank when needed as opposed to all of the previous designs, which require bolting or pinning an apparatus back onto the machine. **Figure 44** shows the proposed tool design.

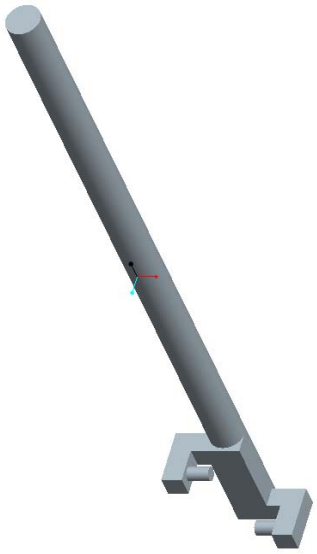

Figure 44 - Redesigned crowbar tool

While it would be feasible to design a tool that only engaged the bracket from one side, the pictured tool provides a safer interface. With the tool only engaging the bracket from a single side, it leaves the possibility for it to slip off. If it happened to slip off during use, it could result in injury to the operator or damage to the equipment. The positives to this kind of design are quicker set up as well as ease of fabrication. When compared with the potential negatives however the two-sided tool is the better option.

8.2 Hard Stop Shimming / Material

In addition to the proposed solutions that were accepted and further explored, a few changes explored represent potential future solutions. Being that the overall goal of the project is to reduce the audible noise emitted from the system, it makes sense to look at the hard stop itself

A solution tried in the past included the insertion of a rubber damper into the hard stop block that featured a protruding nub. This nub would meet the tooling before it hit the hard stop; therefore reducing its velocity before contact. This solution was abandoned despite working at first. The problem lay within the use of the rubber damper. The periodic strikes would cause the rubber nub to deform each time and after numerous strikes, and over the course of just a few weeks, the nub was worn down to the point that it was no longer protruding from the hard stop.

The previous solution, although rejected, presents the idea that the hard stop can be physically modified through the introduction of outside materials to assist in sound and vibration dampening. This goal can be accomplished through a number of solutions as discussed below.

Perhaps one of the best damping materials available is rubber. It is widely used in a variety of applications and industries for this purpose and if properly specified can be extremely effective. In this situation however it is inappropriate for the following reasons. First, rubber is subject to creep. Creep is defined as “an increased tendency toward more strain and plastic

deformation with no change in stress.[1]" Error! Reference source not found. **Figure 45** shows the stress strain curves for rubber that has not been subjected to creep, and the stress strain curve for rubber that has been subjected to creep.

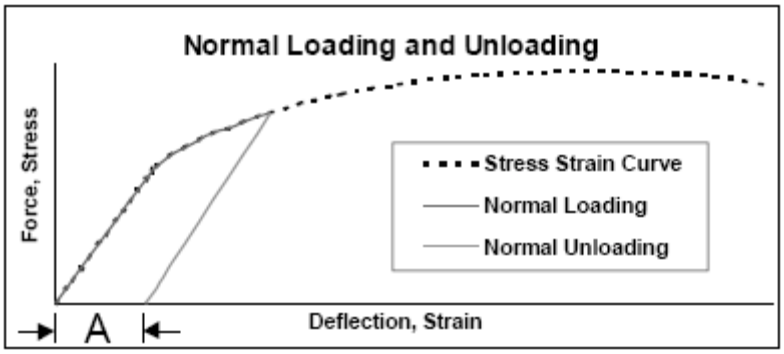

Normal Stress-Strain Curve

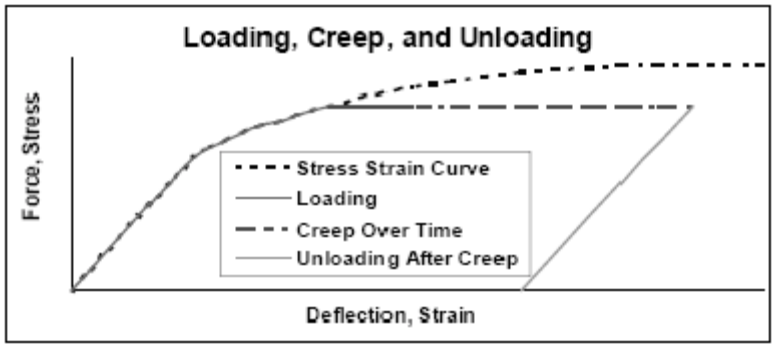

Stress-Strain Curve with Creep

Figure 45 - Stress strain curve with creep

Once the rubber piece reaches this creep point, there is an unpredictable amount of deflection for a given input force. The deflection should increase with time as the rubber is subjected to more strikes and gradually weakens. For a system that relies on precision to deliver

[1] http://www.brushwellman.com/alloy/tech_lit/june00.pdf

the component to a specific location, there is too much variation using a rubber shim to consider it a viable solution.

Another potential solution is the insertion of a metal shim behind the hard stop in the same fashion that the rubber shim would have acted. Although this may not be as effective in damping vibrations as adding a rubber shim, a metal shim would still be a sizable improvement to having the vibration go through only hardened steel.

Perhaps the solution of this nature comes from the implementation of a high-damping material. High damping materials were originally developed for the aeronautical industry where the materials used often featured low damping capacity. The resulting vibrations and resonance have impacts on the safety, reliability, and premature failure of components. For this reason, it is desirable to have a material available that provides better damping that the current materials while maintaining good strength, weight, and cost.

8.3 Plated Tooling

Perhaps the most significant weight within the system lies at the tooling. Being at the very end of the linkage train, the effective mass at the cam follower is a factor of the tooling mass times the link length ratios.

For durability reasons, the entire tooling assembly is made of steel. While hardened steel is a great material for this application as it provides long life and solid operation, it is heavy.

In this case, the strength given by the steel components is not required. Aluminum tooling would provide the necessary strength for normal operation. The aluminum however does not provide the same longevity as the hardened steel does when taking into account the contact between the tooling and its housing. Aluminum components run into problems with galling and

seizing considering this motion, which is why plain aluminum components cannot be considered. There are however two viable ways to work around this problem.

The first is plating the aluminum. By plating the aluminum, a harder surface layer is added which protects the inner aluminum from damage. One popular method of coating aluminum that helps to combat all of its negative properties in this application is chrome plating. The chrome layer prevents galling and seizing of the aluminum, allowing sliding applications because of chromium's low coefficient of friction. Also beneficial is the hardness of the chrome, improving durability of the plated parts.

This solution has lots of potential. The weight savings from machining the whole tooling assembly out of aluminum would be significant, especially when considering its affect on the cam follower. It negates the main downside to aluminum, which is its poor performance in motion situations.

There are however some downsides to using chrome plated aluminum. First is the cost. Aluminum is generally more expensive than steel, although some of this cost is offset by its ease of processing. The other downside is actually having it chrome plated. Exposure typically leaves aluminum with an oxide layer on the surface, which while providing it with excellent corrosion resistance also interferes with the plating process. It must be carefully cleaned and prepped before application. If not, there is the potential for the chrome to peel, something that occurs with poor adhesion. Getting around this initial problem, the chrome plating process is expensive, time consuming, and potentially hazardous. The involvement of the many caustic chemicals and heavy regulation by the Environmental Protection Agency, as well as personal health issues make it a risky endeavor. Having an outside vendor perform this work could potentially be costly considering the volume of parts required.

Chrome plating allows the majority of the assembly to be fabricated from aluminum, dropping effective mass from the greatest offender in the system. It does however come at a price and further investigation into cost vs. performance benefits should be performed before pursuing this.

The second solution is manufacturing tooling that is primarily made of aluminum but features hardened steel inserts that bolt on in high wear areas. This solution guarantees that the steel is present where needed, but aluminum in the places where it is not. This will save some weight from the overall tooling, as aluminum is approximately one third as heavy as steel for the same volume of material.

These wear plates would not necessarily have to be very thick as their periodic replacement would be a simple enough process. They would only need to be as thick as it would take to have a recessed bolt hole for attachment. There are of course pieces of the system that need to withstand impact forces. These pieces could feature a system much like the above-mentioned solution, with hardened steel outer bolted onto a lighter shell.

One benefit is the near infinite life of the aluminum-tooling carrier. Since the only wearable items in the system are made of the hardened steel, the aluminum core should never need to be replaced. This is beneficial over the old system where excessive wear on the tooling carrier would necessitate replacement of the entire unit rather than a couple of bolt on parts.

The downfall to this system is its complication. The current tooling requires a single material fabricated from a single piece of stock. For this proposed solution to be implemented it would be necessary to use two different materials and some attachment bolts. This of course adds some complications for a few reasons. The first is the extra machining/profiling needed to develop the proper tooling profile. Since there are bolts on wear plates, this extra material must

be accounted for and removed from the existing tooling carrier design. The mounting holes must be placed carefully. Since there is the potential mount from different sides, along with other pieces that mount to the tooling careful attention must be paid to the placement and depth of the mounting holes for all attached equipment. Interfering holes would pose a significant problem. The bolts themselves add another element of complication. As with all bolts, care must be taken to protect the threads to ensure that no seizing takes place. Since the bolts would most likely be some sort of steel threaded into aluminum, there is the potential for the two to bond together resulting in either an irreplaceable bolt/wear plate or some sort of destroyed fastener. This sort of scenario would require the application of a compound designed to resist the tendency of the two to bond together. On a related note, the tooling carrier is subject to various vibrations due to impact and normal operating conditions. If this is not accounted for the vibrations may loosen the bolts over time. This would accelerate wear on the system as now the wear plates are unevenly held down and have the potential to vibrate loose and separate from the tooling carrier resulting in a disastrous failure.

The other drawback to this solution is the associated cost, both in materials and extra machining time. Since aluminum is involved the cost of purchasing the materials will be higher. It will also require the stocking of two materials to complete the assembly. The bolts must be factored into it as another cost as well as any compound or treatment applied to them. The other increase in cost shall be associated with the additional machining time required. These can add up and make the cost of the tooling carrier significantly more expensive that it was previously. Again, a cost vs. performance analysis should be performed before considering this as a potential solution.

9. Reflections

This project provided the opportunity to expand upon concepts introduced in the academic curriculum. Creating a dynamic model of the machine to include effective masses and stiffnesses to determine how system characteristics influenced the resulting motions had not been done before. Verifying this data using accelerometers, transducers, high-speed video, and hammer tests had also never been done by us.

Many engineering concepts that the team had briefly worked with prior to this project were expanded upon and required a greater understanding than was previously required. For instance, the analysis of a system and reduction to a single degree of freedom lumped model to generate the dynamic model for the purpose of manipulating cam function to generate desirable velocities at specified positions.

There were of course problems encountered during the testing and redesign phase. The first involved not having access to the machine for the first few weeks of the project. Once access was granted, accelerometer data was taken on multiple occasions to gather sufficient data for all of the necessary tests. It was at times frustrating when the test data did not have adequate coherence due to outside influence. Fortunately, the suggested designs had a significant improvement over the previous components according to gathered data. Unfortunately there was not sufficient time to further explore and perhaps fabricate prototypes for some of the other suggested solutions.

It was a very valuable experience being able to work in a “real world” engineering setting. The sponsoring company was exceptionally accommodating by providing all of the tools and resources required, often dropping their work to give assistance. It was important to retain flexibility due to production requirements as well as the schedules of individuals required to shut

down and perform testing on the machine. The engineers were especially helpful, taking time to discuss the machine in depth as well as review and make suggestions on potential designs. A big thanks must be extended to everyone involved in the many various aspects of this project.

The overall experience gained during this project is invaluable. The team learned first hand how to apply conceptual engineering knowledge in a professional work environment. In the anticipated final year of undergraduate education, being presented with such inspiring subject matter as a means through which to further interest in engineering will continue to affect our careers for many years to come.

10. References

Norton, Robert L. Cam Design and Manufacturing. New York: Industrial P, 2002.

Norton, Robert L. Design of Machinery. 3rd ed. McGraw-Hill Science/Engineering/Math, 2003.

Norton, Robert L. Machine Design: an Integrated Approach. 3rd ed. Upper Saddle River: Prentice Hall, 2005.

Appendix A: Horizontal Motion Mechanism Correctional Factor

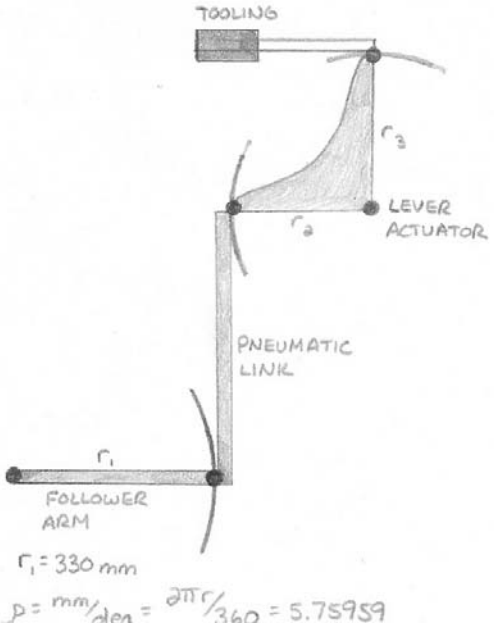

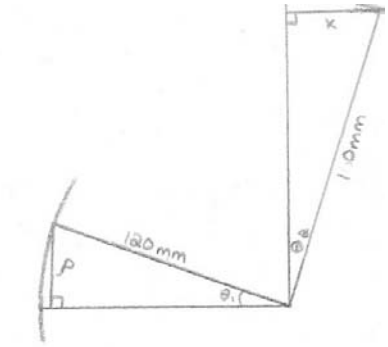

$\sin\theta_1 = \frac{p}{r_1}$

$\theta_1 = \sin^{-1}\frac{p}{r_1} = \sin^{-1}\frac{5.75959}{120}$

$\theta_1 = 2.751°$

$\theta_1 = \theta_2$

$\sin\theta_2 = \frac{x}{r_2}$

$x = r_2 \sin\theta_2 = 160(\sin 2.751)$

$x = 7.67929\ mm/deg$

Appendix B: Vertical Motion Mechanism Correctional Factor

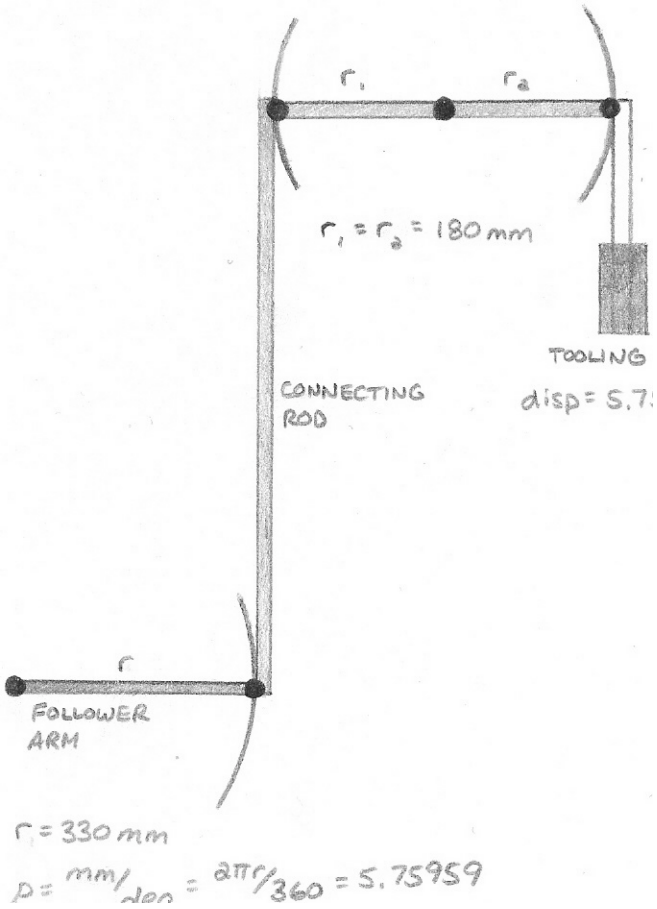

Appendix C: Vertical Motion Lumped Mass Model

CAM 1: Blade Load- Lumped Mass Model

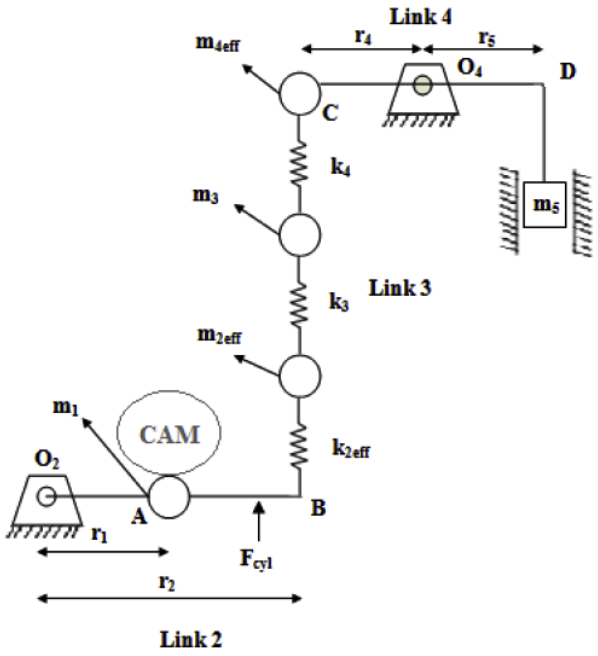

Effective Mass on the CAM

$m_1 := 1.48346 \cdot 10^{-1}$ kg $r_1 := 0.175$ m

$m_3 := 0.6588355$ kg $r_2 := 0.33$ m

$m_5 := 0.7358771$ kg $r_4 := 0.18$ m

$r_5 := 0.18$ m

$I_{zz4} := 1.3911 \cdot 10^{-2}$ $kg \cdot m^2$ moment of inertia about the pivot of Link 4 (lever)

$$m_{4eff} := \frac{I_{zz4}}{r_4^2}$$

$m_{4eff} = 0.4294$ kg Effective mass at point C

$I_{zz2} := 5.2623995 \cdot 10^{-2}$ $kg \cdot m^2$ moment of inertia about the pivot of Link 2 (Cam-Follower)

$$m_{2eff} := \frac{I_{zz2}}{r_2^2}$$

$m_{2eff} = 0.4832$ kg Effective mass at point B

$$m_{5C} := \left(\frac{r_5}{r_4}\right)^2 \cdot m_5$$

$m_{5C} = 0.7359$ kg Effective mass of m5 at point C

$m_C := m_{4eff} + m_{5C}$

$m_C = 1.1652$ kg Total mass at point C

$m_B := m_C + m_3 + m_{2eff}$

$m_B = 2.3073$ kg Total mass at point B

$$m_A := m_1 + \left[m_B \left(\frac{r_2}{r_1} \right)^2 \right]$$

$m_{eff} := m_A$

$m_{eff} = 8.3529$ kg Effective mass on the CAM follower at point A

Effective Masses

$m_1 = 0.1483$ kg Roller Follower

$m_{2eff} = 0.4832$ kg

$m_3 = 0.6588$ kg

$m_{4eff} = 0.4294$ kg

$m_{5C} = 0.7359$ kg

$$M_{2EFF} := m_{2eff} \left(\frac{r_2}{r_1} \right)^2$$ $M_{2EFF} = 1.7183$ kg Lever, CAM Follower

$$M_{3EFF} := m_3 \left(\frac{r_2}{r_1} \right)^2$$ $M_{3EFF} = 2.3428$ kg Conrod

$$M_{4EFF} := m_{4eff} \left(\frac{r_2}{r_1} \right)^2$$ $M_{4EFF} = 1.5267$ kg Lever, Actuator

$$M_{5EFF} := m_{5C} \left(\frac{r_2}{r_1} \right)^2$$ $M_{5EFF} = 2.6167$ kg Hard Stop

Effective Spring Rate on the CAM

$k_4 := 2440200$ Nm-1

$k_2 := 5666000$ Nm-1

Spring Rate for Steel Rod

$OD := 25.4 \cdot 10^{-3}$ m

$ID := 22.1 \cdot 10^{-3}$ m

$$A := \frac{\pi}{4} \cdot \left(OD^2 - ID^2\right)$$

$A = 1.2311 \times 10^{-4}$ m^2

$l := 0.68$ m

$E := 207 \cdot 10^9$ Pa

$$k_3 := \frac{A \cdot E}{l}$$

$k_3 = 3.7476 \times 10^7$ Nm-1 Spring Rate of Conrod

$$k_B := \frac{1}{\frac{1}{k_2} + \frac{1}{k_3} + \frac{1}{k_4}}$$

$k_B = 1.6314 \times 10^6$ Nm-1 Effective Spring Rate at poing B

$$k_A := k_B \cdot \left(\frac{r_2}{r_1}\right)^2$$ Spring Rate at point A

$k_{eff} := k_A$

$k_{eff} = 5.8011 \times 10^6$ Nm-1 Effective Spring Rate on CAM

Appendix D: Lumped Mass Model Horizontal Motion Mechanism

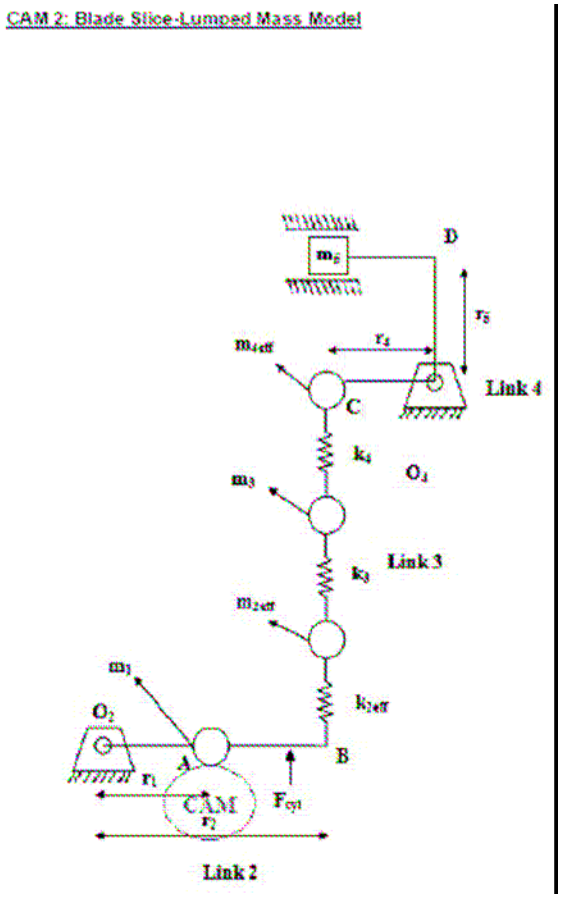

Effective Mass on the CAM

$m_1 := 1.48346 \cdot 10^{-1}$ kg $r_1 := 0.175$ m

$m_3 := 1.1115$ kg $r_2 := 0.33$ m $r_{2new} := 0.315$ m

$m_5 := 0.85916$ kg $r_4 := 0.12$ m $r_{4new} := 0.135$ m

$r_5 := 0.16$ m

$I_{zz4} := 1.0685902 \cdot 10^{-2}$ kg·m^2 moment of inertia about the pivot of Link 4 (Lever)

$I_{zz4new} := 1.1612502 \cdot 10^{-2}$ kg·m^2

$$m_{4eff} := \frac{I_{zz4}}{r_4^2}$$

$m_{4eff} = 0.7421$ kg Effective mass at point C

$I_{zz2} := 5.2623995 \cdot 10^{-2}$ kg·m^2 moment of inertia about the pivot of Link 2 (Cam-Follower)

$I_{zz2new} := 4.9113615 \cdot 10^{-2}$ kg·m^2

$$m_{2eff} := \frac{I_{zz2}}{r_2^2}$$

$m_{2eff} = 0.4832$ kg Effective mass at point B

$$m_{5C} := \left(\frac{r_5}{r_4}\right)^2 \cdot m_5$$

$m_{5C} = 1.5274$ kg Effective mass of m5 at point C

$m_C := m_{4eff} + m_{5C}$

$m_C = 2.2695$ kg Total mass at point C

$m_B := m_C + m_3 + m_{2eff}$

$m_B = 3.8642$ kg Total mass at point B

$$m_A := m_1 + \left[m_B \cdot \left(\frac{r_2}{r_1} \right)^2 \right]$$

$m_{eff} := m_A$

$m_{eff} = 13.8891$ kg Effective mass on the CAM follower at point A

Effective Masses

$m_1 = 0.1483$ kg Roller Follower

$m_{2eff} = 0.4832$ kg

$m_3 = 1.1115$ kg

$m_{4eff} = 0.7421$ kg

$m_{5C} = 1.5274$ kg

$M_{2EFF} := m_{2eff} \left(\frac{r_2}{r_1} \right)^2$ $M_{2EFF} = 1.7183$ kg Lever, CAM Follower

$M_{3EFF} := m_3 \left(\frac{r_2}{r_1} \right)^2$ $M_{3EFF} = 3.9524$ kg Air Cylinder

$M_{4EFF} := m_{4eff} \left(\frac{r_2}{r_1} \right)^2$ $M_{4EFF} = 2.6388$ kg Lever, Actuator

$M_{5EFF} := m_{5C} \left(\frac{r_2}{r_1} \right)^2$ $M_{5EFF} = 5.4313$ kg Hard Stop

Effective Spring Rate

$k_4 := 5.666 \cdot 10^6$ Nm-1

$k_2 := 5.666 \cdot 10^6$ Nm-1

Nm-1 Air Cylinder in Tension

Spring Rate for Air Cylinder

$D := 0.01$ m

$A := \frac{\pi}{4} \cdot D^2$

$A = 7.854 \times 10^{-5}$ m^2

$l := 0.333$ m

$E := 207 \cdot 10^9$ Pa

$k_3 := \frac{A \cdot E}{l}$

$k_3 = 4.8822 \times 10^7$ Nm-1

$$k_B := \frac{1}{\frac{1}{k_2} + \frac{1}{k_3} + \frac{1}{k_4}}$$

$k_B = 2.6776 \times 10^6$ Nm-1 Effective Spring Rate at point B

$k_A := k_B \left(\frac{r_2}{r_1}\right)^2$ Effective Spring Rate at point A

$k_{eff} := k_A$

$k_{eff} = 9.5214 \times 10^6$ Nm-1 Effective Spring Rate on the CAM

Appendix E: LVDT data write up

Since the LVDT was cylindrical in shape and does not have mounting brackets, it was necessary to fabricate custom mountings for the part that would allow for positioning of the LVDT in a way that would allow it to function properly while not interfering with normal machine operations. The brackets below were designed to create a stable platform, while also being easy to machine. The loose dimensions were given inch equivalents to allow the machinist to use US stock while still maintaining metric dimensions.

In order to convert the voltage output of the LVDT into a linear displacement measurement the LVDT had to be calibrated to determine the sensitivity of the sensor precisely. This was done by hooking the LVDT up to a 24-volt output and mounting it on a spare pneumatic link. It was mounted so that the output would be as close to zero as possible. Even though the analyzer only displayed the changed in voltage of the system, keeping it close to zero allowed it to have a full range for its output. The pneumatic link was then placed in its fully compressed state. The distance from the bottom of the cylinder mounting bracket and the top of the pneumatic cylinder was measured and the output voltage was noted. The pneumatic link was then extended to three different position and these distances were measured along with their corresponding output voltages.

This data was put into the Excel spreadsheet below and a trend line was inserted. From this it was determined that for every 0.038 volts the LVDT would move 1 inch. This is shown in **Figure 46Error! Reference source not found.**.

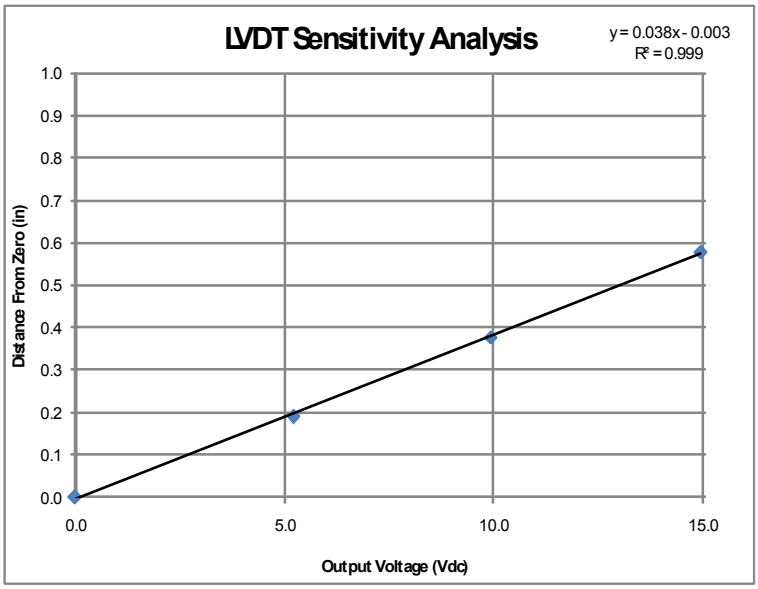

Figure 46 - LVDT sensitivity analysis

The pneumatic link with the LVDT attached (**Figure 47Error! Reference source not found.**) then replaced the current pneumatic link and a pressure sensor placed on the pressurized side of the link. The machine was run and data was taken from both sensors. The data was analyzed to find the maximum pressure difference between the fully compressed pneumatic position and the max extension of the link. These results are in Appendix F.

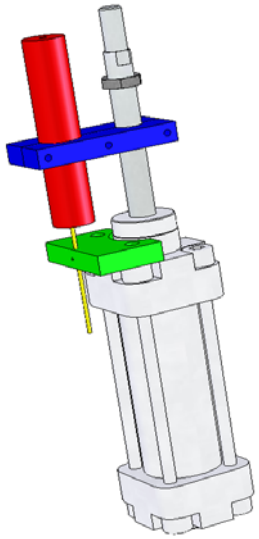

Figure 47 - LVDT setup

Appendix F: LVDT MathCAD Calculations

LVDT Data:

Max Displacement:

$D_{max} := 0.00051$ in

Minimum Displacement:

$D_{min} := -0.0002$ in

Change in Displacement:

$D := D_{max} - D_{min}$

$D = 7.95 \times 10^{-4}$ in

Pressure Sensor Data:

Max Pressure:

$P_{max} := .0588$ psi

Minimum Pressure:

$P_{min} := -.0606$ psi

Pressure Difference:

$P := P_{max} - P_{min}$

$P = 0.119$ psi

Stiffness:

Cylinder Area:

$A_c := 1.12484$ in^2

Force:

$F := P \cdot A_c$

$S := \frac{F}{D}$

$S = 169.024$ $\frac{lb}{in}$

Appendix G: Horizontal Motion Cam Comparison

Displacement:

Over-travel reduced by:	.31mm.

Velocity at hard stop:

Old velocity range at impact:	-28.0 – -19.9
Old velocity at target impact point:	-24.3
New velocity range at impact:	-7.5 – -3
New velocity at median impact point:	-3
% reduction at median impact point:	87.7%

Velocity leaving hard stop:

Old velocity range at impact:	33.8 – 47.4
Old velocity at median impact point:	40.9
New velocity range at impact:	18.5 – 32.3
New velocity at median impact point:	25.8
% reduction at median impact point:	37%

Acceleration:

Old peak acceleration:	7,931
New peak acceleration:	7,841
% decrease in peak acceleration:	1.2%

Vibrations at dwell:

Old first spike amplitude:	42.3
New first spike amplitude:	10.4
% decrease in dwell vibrations:	75.5%

Appendix H: Hammer Tests

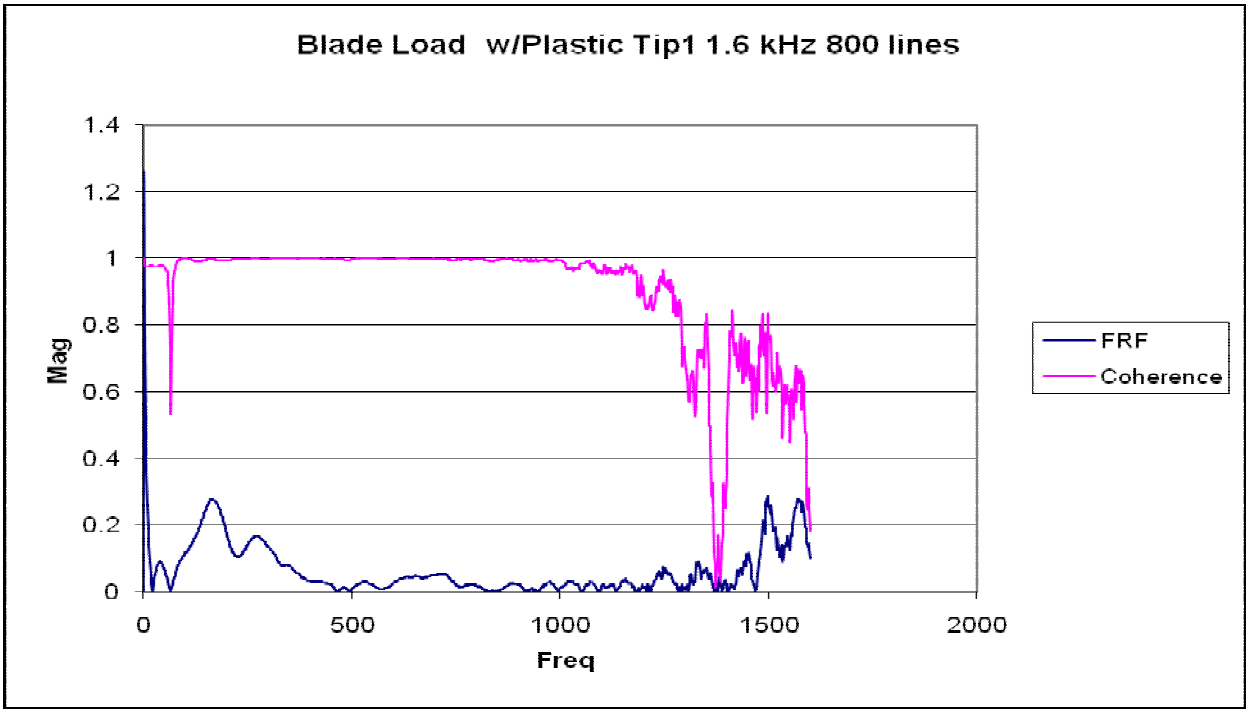

Figure 48 - Experiment 1; FRF and Coherence with accelerometer mounted on vertical slider (on tooling) and plastic hammer tip used

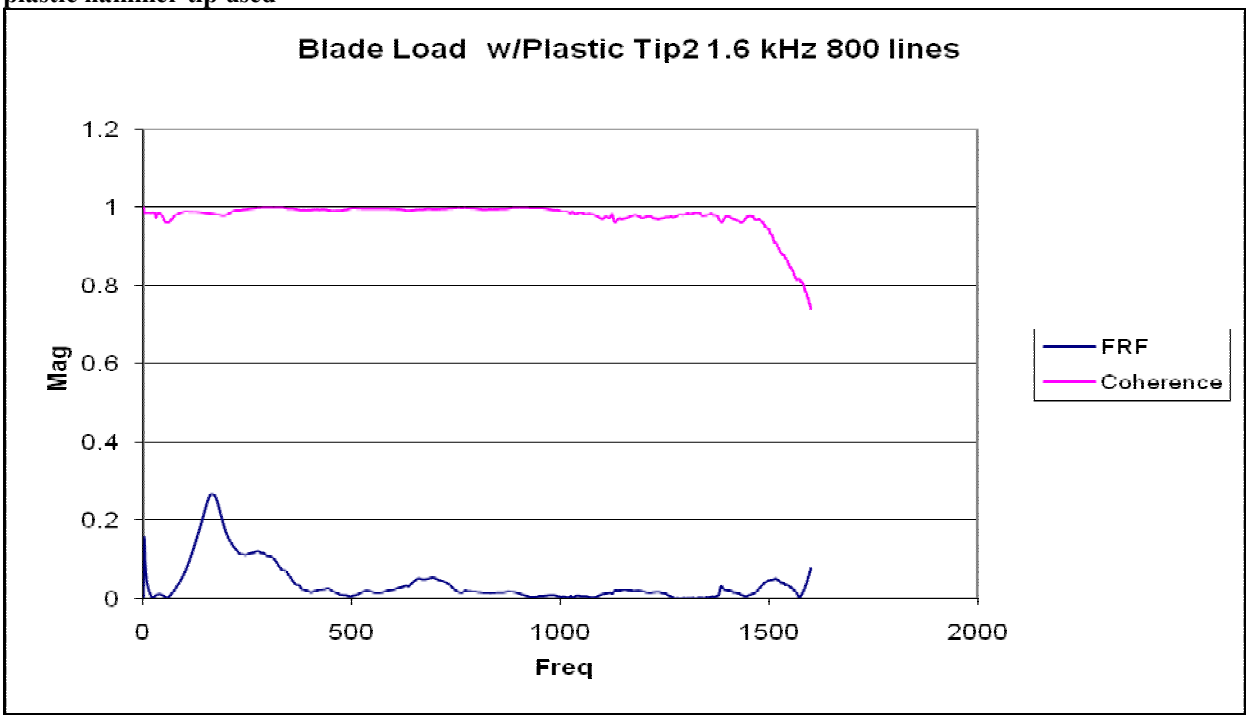

Figure 49 - Experiment 2; FRF and Coherence with accelerometer mounted on vertical slider (on tooling) and plastic hammer tip used

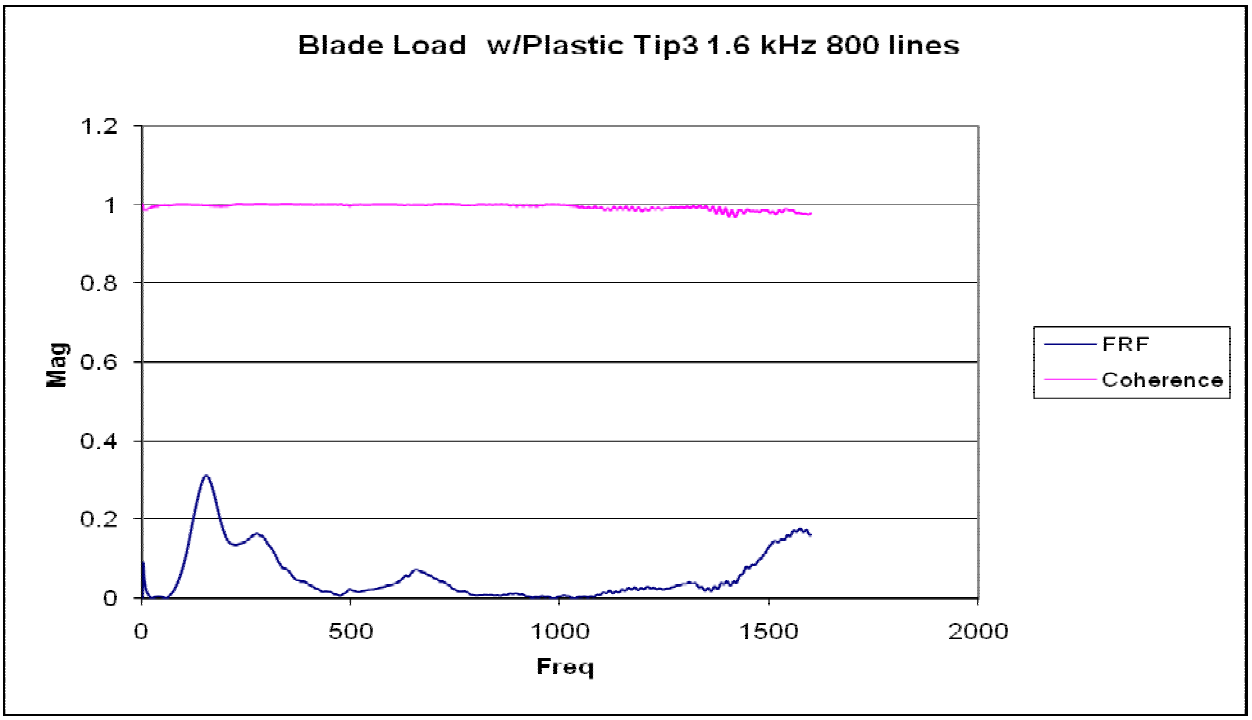

Figure 50 - Experiment 3; FRF and Coherence with accelerometer mounted on vertical slider (on tooling) and plastic hammer tip used

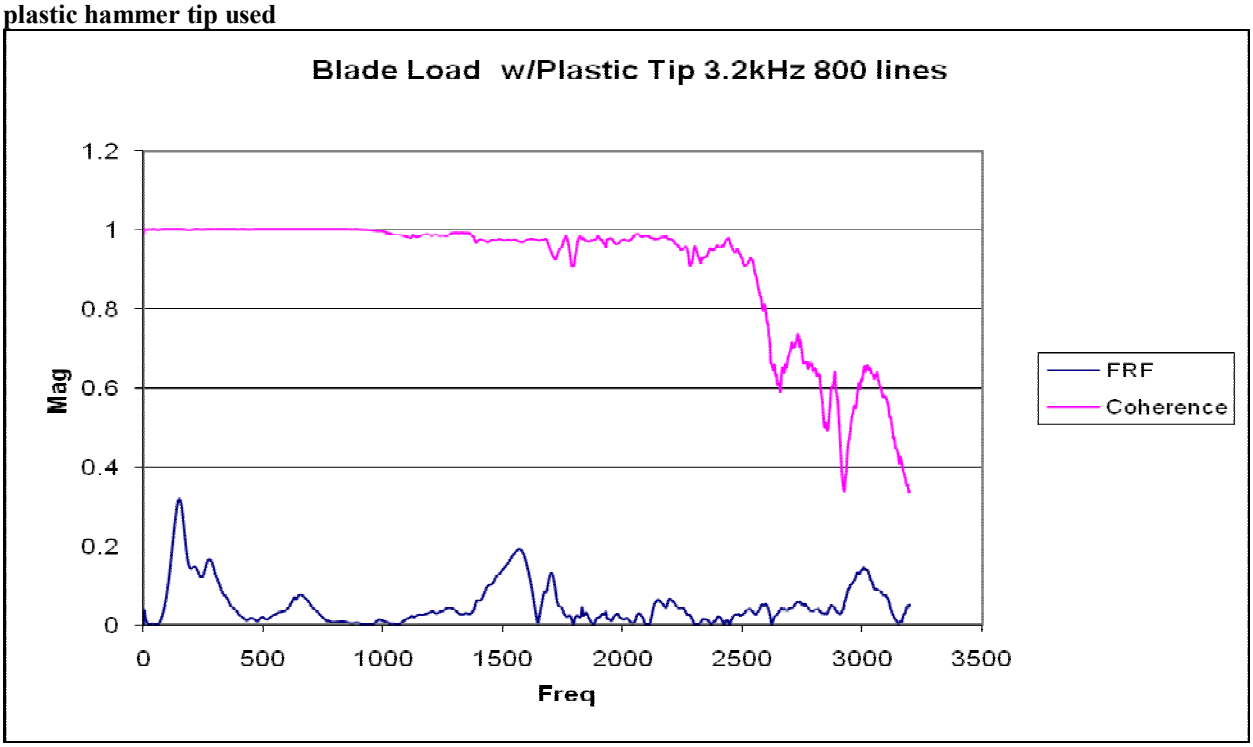

Figure 51 - Experiment 4; FRF and Coherence with accelerometer mounted on vertical slider (on tooling) and plastic hammer tip used

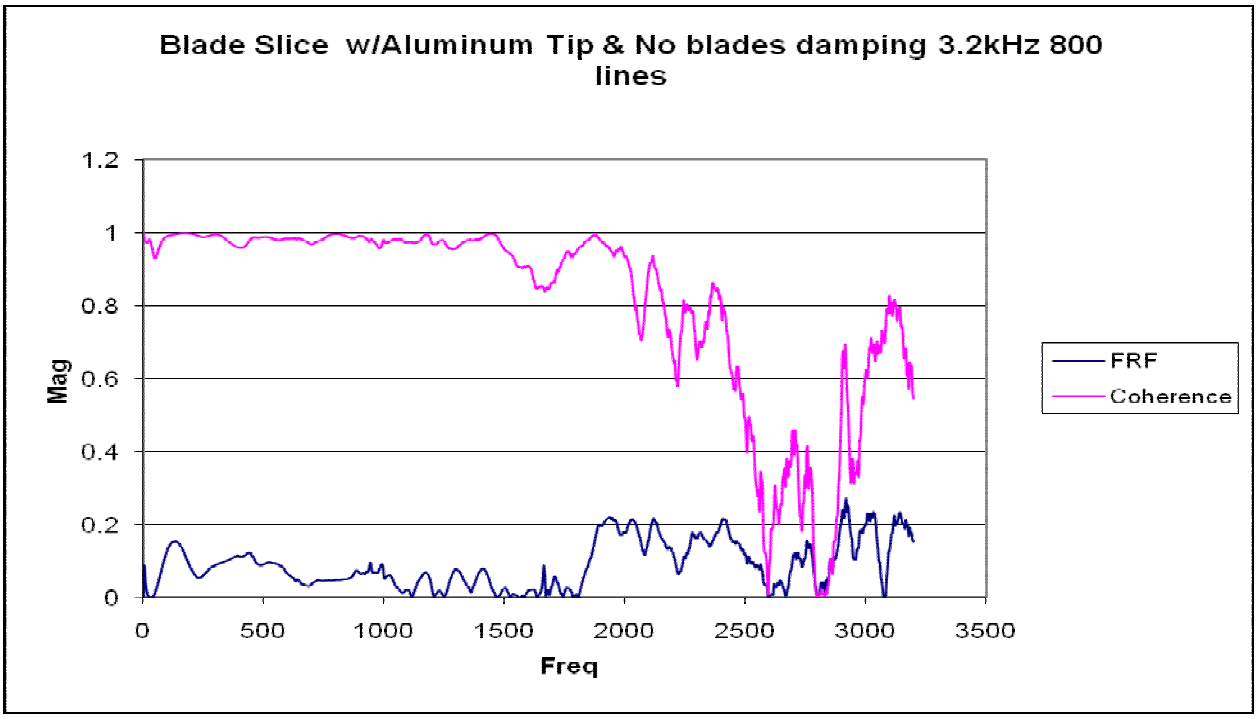

Figure 52 - FRF and Coherence with accelerometer mounted on horizontal slider (on tooling), aluminum hammer tip used and no components in contact with tooling

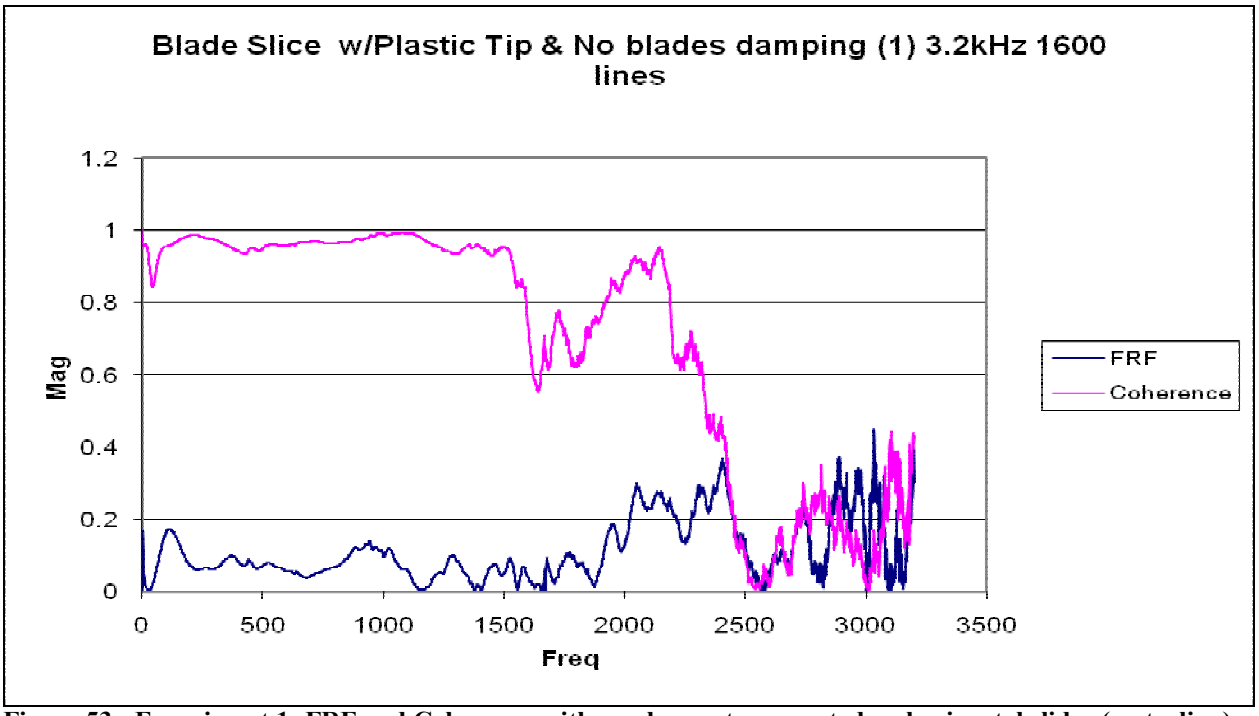

Figure 53 - Experiment 1; FRF and Coherence with accelerometer mounted on horizontal slider (on tooling), plastic hammer tip used and no components in contact with tooling

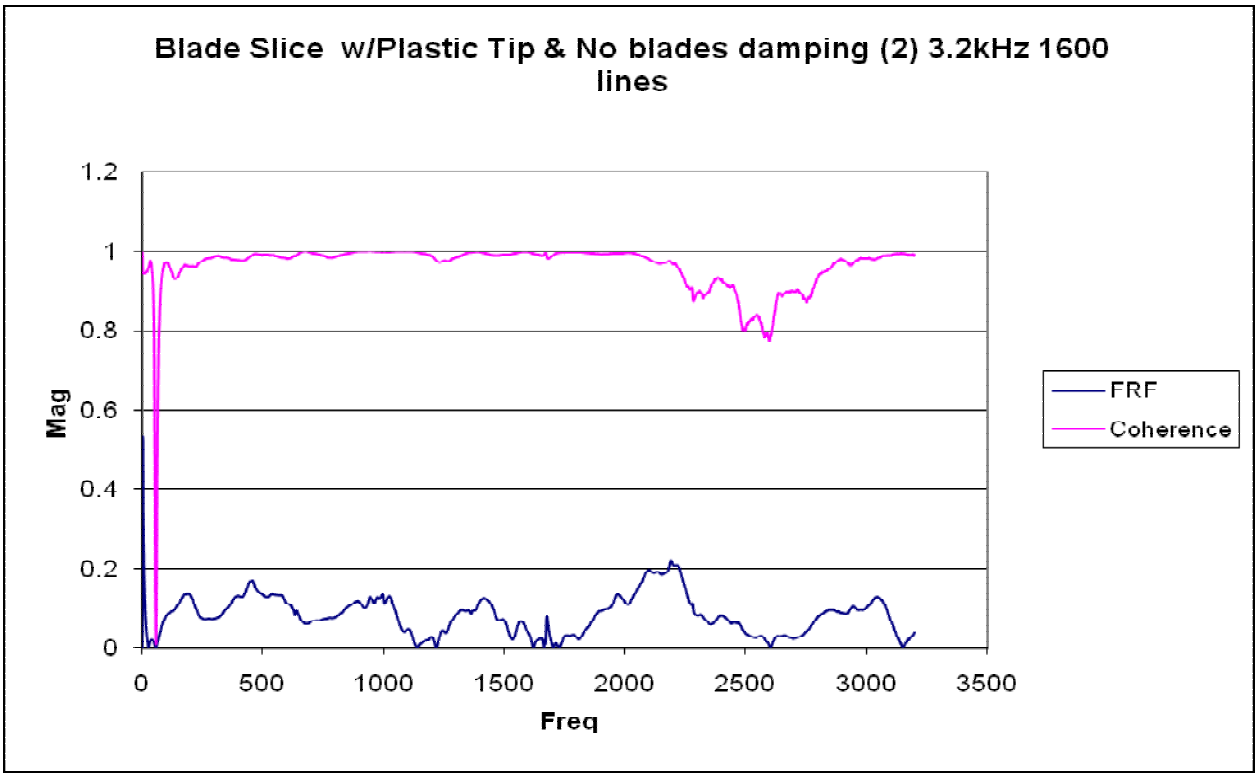

Figure 54 - Experiment 2; FRF and Coherence with accelerometer mounted on horizontal slider (on tooling), plastic hammer tip used and no components in contact with tooling

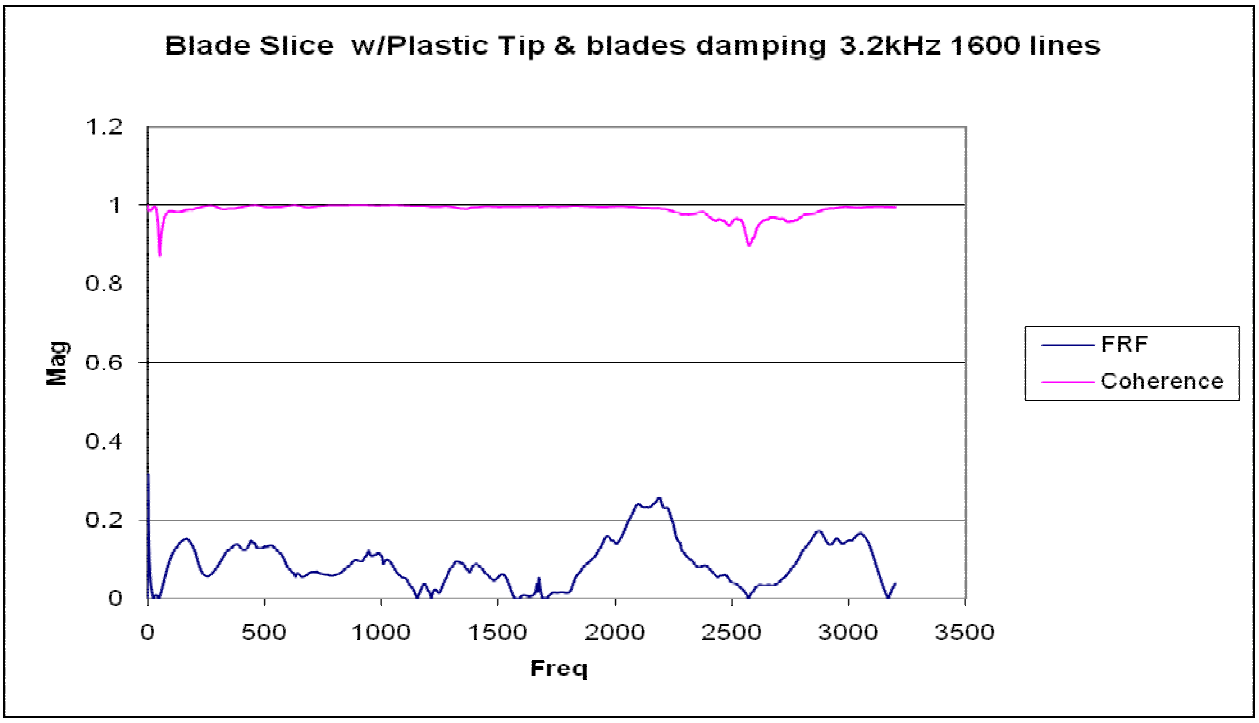

Figure 55 - FRF and Coherence with accelerometer mounted on horizontal slider (on tooling), plastic hammer tip used and components are in contact with tooling

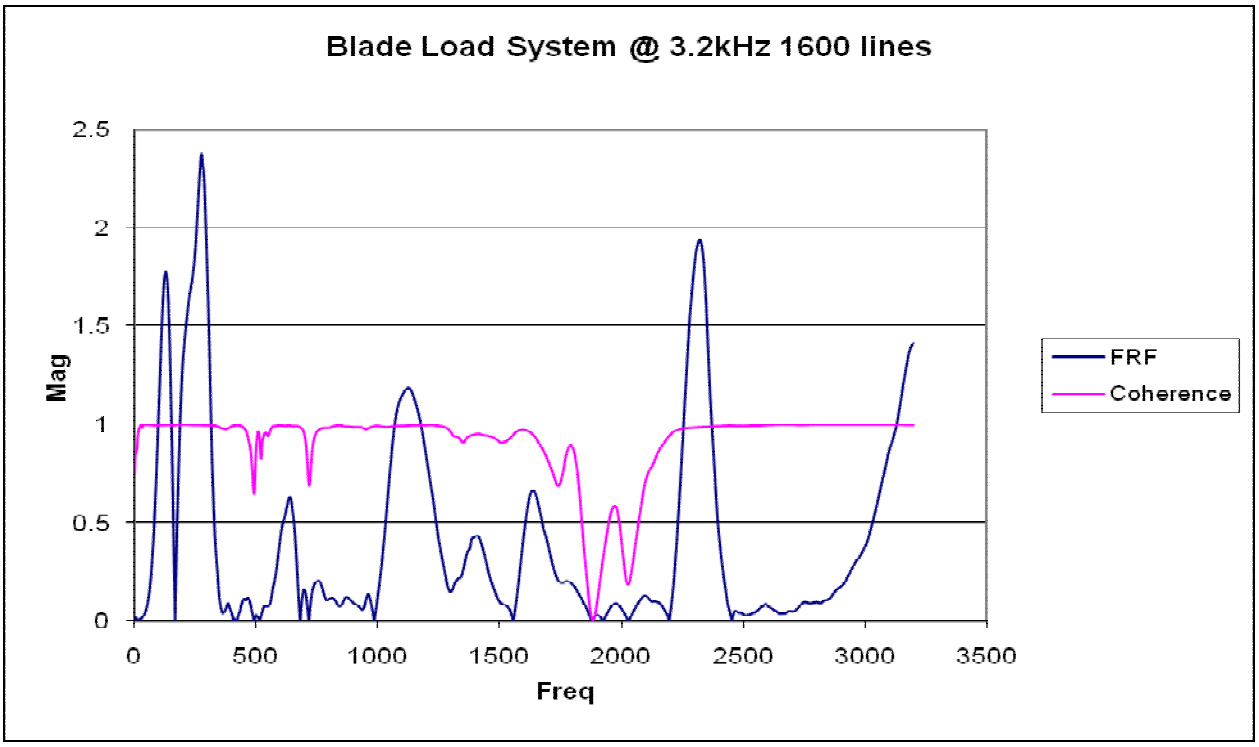

Figure 56 - FRF and Coherence for the vertical mechanism with accelerometer mounted on rocker and hammer hit under cam-follower arm

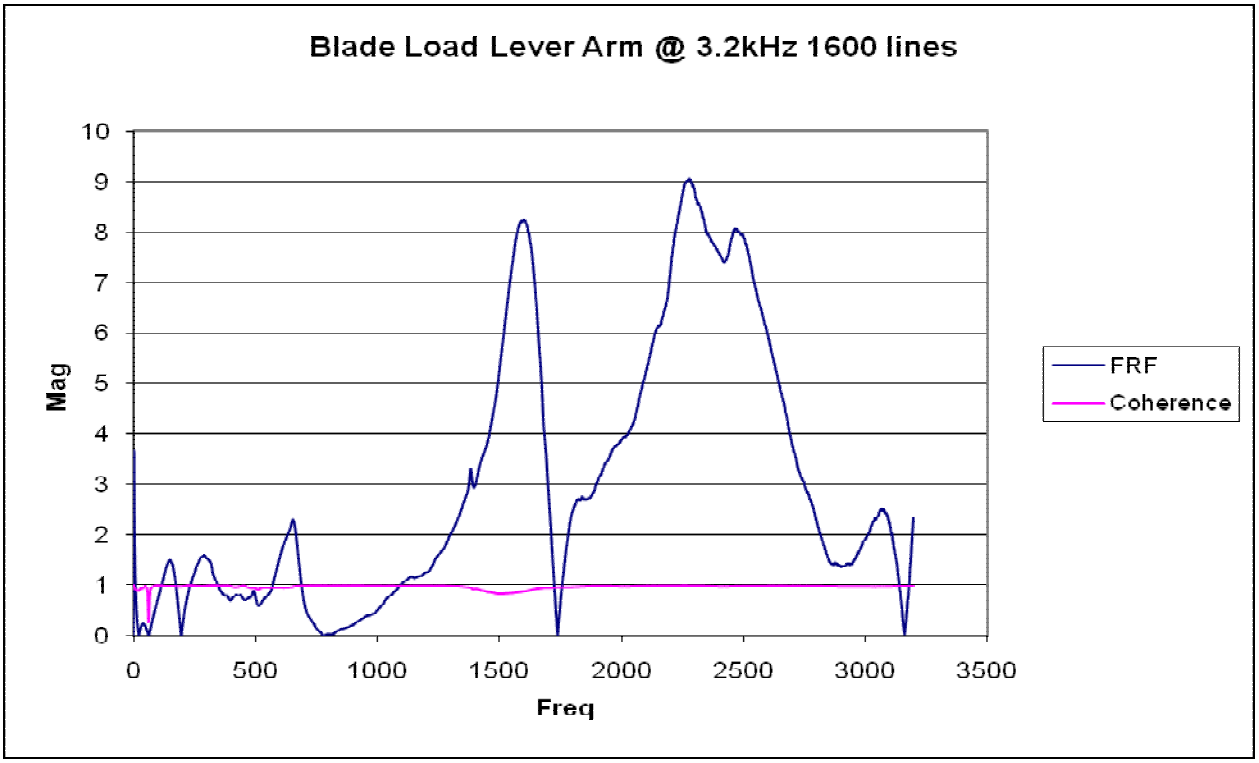

Figure 57 - FRF and Coherence of lever actuator of vertical mechanism with accelerometer mounted on one end and hammer hit on the opposite end

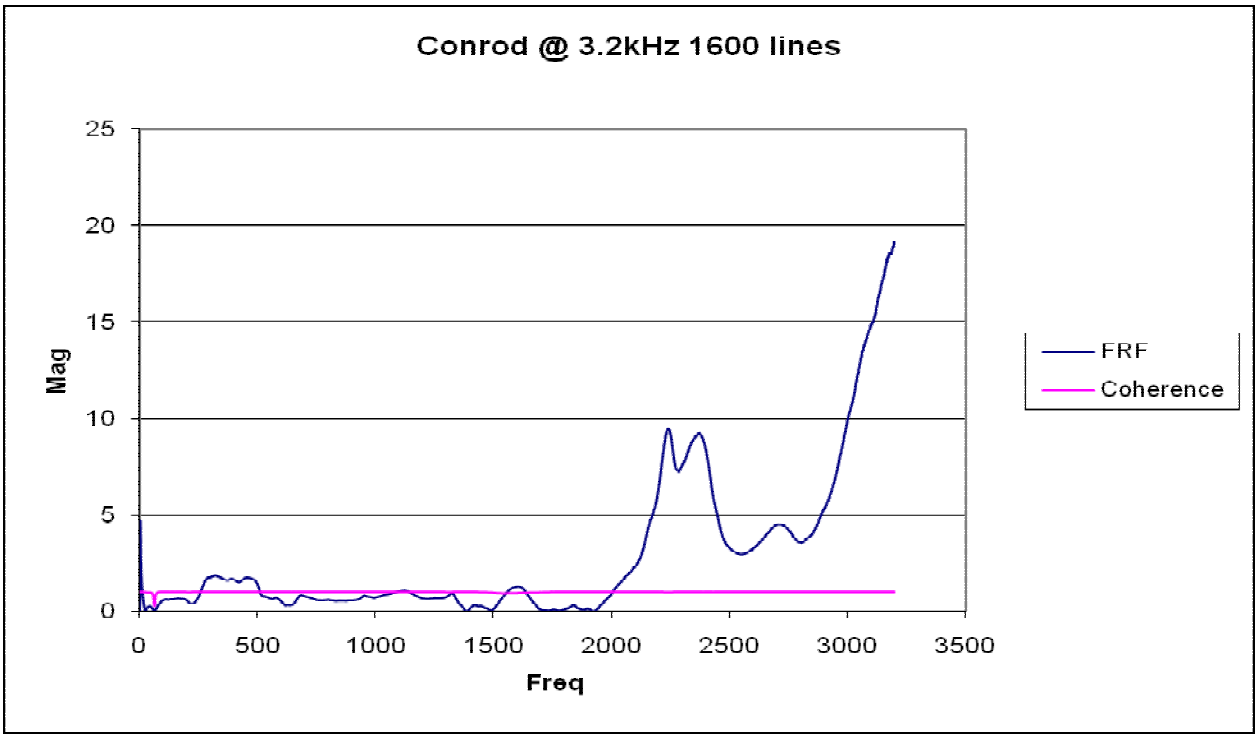

Figure 58 - FRF and Coherence for connecting rod of vertical mechanism with accelerometer mounted on top and hammer hit at the bottom

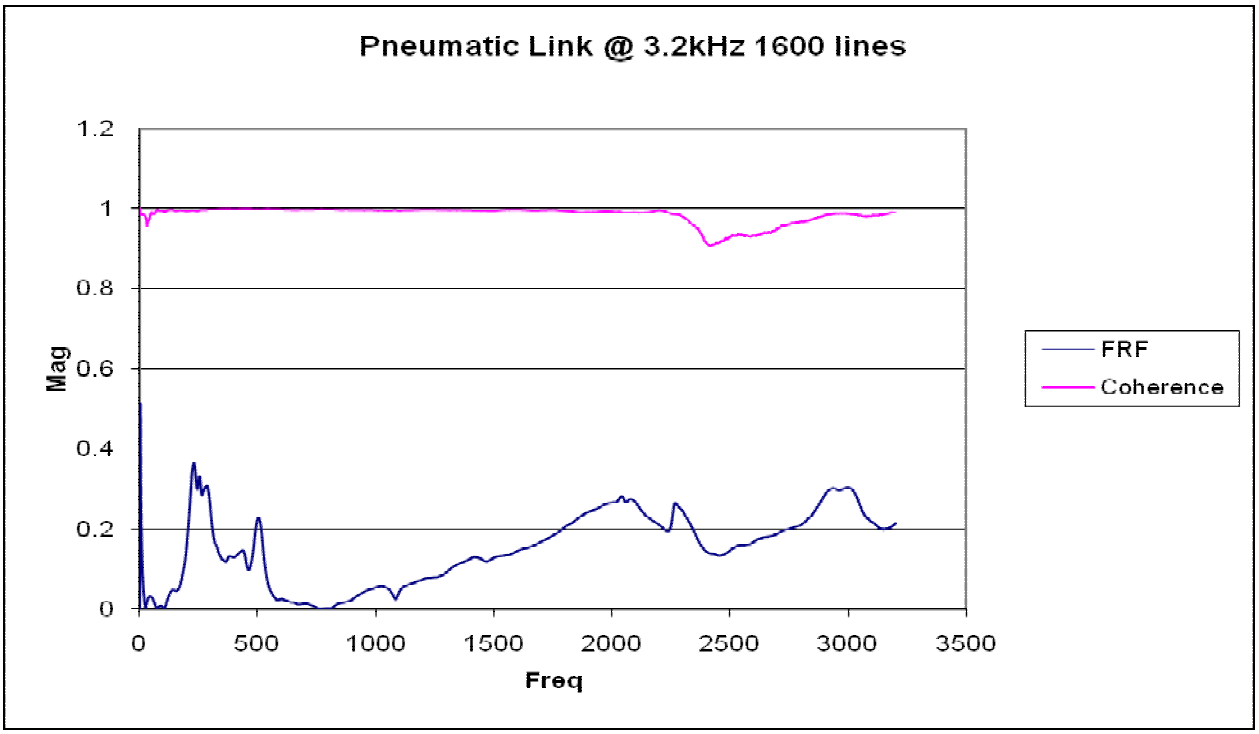

Figure 59 - FRF and Coherence for air-cylinder of horizontal mechanism with accelerometer mounted on top of piston rod and hammer hit at the bottom of pneumatic link

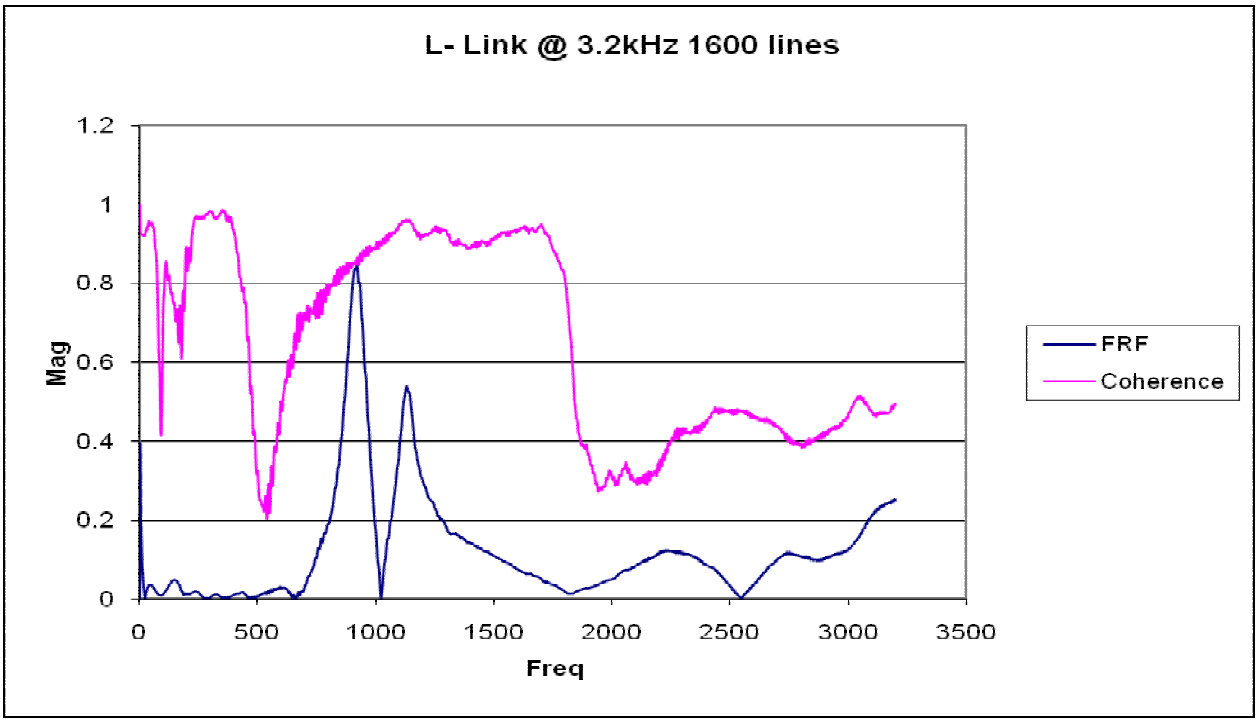

Figure 60 - FRF and Coherence of lever actuator of horizontal mechanism with accelerometer mounted on top edge of vertical arm and hammer hit at the end of the horizontal arm